Confinement of Vibrations for Localized Surface Haptics

Ayoub Ben Dhiab

Doctoral Thesis

Ecole Doctorale des Sciences Mécaniques, Acoustiques, Electronique et Robotique de Paris
ED391

Supervisor: Pr. Jean-Luc ZARADER
Co-supervisor: Dr. Charles HUDIN

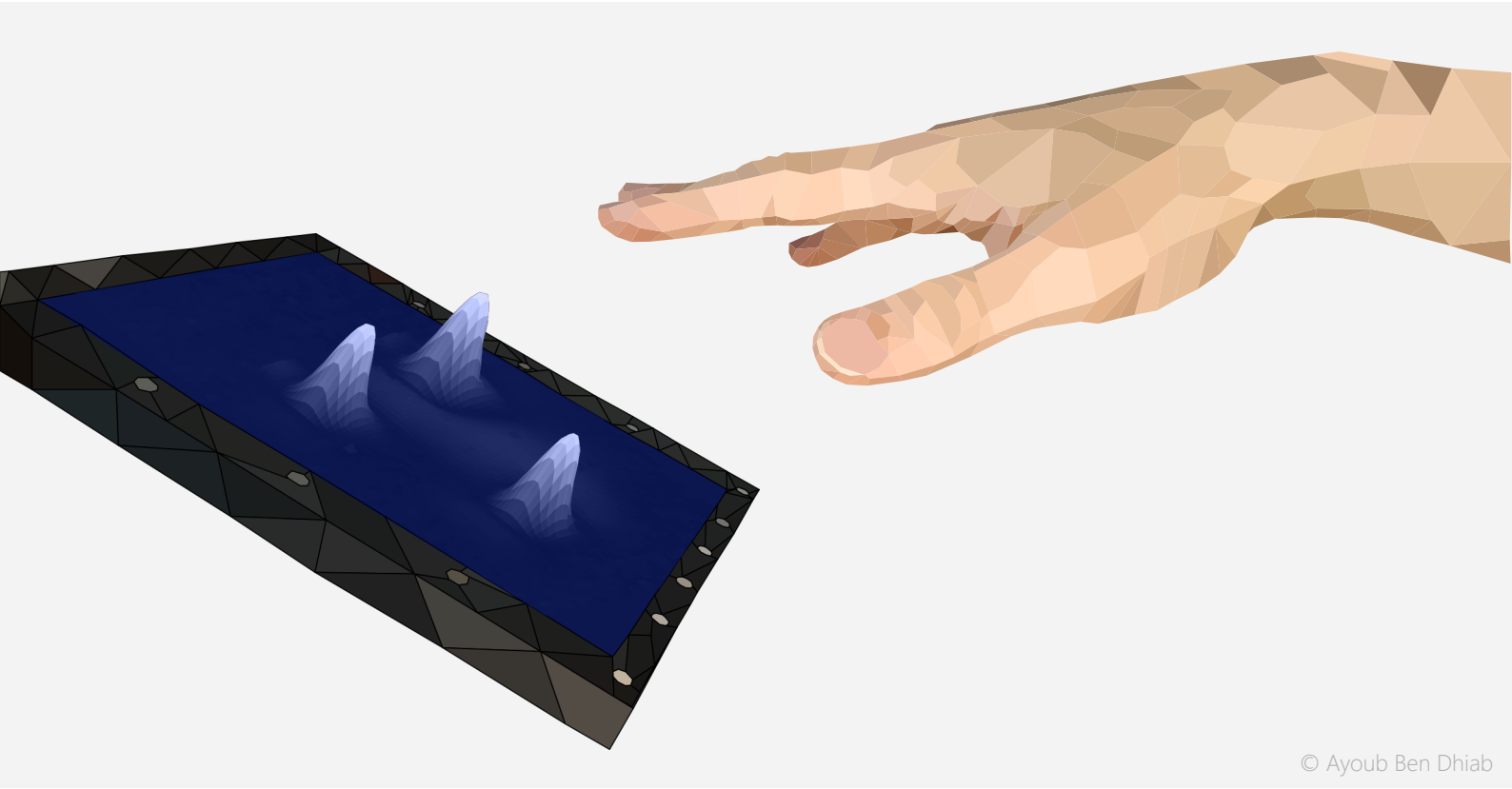

Confinement of Vibrations for Localized Surface Haptics

2021-2022

Ayoub BEN DHIAB

Sorbonne Université

Doctoral Thesis

École Doctorale des Sciences Mécaniques, Acoustique, Électronique et Robotique de Paris

Confinement of Vibrations for Localized Surface Haptics

Presented by

Ayoub BEN DHIAB

A thesis submitted in fulfillment of the requirements for the degree of

Docteur de Sorbonne Université

in the
Laboratory of Sensory and Ambient Interfaces
CEA, LIST, Palaiseau.

Defended on Wednesday the 6th of April 2022 before:

Betty	Lemaire-Semail	Professor,	L2EP, Université de Lille,	Reviewer
Xavier	Boutillon	Director of Research CNRS,	LMS, École Polytechnique,	Reviewer
Vincent	Hayward	Professor,	ISIR, Sorbonne Université,	Examiner
Marc	Rébillat	Associate Professor,	LPIMM, Arts et Métiers Paris,	Examiner
Sinan	Haliyo	Associate Professor,	ISIR, Sorbonne Université,	Examiner
Jean-Luc	Zarader	Professor,	ISIR, Sorbonne Université,	Supervisor
Charles	Hudin	Research Engineer,	LISA, CEA-LIST,	Co-supervisor

License

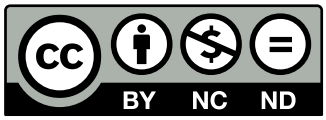

Contents

Summary

On a tactile surface, providing vibrotactile feedback enhance the interaction. Doing so in a localized fashion allows for a more natural multi-finger exploration of these surfaces. While vibration propagation generally prevents this localization, in this thesis we present technical solutions to spatially localize vibratory stimuli on continuous mediums. Taking a different path from control-based approaches, we propose three methods where each actuator provides a stimulus confined in its actuation area. By adjusting the geometry of the propagation medium and the boundary conditions, we show that waveguides exhibit a low frequency band gap that enable localized vibrotactile stimulation on narrow thin plates. Associated theory as well as practical measurements showed that applications for haptics are possible and a prototype was then implemented. The extension of the method to wider surfaces was made possible thanks to the use of periodic supports which also provided a low frequency band-gap. A 2D prototype was designed and allowed the user, through different exploratory procedures, to find a vibrating target area and experience phantom sensations such as apparent movement and saltation. It was shown that the effect of the finger on those geometry was negligible for light and heavy touch. Seeking a full haptic experience, we also wanted to provide, in addition to normal force modulation, lateral force modulation through friction modulation. This was achieved thanks to an interference phenomena appearing at specific ultrasonic frequencies, called non-radiating frequencies, caused by the mechanical coupling of a piezoelectric actuator on a plate. Non-radiating frequencies obtained through a semi-analytical model showed results close to experimental ones. We then realized an array of triangular shaped actuators that covers the entire interaction surface. By powering sets of triangles to form hexagonal piezoelectric actuators, non-radiating frequencies were also found and localized friction modulation was proven possible on an OLED screen, thus paving the way for the integration of localized haptic functions on touch screens.

Résumé

Sur une surface tactile, fournir un retour vibrotactile améliore l'interaction. Le faire de manière localisée permet une exploration multi-doigts plus naturelle de ces surfaces. Alors que la propagation des vibrations empêche généralement cette localisation, nous présentons dans cette thèse des solutions techniques pour localiser spatialement les stimuli vibratoires sur des supports continus. En prenant une voie différente des approches basées sur le contrôle, nous proposons trois méthodes où chaque actionneur fournit un stimulus confiné dans sa zone d'actionnement. En ajustant la géométrie du milieu de propagation et les conditions aux limites, nous montrons que les guides d'ondes constituent des passe-hauts en fréquence permettant une stimulation vibrotactile localisée sur des plaques minces et étroites. La théorie associée ainsi que les mesures pratiques ont montré que des applications pour l'haptique sont possibles et un prototype a ensuite été mis en œuvre. L'extension de la méthode à des surfaces plus larges a été rendue possible grâce à l'utilisation de supports périodiques qui fournissent également des bandes interdites en fréquence. Un prototype 2D a été conçu et a permis à l'utilisateur, à travers différentes procédures exploratoires, de trouver une zone cible vibrante et d'expérimenter des sensations fantômes telles que le mouvement apparent et la saltation. Il a été démontré que l'effet du doigt sur ces géométries était négligeable pour un toucher léger et lourd. A la recherche d'une expérience haptique complète, nous avons également voulu fournir, en plus de la modulation de la force normale, une modulation de la force latérale par la modulation de la friction. Ceci a été réalisé grâce à un phénomène d'interférence apparaissant à des fréquences ultrasonores spécifiques, appelées fréquences non-rayonnantes, provoquées par le couplage mécanique d'un actionneur piézoélectrique sur une plaque. Les fréquences non-rayonnantes obtenues par un modèle semi-analytique ont montré des résultats proches des résultats expérimentaux. Nous avons ensuite réalisé un réseau d'actionneurs de forme triangulaire qui couvre toute la surface d'interaction. En alimentant des ensembles de triangles pour former des actionneurs piézoélectriques hexagonaux, des fréquences non-rayonnantes ont également été trouvées et la modulation localisée de la friction s'est avérée possible sur un écran OLED, ouvrant ainsi la voie à l'intégration de fonctions haptiques localisées sur des écrans tactiles.

Acknowledgements

Throughout those three years, I have been supported by great people.

First I would like to thank my scientific tutor Charles Hudin who every step of the way was responsive to my ideas and took the time to explain their relevance even though a lot of them were not smart. His enthusiasm, pedagogy and thinking became a real inspiration to me and forged my identity as a researcher, for this, I am deeply grateful.

I also wish to thank Pr. Vincent Hayward who supervised my work during the first two years and allowed me to build ties with the ISIR laboratory and participate to the haptic club where I met many people with whom I had awesome exchanges. My third year was supervised by Pr. Jean-Luc Zarader who, after unforeseen events, was kind enough to take me under his wings and provide me with careful advice.

I would also like to express my gratitude to Moustapha Hafez who encouraged me and allowed this adventure to start. And Margarita Anastassova who allowed this adventure to continue. Both of them, open-minded toward innovation and true examples of leadership.

To the LISA lab, a happy bunch where each one of them provided me help when I asked without a second thought or a spec of discomfort. Smart, kind and inclusive towards my beliefs, they are, without a doubt, concrete representation of the ideals of the French Republic.

Special thanks are due to Lucie Pantera who conducted her internship and started her PhD in the LISA at the same time as me. From the RER B to Japan, every journey in life becomes more enjoyable when you are well accompanied. Truly, an unsuspected but welcome friendship which lightened the burden of those three years.

I also find it mandatory to thank my teachers. The first one coming to my mind is Olivier Cassez who inspired me toward engineering with all kind of activities in high-school. Then came the DUT where, in addition to the enormous amount of practical knowledge I was able to absorb, I had my first contact with Japan through Jean-Luc Rigal. From then on, a new wind brought me to the exceptional teachers of the

Baggio ATS prep school in Lille: Daniel Duverney with his tremendous abilities in teaching mathematics; Jean-Marc Playoust making the teaching of physics vibrate with spirit and rhythm; Jean-Baptiste Frossard kindling passion in his student heart for the French language and who enlightened my writing with style and originality; Philippe Marseille illuminating the tortuous wires of electrical engineering; and Didier Cottreel who perfected through simple elements of practical understanding my basics in mechanics. After the ATS came the Arts et Métiers engineering school where I was welcomed by Bernard Charat in my first year then guided to my last year internship by Nazih Mechbal.

I would like to thank Pr. Betty Lemaire-Semail and Pr. Xavier Boutillon, for their attentive and careful reading of my manuscript and the correction they suggested, as well as all the members of the jury. Having researchers giving their time to read, judge and discuss your work brought me more joy than I had expected.

To my friends and family, for their patience, love and continuous support throughout my whole life.

To my future family, Sharmin, a discreet flower that brought an early spring to the end of my doctorate and embalmed it with a sweet peaceful perfume. May Allah grant me perseverance to tirelessly improve my faith to become a better husband and give her peace and happiness until our next life.

この章では、日本で出会った親愛の友達に感謝を申し上げたいと思います。
私は日本での暮らしと交換留学を通して、素晴らしい方々と出会いました。日本人の友達と最初に出会ったのは、森、山、星空、富士山の背景があった清里です。当時未熟な私は、どんな時も仲間達と笑い合って、たのしく過ごしていました。ここで私の人生が大き変里ました。野口さん、福島さん、矢後さん、美智子さん、浦壁さん、加藤さん、村田さん、権さん、桶本さん、エキさん、カーラさん。皆様に心より感謝申し上げます。
次に第二故郷のような小さな町、秋田です。ここで私は、高専の留学生の勇気と決意に触発されました。フィル、モー、ファリス、カビン、アレクシー、アブダラ、ビクター、マチュー、アフィカ、ヌーマズニ、アミラ、ソフィア、ザヤ、皆さんと交流することで、人間として成長することができました。また、技術や人生の知識など、たくさんのことを教えてくれた晴海先生と菅原先生、そして秋田文化を紹介してくれた小沢さんにも大変感謝したいと思います。

この人生とこれからの人生において、幸福をお祈り申し上げます。

طَلَبُ اَلْعِلْمِ فَرِيضَةٌ عَلَى كُلِّ مُسْلِمٍ

Seeking knowledge is an obligation upon every Muslim.

The Prophet Muhammed ﷺ

Source: Sahih Muslim

1

General Introduction

Interacting with nearby object, identifying their characteristics and body movement in general are all enabled thanks to the haptic sense. It plays a central role in our lives for the communication of our feelings and the construction of the concept of self. In turn, it allows for the externalization of the human imagination in the real world through the use of tools. Those tools built to help humans in their interaction with their environment were initially crude but got progressively optimized with time following our senses in search of beauty and comfort. It is a fact that the use of a poorly made tool, such as a kitchen knife with a defective handle, can quickly become uncomfortable, annoying, and even dangerous to use.

As humans kept on evolving, they developed better tools to answer their needs. Our tools nowadays are so advanced that we interact daily with environments that are no longer real but virtual, through our smartphone for example. One of the main technology which allow us to interact with the virtual world is the touch screen. Its birth in the 60s/70s with E.A Johnson's research and Sam Hurst's patents, slow at first, suddenly gained in popularity in 2007 with the release of the iPhone. Since then, touch screens have become an essential part of human machine interfaces: cell phones, TVs, household appliances, ATMs... we are now more than ever likely to interact with these kinds of surfaces that provide in most cases only visual or auditory feedback. The appeal of tactile surfaces has spread very quickly as they are easily integrated, reprogrammed, and use fewer mechanical components than its ancestor, the mechanical button. However, unlike mechanical buttons, touch screens do not necessarily provide tactile feedback. Thus, we cannot confirm if our action was registered by the device or recognize an option presented to us through touch alone (which was possible with buttons by their shapes and mechanics). We then have to rely on our eyesight and hearing to get these kind of feedback. As tactile dashboard

in cars are becoming popular, we can assume that relying on eyesight and hearing alone can be dangerous. We can imagine that a driver interacting with his tactile dashboard would have a hard time keeping their focus on the road as most of the feedback is visual. These new surfaces without tactile feedback moreover limit the accessibility of visually impaired people to everyday interaction. Imagine a scenario in your kitchen where you need to interact with the touch hob while closing your eyes and the associated difficulty and potential danger. Providing haptic feedback is therefore essential in developing secure and inclusive new tools.

The last decade saw a number of innovations to compensate for the lack of haptic feedback in touchscreens. The typical example is the haptic feedback provided by our smartphones. At first a simple vibration obtained through the rotation of an eccentric mass (ERM vibration motor) for notifications purposes, vibration stimuli were slowly refined thanks to the technological development of actuators such as "linear resonant actuators" (LRA) which allowed for instance, through more complex stimuli, the simulation of key-press actions. However, in these surfaces, an inherent problem with the use of vibrations lies in their propagation. This observation reveals two limits: a limit associated with the transmission of information in a passive context of use (e.g. when receiving notifications) and a limit associated with the dynamic interaction with these surfaces (uni-touch) which conflicts with our natural interaction (multi-touch).

Novel work is presented in this thesis to address the issue of vibration propagation. By localizing vibrations for haptic feedback, we seek to enrich the interaction and haptic communication with tactile surfaces by evolving temporally modulated vibratory stimuli to spatio-temporally modulated stimuli. In the following chapters, we first reflect on the current state of the art then proceed by developing three methods to localize vibrations allowing for the creation of different haptic effects that can broaden the use of tactile feedback to several fingers, large areas of the skin and multiple users.

2

Multi-touch Surface Haptics

A short discussion followed by a state of the art are proposed to set context around multi-touch involvements, consequences and needs in the design of future human machine interfaces involving touch-surfaces.

2

Outline

2.1. INTRODUCTION

HAPTIC senses include all the elements involved in the human body's mechanical interaction with its environment. While auditory and visual cues are generally favored during the design of user interfaces, there is a real conceptual difficulty when it comes to the nature of the stimulation as the skin is not a homogeneous organ from a sensory point of view. For example, the feeling of a force can differ greatly depending on the region of the body. Thus, certain notions, such as force, do not really have any meaning in haptics if we do not specify with great precision the conditions in which they are applied (which also removes any generalization of the studied phenomena). The design of devices and algorithms for the stimulation of sensory and motor organs therefore requires a good knowledge of the biological aspects of the haptic senses.

In this field of haptics, some researchers and industrials have been interested in providing tactile feedback in interactive touch surfaces which gave birth to the field of *surface haptics*. This emerging area of research aims to generate haptic effects on physical surfaces such as touch surfaces used in mobile phones, tablets, kiosks, information displays, and the front panels of new generation home appliances and cars. Following the IEEE Special Issue on Surface Haptics [1], related topics of interest of this field are as follow:

- tactile rendering algorithms for displaying virtual shapes and textures on touch surfaces;
- the mechanics and neuroscience of contact between the human fingerpad and touch surfaces displaying haptic feedback; studies on surface haptics investigating human perception, cognition, attention, new HCI paradigms, and user interface design and experience (UIX);
- applications of surface haptics in consumer electronics, the automotive industry, home appliances, designing aids for the visually impaired, online shopping, gaming and entertainment, data visualization, education, tele-touch, and art appreciation;
- and studies on the design and evaluation of various actuation technologies (vibrotactile, electro-adhesive, ultrasonic, electromagnetic, etc.) for displaying haptic feedback through touch surfaces.

This thesis subject "Confinement of Vibration for Localized Surface Haptics" is in line with this last topic and proposes new methods to provide localized haptic feed-

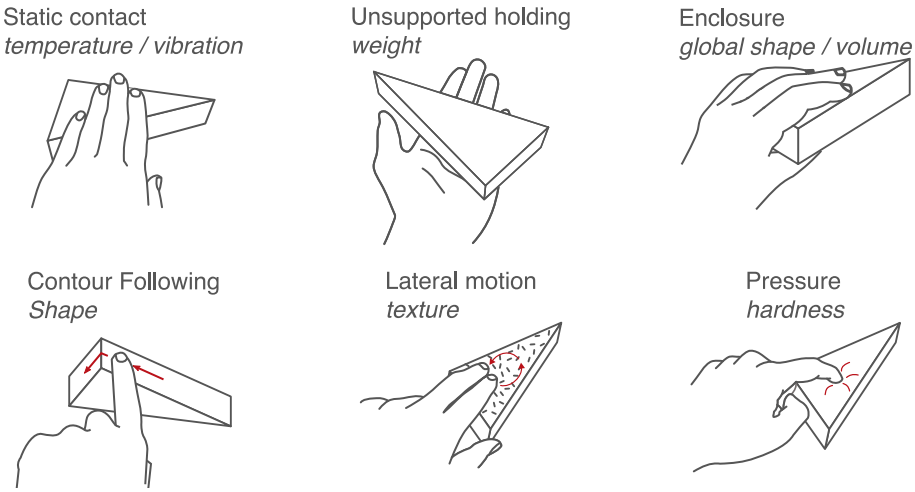

Figure 2.1: Exploratory procedures by Klatzky and Lederman [3] redrawn from Hannaford and Okamura [4].

back by confining vibrations to their area of origin. This subject of haptic feedback localization on touch surfaces is fairly new as most technologies involving vibrations are subjected to vibration propagation which limits applications to a single finger interaction. Thus localizing vibrations could lead to multi-touch/multi-user haptic applications in human machine interfaces.

2.1.1. MULTI-TOUCH INTERACTION

Our natural interaction with the surrounding objects does not only involve the use of one finger but all the mechanisms of the hand. Through different procedures, the hand is able to determine the physical properties of a material. We can identify *exploration procedures (EPs)* which usage depends on the property we wish to determine [2, 3]. Among all the possible movements, we can observe that some dominate (Figure 2.1): static contact for thermal properties, unilateral support for weight, envelopment for size, and especially regarding surface exploration: contour tracking for shape, lateral sliding for texture and indentation for rigidity. Those exploration procedures are optimized to make full use of our sensory system to extract the desired information.

It then seems that limiting the use of haptic feedback to a single finger hinders the user. It reduces the possibilities of interaction and restricts the amount and richness of tactile information that can be conveyed. Leading therefore to reduced haptic performance. This observation though logic at first glance, is yet to be properly proven as no tactile device providing full multi-touch haptic feedback exists.

However, studies can be found in the literature trying to determine if using more fingers improves performance on other kind of apparatus like tactile maps (printed

maps designed to be read by touch for blind and partially sighted users). Unfortunately, observations on this topic are diverging. For Overvliet et al. [5], using more fingers do not necessarily reduce search times in haptic search of a target. Using more fingers seems to add commutation time between each finger on the targeted area. Also, Catala et al. [6] experimented with a user wearing a glove equipped with vibration actuators. The user had to scan a tactile surface with virtual targets blindly with one and two fingers (same hand and different hands). The actuator attached to the finger was activated when the finger was passing over a virtual target. The results indicated that the use of one finger in one hand is more efficient than the use of two fingers in one or two hands in the studied task. Also, users demonstrated greater confidence, shorter exploration time, more correct answers, and greater speed of exploration with one finger.

On the other hand, other articles show that the use of several hands and fingers improve haptic performances [7, 8]. In particular, Morash et al. [7] prove that a range of perceptual tasks are better performed with two hands and more fingers and provided benefits are task-specific. For example, search is always enhanced by more fingers, but line-following is best performed with two index fingers. In Metzger et al. [8] case, they associate different role for each finger during multi-touch exploration (index and middle finger are suggested to be specialized for fine analysis). They then argue that haptic target search involves a two-phase search and analysis process similar to vision: peripheral detection and foveation for high-resolution processing.

All those results about multi-touch performances seem to point that the need for multi-touch haptic feedback is task specific. However those results are also a bit limited in our case since they do not involve localized vibration on a continuous medium. Multi-touch interaction is complex and still contains many conceptual difficulties and misunderstandings that could be alleviated provided the conception of innovative devices.

2.1.2. MULTI-TOUCH STIMULATION

Adding to the previous section, even if we localize haptic feedback both in space and time for the creation of more complex and precise interactions, the use of spatially distributed stimuli also brings a new set of interrogations. Indeed, our sensory system, despite its fine tuning and its multi-functionality, remains subjected to tactile illusions and masking phenomena. For instance, if we take two discrete points of stimulation we can observe different perceptual effects depending on how the actuation is made.

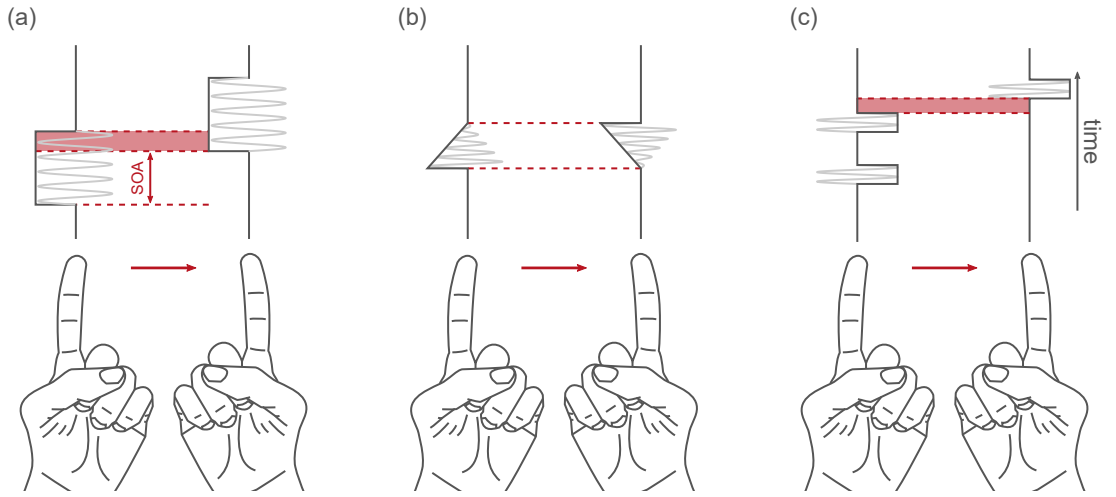

Figure 2.2: Phantom sensations. (a) apparent movement. (b) funneling illusion. (c) saltation.

For example, when two vibration are overlapping in time they can be perceived as a single moving stimuli (Figure 2.2.a). This effect is known as *apparent motion*. Extensive research have been made to understand and control variables implying such illusion. It was shown that the stimuli duration and the time between onsets of subsequent actuations (SOA) can allow us to produce robust apparent tactile motion [9]. A another effect is the *funneling illusion* which generates a midway phantom sensation between two equal stimuli when they are presented simultaneously but separately at adjacent locations on the skin. The location of the funneled sensation can be modified by adjusting intensities of the two stimuli (producing a sensation that moves along the skin between the two actuators is also possible)(Figure 2.2.b) [10–13]. A related illusion is *saltation*, which is similar to the funneling illusion, but instead of modulating the amplitude it modulates the inter-stimulus time interval (Figure 2.2.c) [14].

An other observation when stimulating two areas of the skin is that one stimulus can be masked by an other. For instance, a *masking effect* was observed by Kim et al. [15] when stimulating two fingers with different amplitudes of vibration, the stronger one perceptually masks the other if there is a minimum of 20 dB difference between the two. Adding to this, we can also find a *gating effect* which corresponds to a reduction in the ability to perceive tactile stimuli during movement [16, 17]. Once again, multi-touch interactions is complex and is yet to be fully understood.

In any case, our interaction with a surface, whether it is single-touch or multi-touch, creates normal and tangential forces which amplitudes varies depending on the task to be carried. The idea behind *surface haptics* is to modulate those forces to create a stimulation to the finger. In our case we seek to modulate those forces using

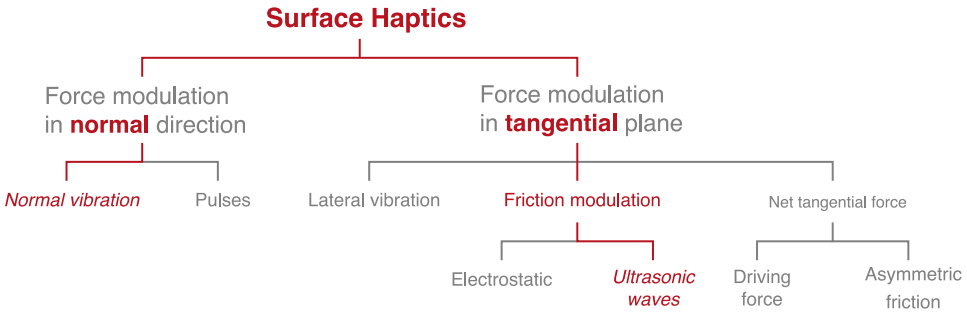

Figure 2.3: Classification of Basdogan et al. [21] of the current technologies for surface haptics displays based on the stimulation direction and method. Methods developed in this thesis are part of the highlighted elements.

vibrations.

2.2. SURFACE HAPTICS TECHNOLOGIES

TAXONOMIES have been proposed by Srinivasan and Basdogan [18], Grant et al. [19], Bluteau [20, chapter 2] and many others to classify haptic technologies. Surface haptics is a special case that focuses primarily on the tactile aspects of haptics. We will follow a recent review by Basdogan et al. [21] to situate our thesis in current researches on surface haptics. As highlighted on Figure 2.3, we will here focus on normal vibration and friction modulation.

2.2.1. NORMAL FORCE MODULATION

Concerning normal vibration, a simple actuator applied to a surface can be enough to modulate normal forces and allow vibrotactile stimulation (which refers to the use of frequency inside the range of tactile perception going from 10 to 1000 Hz [22]). For example by sending vibrations modulated in time, amplitude and frequency, one can simulate clicks and reproduce to a certain extent force-displacement curves associated with real buttons [23, 24]. Vibrotactile stimulation can be noticed with both static and moving fingers.

By multiplying the number of actuators, different methods can be applied to provide striking effects. As we discussed before, the creation of phantom sensations by saltation, funneling or apparent movement can be used to give, from a sensory point of view, spatial tactile feedback. On the other hand, providing “physically” localized stimulation on a touch screen is not trivial.

FREQUENCY/AMPLITUDE OPTIMIZATION SCHEME

By measuring the frequency behavior of a surface subjected to several actuators at a discrete number of points, it is possible to construct a transfer function map (from

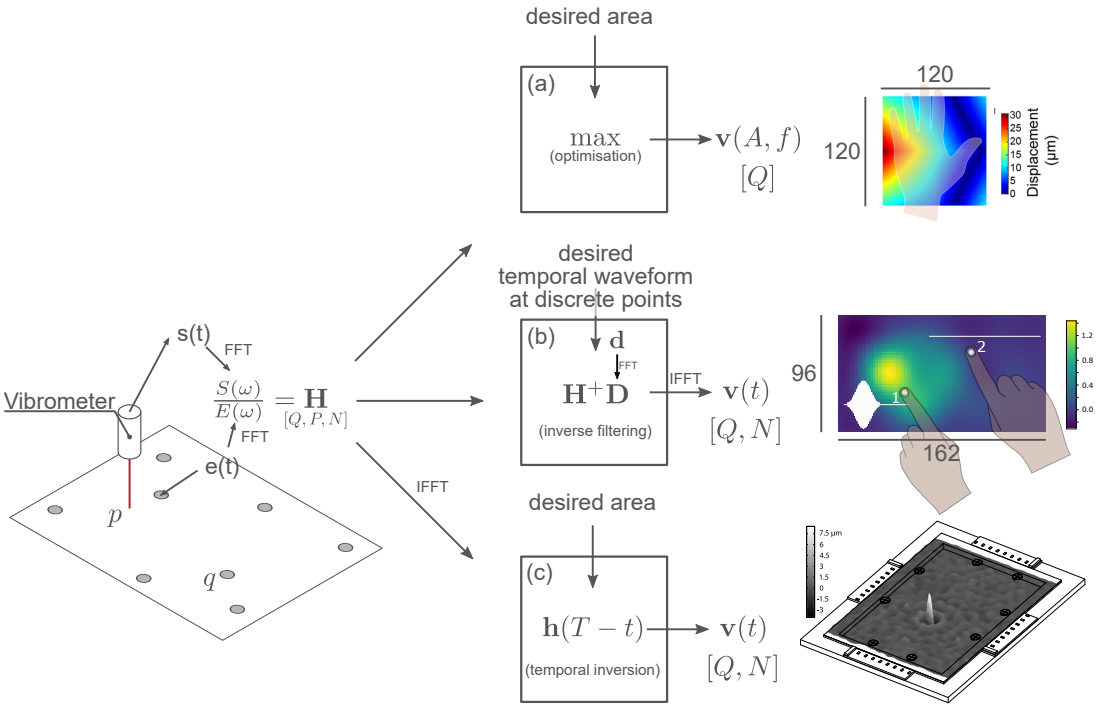

Figure 2.4: Normal force modulation techniques based on a frequency response function matrix. The transfer matrix $\mathbf{H}$ is obtained by the ratio of the Fourier transforms of the measured signals $s(t)$ and sent signals $e(t)$ (of lengths N) by the actuator q at position p. (a) Emgin et al. [25] find the working frequency through $\mathbf{H}$ which maximize the amplitude at the desired position. (b) Pantera and Hudin [26] find the signals $\mathbf{v}(t)$ to be sent to the actuators to obtain the desired stimuli at the desired positions by realizing an inverse Fourier transform of the dot product between the pseudo-inverse of the transfer matrix $\mathbf{H}^+$ with the Fourier transform of desired stimuli signals $\mathbf{D}$. (c) Hudin et al. [27] find the signals $\mathbf{v}(t)$ to be sent to the actuators to obtain focalization at the desired position by reversing the impulsion response $\mathbf{h}(T-t)$ of the plate (obtained by inverse Fourier transform of the transfer matrix).

actuator supply voltage to plate displacement) that can then be used to provide localized haptic feedback. Emgin et al. [25] (Figure 2.4(a)) used this frequency map to identify frequencies which present a maximum amplitude at each measured points. By exciting the surface at the adapted frequency during interaction, a localized haptic effect can be generated at and around the point of interest. They also try to maximize obtained amplitude at the said point while minimizing every other region. This technique uses different frequencies in the tactile sensitivity range (10 to 1000 Hz) to assure localized feedback throughout the screen.

INVERSE FILTERING

Introduced by Hudin and Panëels [28] and developed by Pantera and Hudin [26, 29] the inverse filtering technique (Figure 2.4(b)) uses the frequency map as a matrix and apply an inverse filter method in order to manage a certain number of control points at desired frequencies, amplitudes and phase. While Emgin et al. [25] try to optimize the whole plate displacement and have to use different frequencies to assure localization, Pantera and Hudin [29] technique only assures a number of control points,

typically corresponding to the number of fingers in contact with the surface. The inverse method is particularly interesting as it allow full control at each control points over the amplitude, frequency and phase thus allowing the delivery of rich stimuli. But, it cannot yet provide localized stimuli if the whole hand is resting on the surface as the frequencies in the tactile range implies large wavelengths thus transmitting energy throughout the plate.

Time-reversal wave focusing

The method of time-reversal wave focusing consists in focusing waves in one or more points of space through an array of actuator (Figure 2.4(c)). This technique is widely studied in biomedical engineering and find applications for example in brain therapy [30–32]. Researchers such as Bai and Tsai [33], Wöckel et al. [34][35] and Hudin et al. [27][36, 37] reapplied this technique to focus bending waves in a thin plate by means of actuators placed on its periphery. This method is a two step process as it first requires the recording, through the actuator array of the out-of-plane displacements produced by flexural waves resulting from an impulsive source. Then, those recorded signals corresponding to impulse responses are time-reversed and used as driving voltage for re-emission [27]. Hudin et al. [27] achieved localized displacements reaching 7 μm on a spot diameter of 5.2 mm (smaller than typical finger diameter). Even though the bandwidth used to achieve their impulsive focusing goes from 20 to 70 kHz, a haptic effect can be felt as the focal point produce such a strong acceleration that it eject the finger pulp from the plate [27, 37]. This technique can be extended to several fingers and can possibly (depending on wave scattering) provide localized stimuli in the case of a hand placed entirely on the device.

Modal superimposition

Enferad et al. [38, 39] used modal superimposition to produce an arbitrary vibration field based on control in the modal space. They experimented this method on a beam covered with piezoelectric actuators which displayed encouraging results with the obtainment of a desired velocity field. Authors offered a psychophysical evaluation proving that users could differentiate and localize the stimulation with two fingers on the setup, therefore confirming its possible use in multi-touch applications. Enferad et al. [39] consider that the difficulty of this technique resides in the number of mode required which increases the number of uncertainties and could lead to problems regarding power-consumption and control.

Others

An other promising solution is the creation of vibrations, based on a localized electric field producing an electrostrictive deformation of an relaxor ferroelectric polymer

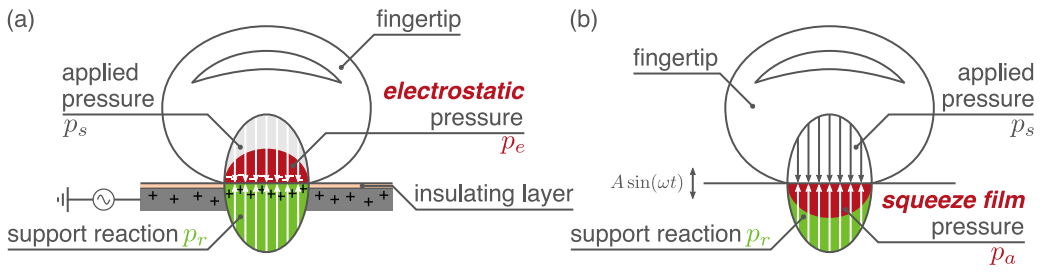

Figure 2.5: Balance of time-averaged pressure during (a) electrostatic charge displacement (b) ultrasonic vibrations. (Inspired from [42])

film, during the application of normal pressure of a finger [40]. We can also cite the work of Papetti et al. [41] which relies on attenuation to provide multi-point localized vibrotactile feedback by using a dense honeycomb-distributed array of piezoelectric actuator discs integrated in a multi-layered structure.

2.2.2. FRICTION MODULATION

Lateral forces can be indirectly produced by modulating the friction between the finger and the surface. To do so, methods using electrostatic forces and ultrasonic waves have been extensively researched.

ELECTROSTATIC FORCES

The effect of electrostatic forces was proved by Mallinckrodt et al. [43]. who perceived different sensation while moving a finger over a metal surface subjected to an alternating voltage and covered with a thin insulating layer. This effect was explained by a displacement of charges due to the formation of a capacitor between the metal surface and the insulating layer (Figure 2.5.a). As a tangential displacement of the finger on the electrode is subject to a resultant force of friction, the relative movement of the finger is necessary for the effect to take place. This force depends: on the normal force applied by the user; on the electrostatic force (depending on the applied voltage, the thickness of the insulator and the area of the finger contact); and on the dynamic friction coefficient. The modulation of the friction then creates perceptible sensations.

In 2010, Bau et al. [44] proposed the first electrostatic touch screen integrated into a visual display. Using a projector installed behind a glass plate, the visual image was projected onto a diffusion plane and tactile stimuli were modulated according to the visual information. They thus allow the user to feel virtual elements through touch. Radivojevic et al. [45] also proposed a display combining a visual display of a mobile device and an electrostatic touch screen. These electrostatic devices require high supply voltages and are sensitive to skin and air humidity. Despite the amount

of research on the subject, the exact mechanism leading to an increase in tangential frictional forces is still not known completely and extensive studies can be found especially regarding the fingerpulp contact area during electro-vibration [46].

ULTRASONIC WAVES

The use of ultrasonic vibrations allows for the creation of ultrasonic lubrication. When a finger slides on a high frequency vibrating plate, a *bouncing motion* of the skin and the existence of a *squeeze film* creates an over-pressure of air that partially supports the normal load and releases some asperities of the skin from contact (Figure 2.5.b) [42]. Those two mechanisms are at play in friction reduction [47, 48].

For the creation of ultrasonic waves, piezoelectric actuators are glued to a surface and powered with a sine signal at a plate resonance above 20 kHz (carrier frequency). Therefore, the entire plate moves and limit the user interaction to one finger. To bypass this limitation, Katumu and Gorlewicz [49] and Ghenna et al. [50, 51], Ghenna [52] superimposed two vibration mode and managed to give different tactile stimuli to two fingers at different position. Also, as resonance are used in order to extract maximum amplitude from the plate, the finger pulp introduces complications during interaction due to its highly non-linear nature which researchers tried to compensate through closed-loop control [53–55].

As lateral forces applied on the finger pulp during tactile exploration of a surface constitute important cues for the identification of asperities, their modulation (with a low-frequency signal inside the vibrotactile sensitivity range) allow the simulation of material properties such as texture [53, 56]. A number of devices (as well as start-ups Figure 2.6) based on this effect have been created. For example, the STIMTAC by Amberg et al. [57] or the T-PaD by Winfield et al. [58] which led later to the "PaD series" with the ShiverPaD [59] (adding lateral low-frequency vibrations), the ActivePaD [60] (using an impedance controlled planar mechanism), the LateralPaD [61] (adding lateral high-frequency vibrations).

It is important to specify that ultrasonic lubrication can only exist for a moving finger and that detection of friction-modulated textures is limited by vibrotactile sensitivity [62] (10 to 1000 Hz [22]). Also, the amplitude needed to provide a haptic feedback is potentially depending on the carrier frequency. Giraud et al. [63] showed by comparing a 66 kHz and 225 kHz carrier frequency that the latter needed 10 times less amplitude than the former to produce the same perceived sensation.

Moreover, some recent studies showed that across a broad frequency range, gratings induced by normal displacement of a touch surface and those induced by lateral force modulation are perceived as being equivalent in intensity when the magnitude of velocity at the fingertip matches [64]. Grigorii et al. [64] argue that there is a lot of

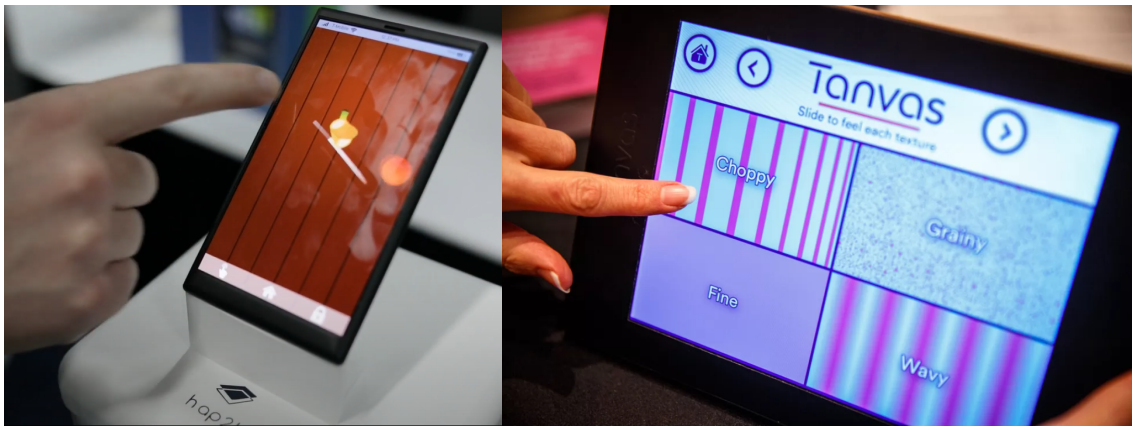

Figure 2.6: Left: Startup Hap2U using modal-based friction modulation to provide in-game haptic feedback on a smartphone-like demonstrator. Right: Startup Tanvas using electrostatic-based friction modulation to simulate texture to a user's finger (Josh Miller/CNET).

similarity between the two actuation types (normal and lateral) and that they tend to improve with increasing frequency. They explain their results by referring to perception being a blend of direction-sensitive kinesthetic sensing and tactile sensing at the lower frequencies which transition to primarily spatially and direction-insensitive tactile sensing at the higher frequencies. They thus stress the need for both type of actuation (normal and lateral forces modulation) to provide enhanced haptic interfaces.

There are also techniques that differ from control approaches. One can mention Hudin [65] who used an interference phenomenon to create a localized friction modulation in the area covered by a piezoelectric actuator (Chapter 5 furthers this technique). More recently, Daunizeau et al. [66] used periodical resonant structures known as phononic crystals as boundaries to create a meta-materials with two distinct region with a waveguide form (of size 32×140 mm^2). Their structure created a frequency band-gap at a desired frequency leading to the localization of ultrasonic standing waves in the excited waveguide region.

2.3. THESIS'S POSITION IN THE STATE OF THE ART

As observed in last section, there are a lot of techniques to provide haptic feedback depending on the desired application requirements. Few of them allowed for the localization of stimuli by mainly relying on learning phases (of the plate frequency behavior) and/or wave propagation (control approach).

The work described in this thesis takes the opposite direction and propose three methods of wave localization through geometrical means. With those techniques each transducer of a dense matrix of actuators modulates the forces through vibra-

tions over a limited area of a continuous surface.

Chapter 3 and chapter 4 introduce techniques relying on the propagation medium geometry to localize vibrotactile stimuli (10 to 1000 Hz). While chapter 5 harnesses an interference phenomenon resulting from the geometry of piezoelectric actuators to create a localized ultrasonic lubrication effect.

NOMENCLATURE

ABBREVIATIONS

Abbreviation	Definition
ERM	Eccentric Rotating Mass
EPs	Exploration Procedures
FRF	Frequency Response Function
FFT	Fast Fourier Transform
DFT	Discrete Fourier Transform
HCI	Human-Computer Interaction
IF	Inverse Filtering
iFFT	Inverse Fast Fourier Transform
LRA	Linear Resonant Actuator
SOA	Stimulus Onset Asynchrony
UIX	User Interaction and Experience

SYMBOLS

Symbol	Definition	Unit
A	Amplitude	V or μm
f	Frequency	Hz
N	Number of samples	~
Q	Number of actuators	~
P	Number of measured positions	~
q	Actuator index	~
p	Position index	~
t	Time	s
$e(t)$	Signal sent for acquisition	V
$E(\omega)$	Fourier transform of $e(t)$	V
$s(t)$	Signal measured	m
$S(\omega)$	Fourier transform of $s(t)$	m
$\mathbf{d}$	Desired signals matrix in time space	m
$\mathbf{D}$	Fourier Transform of $\mathbf{d}$	m
$\mathbf{H}$	Transfer matrix	m/V
$\mathbf{H}^+$	Pseudo-Inverse of the transfer matrix	m/V
$\mathbf{h}(T-t)$	Temporally inverted impulsion response	m/V
$\mathbf{v}(t)$	Signals to be sent to actuators	V

References

[1] Special Issue on Surface Haptics. *IEEE Transactions on Haptics*, 13(3):448–449, July 2020. ISSN 2329-4051. doi: 10.1109/TOH.2020.3013079. Conference Name: IEEE Transactions on Haptics.

[2] Susan J Lederman and Roberta L Klatzky. Hand movements: A window into haptic object recognition. *Cognitive Psychology*, 19(3):342–368, July 1987. ISSN 0010-0285. doi: 10.1016/0010-0285(87)90008-9. URL https://www.sciencedirect.com/science/article/pii/0010028587900089.

[3] Roberta L. Klatzky and Susan J. Lederman. Touch. In *Handbook of psychology: Experimental psychology, Vol. 4, 2nd ed*, pages 152–178. John Wiley & Sons, Inc., Hoboken, NJ, US, 2013. ISBN 978-0-470-64993-0 978-1-118-28515-2 978-1-118-28194-9 978-1-118-28377-6.

[4] Blake Hannaford and Allison M. Okamura. Haptics. In Bruno Siciliano and Oussama Khatib, editors, *Springer Handbook of Robotics*, pages 719–739. Springer, Berlin, Heidelberg, 2008. ISBN 978-3-540-30301-5. doi: 10.1007/978-3-540-30301-5_31. URL https://doi.org/10.1007/978-3-540-30301-5_31.

[5] K. E. Overvliet, J. B. J. Smeets, and E. Brenner. Haptic search with finger movements: using more fingers does not necessarily reduce search times. *Experimental Brain Research*, 182(3):427–434, September 2007. ISSN 1432-1106. doi: 10.1007/s00221-007-0998-9. URL https://doi.org/10.1007/s00221-007-0998-9.

[6] Alejandro Catala, Miguel Oliver, Jose Pascual Molina, and Pascual Gonzalez. Involving multiple fingers in exploring a haptic surface: an evaluation study. *The Visual Computer*, 32(6):921–932, June 2016. ISSN 1432-2315. doi: 10.1007/s00371-016-1250-z. URL https://doi.org/10.1007/s00371-016-1250-z.

[7] Valerie S Morash, Allison E Connell Pensky, and Joshua A Miele. Effects of Using Multiple Hands and Fingers on Haptic Performance. *Perception*, 42(7):759–777, July 2013. ISSN 0301-0066. doi: 10.1068/p7443. URL https://doi.org/10.1068/p7443.

[8] Anna Metzger, Matteo Toscani, Matteo Valsecchi, and Knut Drewing. Dynamics of exploration in haptic search*. In *2019 IEEE World Haptics Conference (WHC)*, pages 277–282, July 2019. doi: 10.1109/WHC.2019.8816174.

[9] Carl E. Sherrick and Ronald Rogers. Apparent haptic movement. *Perception & Psychophysics*, 1(6):175–180, June 1966. ISSN 0031-5117, 1532-5962. doi: 10.3758/BF03215780. URL http://link.springer.com/10.3758/BF03215780.

[10] G. v. Békésy. Funneling in the Nervous System and its Role in Loudness and Sensation Intensity on the Skin. *The Journal of the Acoustical Society of America*, 30(5):399–412, May 1958. ISSN 0001-4966. doi: 10.1121/1.1909626. URL https://asa.scitation.org/doi/10.1121/1.1909626. Publisher: Acoustical Society of America.

[11] David S. Alles. Information Transmission by Phantom Sensations. *IEEE Transactions on Man-Machine Systems*, 11(1):85–91, March 1970. ISSN 2168-2860. doi: 10.1109/TMMS.1970.299967. Conference Name: IEEE Transactions on Man-Machine Systems.

[12] Jaedong Lee, Sangyong Lee, and Gerard J. Kim. Funneling and Saltation Effects for Tactile Interaction with "Detached" Out of the Body Virtual Objects. In Paula Kotzé, Gary Marsden, Gitte Lindgaard, Janet Wesson, and Marco Winckler, editors, *Human-Computer Interaction –INTERACT 2013*, Lecture Notes in Computer Science, pages 104–121, Berlin, Heidelberg, 2013. Springer. ISBN 978-3-642-40483-2. doi: 10.1007/978-3-642-40483-2_8.

[13] Payal Patel, Rahul Kumar Ray, and Muniyandi Manivannan. Power Law Based "Out of Body" Tactile Funneling for Mobile Haptics. *IEEE Transactions on Haptics*, 12(3):307–318, July 2019. ISSN 2329-4051. doi: 10.1109/TOH.2019.2933822. Conference Name: IEEE Transactions on Haptics.

[14] F. A. Geldard and C. E. Sherrick. The Cutaneous "Rabbit": A Perceptual Illusion. *Science*, 178(4057):178–179, October 1972. ISSN 0036-8075, 1095-9203. doi: 10.1126/science.178.4057.178. URL https://www.sciencemag.org/lookup/doi/10.1126/science.178.4057.178.

[15] Jin Ryong Kim, Xiaowei Dai, Xiang Cao, Carl Picciotto, Desney Tan, and Hong Z. Tan. A Masking Study of Key-Click Feedback Signals on a Virtual Keyboard. In Poika Isokoski and Jukka Springare, editors, *Haptics: Perception, Devices, Mobility, and Communication*, Lecture Notes in Computer Science, pages 247–257. Springer Berlin Heidelberg, 2012. ISBN 978-3-642-31401-8.

[16] D. N. RUSHTON, J. C. ROGHWELL, and M. D. CRAGGS. Gating of Somatosensory Evoked Potentials during Different Kinds of Movements in Man. *Brain*, 104 (3):465–491, September 1981. ISSN 0006-8950. doi: 10.1093/brain/104.3.465. URL https://doi.org/10.1093/brain/104.3.465.

[17] C. E. Chapman, M. C. Bushnell, D. Miron, G. H. Duncan, and J. P. Lund. Sensory perception during movement in man. *Experimental Brain Research*, 68(3):516–524, November 1987. ISSN 1432-1106. doi: 10.1007/BF00249795. URL https://doi.org/10.1007/BF00249795.

[18] Mandayam A. Srinivasan and Cagatay Basdogan. Haptics in virtual environments: Taxonomy, research status, and challenges. *Computers & Graphics*, 21(4):393–404, July 1997. ISSN 0097-8493. doi: 10.1016/S0097-8493(97)00030-7. URL http://www.sciencedirect.com/science/article/pii/S0097849397000307.

[19] Danny Grant, Oliver R. Astley, Vincent Hayward, Manuel Cruz-Hernandez, and Gabriel Robles-De-La-Torre. Haptic interfaces and devices. *Sensor Review*, 24(1):16–29, March 2004. ISSN 0260-2288. doi: 10.1108/02602280410515770. URL https://www.emeraldinsight.com/doi/full/10.1108/02602280410515770.

[20] Jérémy Bluteau. Evaluation des effets de l'ajout d'interfaces haptiques sur le suivi manuel de trajectoires. June 2010. URL https://tel.archives-ouvertes.fr/tel-00524533.

[21] Cagatay Basdogan, Frederic Giraud, Vincent Levesque, and Seungmoon Choi. A Review of Surface Haptics: Enabling Tactile Effects on Touch Surfaces. *IEEE Transactions on Haptics*, pages 1–1, 2020. ISSN 2329-4051. doi: 10.1109/TOH.2020.2990712.

[22] Ronald T. Verrillo. Psychophysics of vibrotactile stimulation. *The Journal of the Acoustical Society of America*, 77(1):225–232, January 1985. ISSN 0001-4966. doi: 10.1121/1.392263. URL https://asa.scitation.org/doi/abs/10.1121/1.392263.

[23] Sunjun Kim and Geehyuk Lee. Haptic Feedback Design for a Virtual Button Along Force-displacement Curves. In *Proceedings of the 26th Annual ACM Symposium on User Interface Software and Technology*, UIST '13, pages 91–96, New York, NY, USA, 2013. ACM. ISBN 978-1-4503-2268-3. doi: 10.1145/2501988.2502041. URL http://doi.acm.org/10.1145/2501988.2502041.

[24] Seokhee Jeon, Hongchae Lee, Jiyoung Jung, and Jin Ryong Kim. User-Adaptive Key Click Vibration on Virtual Keyboard. *Mobile Information Systems*, 2018: e6126140, October 2018. ISSN 1574-017X. doi: 10.1155/2018/6126140. URL https://www.hindawi.com/journals/misy/2018/6126140/. Publisher: Hindawi.

[25] Senem Ezgi Emgin, Amirreza Aghakhani, T. Metin Sezgin, and Cagatay Basdogan. HapTable: An Interactive Tabletop Providing Online Haptic Feedback for Touch Gestures. *IEEE Transactions on Visualization and Computer Graphics*, 25(9):2749–2762, September 2019. ISSN 1941-0506. doi: 10.1109/TVCG.2018.2855154. Conference Name: IEEE Transactions on Visualization and Computer Graphics.

[26] Lucie Pantera and Charles Hudin. Multitouch Vibrotactile Feedback on a Tactile Screen by the Inverse Filter Technique: Vibration Amplitude and Spatial Resolution. *IEEE Transactions on Haptics*, pages 1–1, 2020. ISSN 2329-4051. doi: 10.1109/TOH.2020.2981307.

[27] C. Hudin, J. Lozada, and V. Hayward. Localized Tactile Feedback on a Transparent Surface through Time-Reversal Wave Focusing. *IEEE Transactions on Haptics*, 8(2):188–198, April 2015. ISSN 1939-1412. doi: 10.1109/TOH.2015.2411267.

[28] Charles Hudin and Sabrina Panëels. Localisation of Vibrotactile Stimuli with Spatio-Temporal Inverse Filtering. In Domenico Prattichizzo, Hiroyuki Shinoda, Hong Z. Tan, Emanuele Ruffaldi, and Antonio Frisoli, editors, *Haptics: Science, Technology, and Applications*, Lecture Notes in Computer Science, pages 338–350. Springer International Publishing, 2018. ISBN 978-3-319-93399-3.

[29] L. Pantera and C. Hudin. Sparse Actuator Array Combined with Inverse Filter for Multitouch Vibrotactile Stimulation. In *2019 IEEE World Haptics Conference (WHC)*, pages 19–24, July 2019. doi: 10.1109/WHC.2019.8816107.

[30] Mathias Fink, Gabriel Montaldo, and Mickael Tanter. Time-Reversal Acoustics in Biomedical Engineering. *Annual Review of Biomedical Engineering*, 5(1):465–497, August 2003. ISSN 1523-9829, 1545-4274. doi: 10.1146/annurev.bioeng.5.040202.121630. URL http://www.annualreviews.org/doi/10.1146/annurev.bioeng.5.040202.121630.

[31] Mathias Fink and Claire Prada. Acoustic time-reversal mirrors. *Inverse Problems*, 17(1):R1–R38, January 2001. ISSN 0266-5611. doi: 10.1088/0266-5611/17/1/201. URL https://doi.org/10.1088/0266-5611/17/1/201. Publisher: IOP Publishing.

[32] Alexander Sutin and Hady Salloum. Prospective medical applications of Nonlinear Time Reversal Acoustics. page 020003, Santa Fe, New Mexico, USA, 2018. doi: 10.1121/2.0000920. URL http://asa.scitation.org/doi/abs/10.1121/2.0000920.

[33] Mingsian R. Bai and Yao Kun Tsai. Impact localization combined with haptic feedback for touch panel applications based on the time-reversal approach. *The Journal of the Acoustical Society of America*, 129(3):1297–1305, March 2011. ISSN 0001-4966. doi: 10.1121/1.3533725. URL https://asa.scitation.org/doi/10.1121/1.3533725.

[34] S. Wöckel, U. Steinmann, and H. Arndt. Modelling of time reversal for localized tactile feedback on displays. *Procedia Engineering*, 120:302–305, January 2015. ISSN 1877-7058. doi: 10.1016/j.proeng.2015.08.621. URL https://www.sciencedirect.com/science/article/pii/S1877705815022845.

[35] S. Wöckel, U. Steinmann, and H. Arndt. Haptics by time reversal of elastic waves. In *2016 IEEE International Ultrasonics Symposium (IUS)*, pages 1–3, September 2016. doi: 10.1109/ULTSYM.2016.7728754. ISSN: 1948-5727.

[36] Charles Hudin, José Lozada, Michael Wiertlewski, and Vincent Hayward. Tradeoffs in the Application of Time-Reversed Acoustics to Tactile Stimulation. In Poika Isokoski and Jukka Springare, editors, *Haptics: Perception, Devices, Mobility, and Communication*, Lecture Notes in Computer Science, pages 218–226, Berlin, Heidelberg, 2012. Springer. ISBN 978-3-642-31401-8. doi: 10.1007/978-3-642-31401-8_20.

[37] Charles Hudin, Jose Lozada, and Vincent Hayward. Localized tactile stimulation by time-reversal of flexural waves: Case study with a thin sheet of glass. In *2013 World Haptics Conference (WHC)*, pages 67–72, April 2013. doi: 10.1109/WHC.2013.6548386.

[38] Ehsan Enferad, Christophe Giraud-Audine, Frédéric Giraud, Michel Amberg, and Betty Lemaire-Semail. Differentiated haptic stimulation by modal synthe-

sis of vibration field. In *2018 IEEE Haptics Symposium (HAPTICS)*, pages 216–221, March 2018. doi: 10.1109/HAPTICS.2018.8357179. ISSN: 2324-7355.

[39] Ehsan Enferad, Christophe Giraud-Audine, Frédéric Giraud, Michel Amberg, and Betty Lemaire Semail. Generating controlled localized stimulations on haptic displays by modal superimposition. *Journal of Sound and Vibration*, 449: 196–213, June 2019. ISSN 0022-460X. doi: 10.1016/j.jsv.2019.02.039. URL http://www.sciencedirect.com/science/article/pii/S0022460X19301476.

[40] Quang Van Duong, Vinh Phu Nguyen, Fabrice Domingues Dos Santos, and Seung Tae Choi. Localized Fretting-Vibrotactile Sensations for Large-Area Displays. *ACS Applied Materials & Interfaces*, 11(36):33292–33301, September 2019. ISSN 1944-8244. doi: 10.1021/acsami.9b09691. URL https://doi.org/10.1021/acsami.9b09691. Publisher: American Chemical Society.

[41] Stefano Papetti, Sébastien Schiesser, and Martin Fröhlich. Multi-Point Vibrotactile Feedback for an Expressive Musical Interface. In *Proceedings of the International Conference on New Interfaces for Musical Expression*, NIME 2015, pages 235–240, Baton Rouge, Louisiana, USA, 2015. The School of Music and the Center for Computation and Technology (CCT), Louisiana State University. ISBN 978-0-692-49547-6. URL http://dl.acm.org/citation.cfm?id=2993778.2993839. event-place: Baton Rouge, Louisiana, USA.

[42] Michaël Wiertlewski, Rebecca Fenton Friesen, and J. Edward Colgate. Partial squeeze film levitation modulates fingertip friction. *Proceedings of the National Academy of Sciences*, 113(33):9210–9215, August 2016. ISSN 0027-8424, 1091-6490. doi: 10.1073/pnas.1603908113. URL https://www.pnas.org/content/113/33/9210. Publisher: National Academy of Sciences Section: Physical Sciences.

[43] Edward Mallinckrodt, A. L. Hughes, and William Sleator. Perception by the Skin of Electrically Induced Vibrations. *Science*, 118(3062):277–278, September 1953. doi: 10.1126/science.118.3062.277. URL https://www.science.org/doi/10.1126/science.118.3062.277. Publisher: American Association for the Advancement of Science.

[44] Olivier Bau, Ivan Poupyrev, Ali Israr, and Chris Harrison. TeslaTouch: electrovibration for touch surfaces. In *Proceedings of the 23nd annual ACM symposium on User interface software and technology*, UIST '10, pages 283–292, New York, NY, USA, October 2010. Association for Computing Machinery. ISBN 978-1-4503-0271-5. doi: 10.1145/1866029.1866074. URL https://doi.org/10.1145/1866029.1866074.

[45] Z. Radivojevic, P. Beecher, C. Bower, S. Haque, P. Andrew, T. Hasan, F. Bonaccorso, A. C. Ferrari, and B. Henson. Electrotactile touch surface by using transparent graphene. In *Proceedings of the 2012 Virtual Reality International Conference*, VRIC '12, pages 1–3, New York, NY, USA, March 2012. Association for Computing Machinery. ISBN 978-1-4503-1243-1. doi: 10.1145/2331714.2331733. URL https://doi.org/10.1145/2331714.2331733.

[46] Omer Sirin, Allan Barrea, Philippe Lefèvre, Jean-Louis Thonnard, and Cagatay Basdogan. Fingerpad contact evolution under electrovibration. *Journal of The Royal Society Interface*, 16(156):20190166, July 2019. doi: 10.1098/rsif.2019.0166. URL https://royalsocietypublishing.org/doi/10.1098/rsif.2019.0166. Publisher: Royal Society.

[47] T. Watanabe and S. Fukui. A method for controlling tactile sensation of surface roughness using ultrasonic vibration. In *Proceedings of 1995 IEEE International Conference on Robotics and Automation*, volume 1, pages 1134–1139 vol.1, May 1995. doi: 10.1109/ROBOT.1995.525433. ISSN: 1050-4729.

[48] Mélisande Biet, Frédéric Giraud, and Betty Lemaire-Semail. Squeeze film effect for the design of an ultrasonic tactile plate. *IEEE Transactions on Ultrasonics, Ferroelectrics, and Frequency Control*, 54(12):2678–2688, December 2007. ISSN 1525-8955. doi: 10.1109/TUFFC.2007.596. Conference Name: IEEE Transactions on Ultrasonics, Ferroelectrics, and Frequency Control.

[49] Karl Katumu and Jenna L. Gorlewicz. Using modal superposition for generating localized tactile effects on variable friction touchscreens. In *2016 IEEE Haptics Symposium (HAPTICS)*, pages 211–216, April 2016. doi: 10.1109/HAPTICS.2016.7463179. ISSN: 2324-7355.

[50] Sofiane Ghenna, Frederic Giraud, Christophe Giraud-Audine, Michel Amberg, and Betty Lemaire-Semail. Preliminary design of a multi-touch ultrasonic tactile stimulator. In *2015 IEEE World Haptics Conference (WHC)*, pages 31–36, June 2015. doi: 10.1109/WHC.2015.7177687.

[51] Sofiane Ghenna, Christophe Giraud-Audine, Frederic Giraud, Michel Amberg, and Betty Lemaire-Semail. Modal Superimposition for Multi-fingers Variable Friction Tactile Device. In Fernando Bello, Hiroyuki Kajimoto, and Yon Visell, editors, *Haptics: Perception, Devices, Control, and Applications*, Lecture Notes in Computer Science, pages 521–530, Cham, 2016. Springer International Publishing. ISBN 978-3-319-42321-0. doi: 10.1007/978-3-319-42321-0_49.

[52] Sofiane Ghenna. *Approche multimodale pour la conception d'interfaces à retour tactile à plusieurs doigts*. phdthesis, Université Lille 1 - Sciences et Technologies, November 2016. URL https://hal.inria.fr/tel-01526451.

[53] Eric Vezzoli, Thomas Sednaoui, Michel Amberg, Frédéric Giraud, and Betty Lemaire-Semail. Texture Rendering Strategies with a High Fidelity - Capacitive Visual-Haptic Friction Control Device. In Fernando Bello, Hiroyuki Kajimoto, and Yon Visell, editors, *Haptics: Perception, Devices, Control, and Applications*, Lecture Notes in Computer Science, pages 251–260. Springer International Publishing, 2016. ISBN 978-3-319-42321-0.

[54] Wael Ben Messaoud, Frédéric Giraud, Betty Lemaire-Semail, Michel Amberg, and Marie-Ange Bueno. Amplitude Control of an Ultrasonic Vibration for a Tactile Stimulator. *IEEE/ASME Transactions on Mechatronics*, 21(3):1692–1701, June 2016. ISSN 1941-014X. doi: 10.1109/TMECH.2016.2535300. Conference Name: IEEE/ASME Transactions on Mechatronics.

[55] Anis Kaci, Angelica Torres, Frederic Giraud, Christophe Giraud-Audine, Michel Amberg, and Betty Lemaire-Semail. Fundamental Acoustical Finger Force Calculation for Out-of-Plane Ultrasonic Vibration and its Correlation with Friction Reduction. In *2019 IEEE World Haptics Conference (WHC)*, pages 413–418, July 2019. doi: 10.1109/WHC.2019.8816168.

[56] Michaël Wiertlewski, Daniele Leonardis, David J. Meyer, Michael A. Peshkin, and J. Edward Colgate. A High-Fidelity Surface-Haptic Device for Texture Rendering on Bare Finger. In Malika Auvray and Christian Duriez, editors, *Haptics: Neuroscience, Devices, Modeling, and Applications*, Lecture Notes in Computer Science, pages 241–248, Berlin, Heidelberg, 2014. Springer. ISBN 978-3-662-44196-1. doi: 10.1007/978-3-662-44196-1_30.

[57] Michel Amberg, Frédéric Giraud, Betty Semail, Paolo Olivo, Géry Casiez, and Nicolas Roussel. STIMTAC: a tactile input device with programmable friction. In *Proceedings of the 24th annual ACM symposium adjunct on User interface software and technology*, UIST '11 Adjunct, pages 7–8, New York, NY, USA, October 2011. Association for Computing Machinery. ISBN 978-1-4503-1014-7. doi: 10.1145/2046396.2046401. URL https://doi.org/10.1145/2046396.2046401.

[58] Laura Winfield, John Glassmire, J. Edward Colgate, and Michael Peshkin. T-PaD: Tactile Pattern Display through Variable Friction Reduction. In *Second Joint EuroHaptics Conference and Symposium on Haptic Interfaces for Virtual Environment and Teleoperator Systems (WHC'07)*, pages 421–426, March 2007. doi: 10.1109/WHC.2007.105.

[59] Erik C. Chubb, J. Edward Colgate, and Michael A. Peshkin. ShiverPaD: A Glass Haptic Surface That Produces Shear Force on a Bare Finger. *IEEE Transactions on Haptics*, 3(3):189–198, July 2010. ISSN 2329-4051. doi: 10.1109/TOH.2010.7. Conference Name: IEEE Transactions on Haptics.

[60] Joe Mullenbach, Dan Johnson, J. Edward Colgate, and Michael A. Peshkin. ActivePaD surface haptic device. In *2012 IEEE Haptics Symposium (HAPTICS)*, pages 407–414, March 2012. doi: 10.1109/HAPTIC.2012.6183823. ISSN: 2324-7355.

[61] Xiaowei Dai, J. Edward Colgate, and Michael A. Peshkin. LateralPaD: A surface-haptic device that produces lateral forces on a bare finger. In *2012 IEEE Haptics Symposium (HAPTICS)*, pages 7–14, March 2012. doi: 10.1109/HAPTIC.2012.6183753. ISSN: 2324-7355.

[62] Corentin Bernard, Sølvi Ystad, Jocelyn Monnoyer, and Michaël Wiertlewski. Detection of Friction-Modulated Textures is Limited by Vibrotactile Sensitivity. *IEEE Transactions on Haptics*, 13(3):542–551, July 2020. ISSN 2329-4051. doi: 10.1109/TOH.2020.2985364. Conference Name: IEEE Transactions on Haptics.

[63] F. Giraud, T. Hara, C. Giraud-Audine, M. Amberg, B. Lemaire-Semail, and M. Takasaki. Evaluation of a friction reduction based haptic surface at high frequency. In *2018 IEEE Haptics Symposium (HAPTICS)*, pages 210–215, March 2018. doi: 10.1109/HAPTICS.2018.8357178.

[64] Roman V Grigorii, Evan Li, Michael A. Peshkin, and Edward Colgate. Comparison of wide-band vibrotactile and friction modulation surface gratings. *IEEE Transactions on Haptics*, pages 1–1, 2021. ISSN 2329-4051. doi: 10.1109/TOH.2021.3075905. Conference Name: IEEE Transactions on Haptics.

[65] C. Hudin. Local friction modulation using non-radiating ultrasonic vibrations. In *2017 IEEE World Haptics Conference (WHC)*, pages 19–24, June 2017. doi: 10.1109/WHC.2017.7989850.

[66] Thomas Daunizeau, David Gueorguiev, Sinan Haliyo, and Vincent Hayward. Phononic Crystals Applied to Localised Surface Haptics. *IEEE Transactions on Haptics*, 14(3):668–674, July 2021. ISSN 2329-4051. doi: 10.1109/TOH.2021.3072566. Conference Name: IEEE Transactions on Haptics.

3

Vibrotactile Stimulation Confinement in Waveguides

On a touch surface, providing a local vibrotactile feedback enables multi-user and multi-touch interactions. While the vibration propagation usually impedes this localization, we show in this chapter that narrow strip-shaped plates constitute waveguides in which bending waves below a cut-off frequency do not propagate. We provide a theoretical explanation of the phenomenon and experimental validations. We thus show that vibrations up to a few kilohertz are well confined on top of the actuated area with vibration amplitude over one micrometer. The principle was validated with piezoelectric actuators of various shapes, a linear resonant actuator (LRA) and an eccentric rotating mass vibration motor (ERM). Investigation of the effect of a fingertip load on the system through theory and experimentation was conducted and revealed that almost no attenuation was brought by the fingertip when using low frequency evanescent waves. Finally, a perceptual validation was conducted and showed dynamic stimuli with a large frequency spectrum could be felt and distinguished.

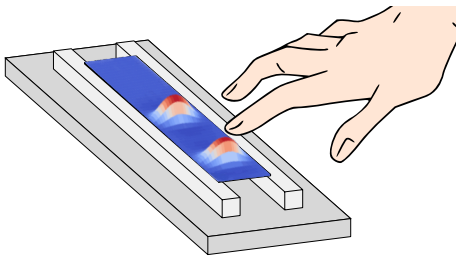

Parts of this chapter have been published in A. B. Dhiab et C. Hudin, « Confinement of Vibrotactile Stimuli in Narrow Plates: Principle and Effect of Finger Loading », IEEE Transactions on Haptics, vol. 13, n° 3, p. 471-482, juill. 2020, doi: 10.1109/TOH.2020.2986727.

3

Outline

3.1. INTRODUCTION

VIBRATIONS within the tactile sensitivity range of frequency (10 to 1000 Hz [1]) are used to convey information, but also, when correlated with finger motion and force, to simulate clicks [2, 3], bumps, texture [4, 5] or compliance [6, 7]. Wave propagation and reverberation effects usually lead to a uniform distribution of vibration energy across the surface. Actuators, acting as local sources of vibration, produce a global and uniform stimulation. Providing different feedback at different positions is then only achievable for single finger exploration through a temporal variation correlated to the finger position [8]. This approach however raises two issues. Firstly, the whole contact area experiences the same vibration thus making it impossible to display, for a static finger, variations at a scale smaller than finger size. Secondly, is the impossibility to provide distinct feedback to multiple fingers. The vibrotactile feedback provided on standard interactive surfaces is therefore irrelevant for multi-touch or multi-user interactions. Those two issues can be solved by localizing the vibration, that is by ensuring that vibration produced at a chosen position cannot be felt at another. The aim of the presented work is to introduce a method for localizing those vibrations on a thin narrow plate.

Existing approaches for localized haptics can be sorted into two types: on one hand, wavefield shaping approaches like Time Reversal [9–11], Inverse Filter [12–14], Modal Superimposition [15, 16] or Airborn Ultrasound [17] use signal processing and control strategies to create high amplitude vibrations at specific positions while maintaining low level vibration at others. On the other hand, confinement approaches like non-radiating frequencies [18], patterned or damped surfaces [19, 20] and tapered membranes [21] prevent, to some extent, vibrations from propagating. The work presented here is of the second type as it relies on the geometry of the propagation surface to confine vibrations within the actuated area, and does not involve any specific signal processing. This approach, however, differs from the non-radiating approach in three ways. First, it allows for the localization of low frequencies (below a few kilohertz) while non-radiating frequencies are ultrasonic frequencies well-suited for friction modulation only [22]. Second, the non-propagating behavior is observed over the whole bandwidth from DC to the cut-off frequency and not at specific discrete frequencies. Finally, the vibration confinement results from the surface geometry and boundary conditions and not from the actuator geometry. As a consequence, the method presented in this chapter works for piezoelectric actuators of different shapes and also for electromagnetic vibration motors, as it will be shown in the experimental validation. This method is however limited to narrow plates. It is therefore not well-suited for screens but is very effective for 1D tactile

interfaces like slidebars or single row keyboards.

In this chapter, we first derive a mathematical model explaining how localization can be obtained. Then, we prove experimentally that vibrotactile stimuli can be confined above actuated areas. As the purpose of this system is to deliver multi-touch haptic feedbacks, we studied the effect of the finger on stimuli amplitudes and conducted a short perceptual validation on a group of 5 people to confirm that stimuli could be felt and distinguished.

3.2. PRINCIPLE

In this section, we explain how non-propagative vibrations can be obtained at low frequencies using the geometric properties of a waveguide. A waveguide is a medium where the wave propagation is bounded in two directions of space and free in the third [23, Chapter 24]. They find applications in different fields of wave physics [24]. Electromagnetic waveguides are used as filters in radiocommunication. Single and multimode fiber optics rely on propagation modes to convey information [25]. Acoustic waveguides are used to design horns and high frequency electronic filters [26]. In our case the propagation medium is a thin narrow plate with finite thickness and width but with an arbitrary length. The propagation of waves in a waveguide can be described in terms of propagation modes. Each of these modes is defined by its cross section profile, wave velocity and cut-off frequency [27, p. 201]. While in most waveguides the zero order propagation mode with a cut-off frequency equal to 0 Hz exist, we show that in the case of a narrow plate simply supported or clamped on its longer sides that the zero order mode has a null amplitude and therefore does not contribute to the propagation. As a result, bending waves cannot propagate in such guide below the cut-off frequency of the first propagation mode. We derive the expression of this frequency and show that in practical cases it can be greater than the frequency bandwidth of tactile stimuli.

3.2.1. THEORY

HOMOGENEOUS SOLUTION

The equation governing the transverse motion u of an isotropic homogeneous plate of constant thickness h is given as [28, p. 233]:

$$\rho h \frac{\partial^2 u}{\partial t^2} + D\nabla^4 u = 0 \tag{3.1}$$

with rho the mass density, D the bending stiffness and ∇^4 the biharmonic operator. Under Kirchhoff thin plate assumptions, D can be expressed as [28, p. 233]:

$$D = \frac{Eh^3}{12(1-\nu^2)} \tag{3.2}$$

where E and ν are the Young's modulus and Poisson's ratio. Since we are considering an homogeneous system, with constant mechanical and dimensional properties and constant boundary conditions, the solutions of (3.1) are invariant with respect to space and time translation. As a consequence we can separate variables and write:

$$u(x,y,t) = \Psi(x)\Phi(y)\Theta(t) \tag{3.3}$$

For harmonic behavior, the response can be written in exponential terms with :

$$\left.\begin{aligned} \Psi(x) &= \mathrm{e}^{px} \\ \Phi(y) &= \mathrm{e}^{qy} \\ \Theta(t) &= \mathrm{e}^{rt} \end{aligned}\right\} \tag{3.4}$$

where p, q and r are quantities we search to define. Putting expressions from (3.4) in (3.1) yields to the following dispersion relation:

$$r^2 + \frac{D}{\rho h}\left(p^2+q^2\right)^2 = 0 \tag{3.5}$$

which leads to:

$$r = \pm \mathrm{j}\sqrt{\frac{D}{\rho h}}\left(p^2+q^2\right) = \pm \mathrm{j}\sqrt{\frac{D}{\rho h}}k^2 = \pm \mathrm{j}\omega$$

with $\omega = 2\pi f$ the circular frequency.
To find $\Phi(y)$, we use the differential equation obtained by injecting (3.3) in (3.1):

$$\Phi^{(4)} + 2\frac{\Phi^{(2)}}{\Phi}\Phi^{(2)} + \left[\frac{\rho h}{D}\frac{\Theta^{(2)}}{\Theta} + \frac{\Psi^{(4)}}{\Psi}\right]\Phi = 0$$

then replace Ψ and Θ by (3.4):

$$\Phi^{(4)} + 2p^2\Phi^{(2)} + \left[\frac{\rho h}{D}r^2 + p^4\right]\Phi = 0 \tag{3.6}$$

Equation (3.6) is of fourth order and composed of even-order derivatives which gives the following solution:

$$\Phi(y) = A_1 e^{q_1 y} + A_2 e^{-q_1 y} + A_3 e^{q_2 y} + A_4 e^{-q_2 y} \tag{3.7}$$

The boundary conditions for a simply supported plate are defined as:

$$\left| \begin{array}{l} \Phi(y) = 0 \\ \dfrac{\partial^2 \Phi(y)}{\partial y^2} = 0 \end{array} \right. \quad \text{for } y = 0, W \tag{3.8}$$

where W is the plate width.
Applying those boundary conditions (3.8) together with orthogonality properties of modes $\int_0^W \Phi_n^2(y)\, dy = 1$, equation (3.7) reduces to:

$$\Phi(y) = A_1 \left(e^{q_1 y} - e^{-q_1 y} \right) \tag{3.9}$$

$$= \pm \sqrt{\frac{2}{W}} \sin(k_y y) \tag{3.10}$$

with:

$$q_1 = \mathrm{j} k_y = \mathrm{j} \frac{n\pi}{W} \tag{3.11}$$

where n is an integer corresponding to the mode index.
For $\Psi(x)$ we use the dispersion relation (3.5) to extract x-related quantity p:

$$p = \pm \sqrt{-q^2 \pm \sqrt{-\frac{\rho h}{D} r^2}}$$

$$p = \pm \sqrt{k_y^2 \pm k^2}$$

$$p_1 = \sqrt{k_y^2 + k^2}, \; p_2 = \sqrt{k_y^2 - k^2} \tag{3.12}$$

Leading us to :

$$\begin{array}{ll} \Psi(x) = \alpha_n^+ e^{-p_1 x} + \beta_n^+ e^{-p_2 x} & \text{if } x > 0 \\ \Psi(x) = \alpha_n^- e^{p_1 x} + \beta_n^- e^{p_2 x} & \text{if } x < 0 \end{array} \tag{3.13}$$

We can see that the expression of p_1 implies the production of evanescent waves regardless of the frequency because the content of the square root is always positive. Whereas p_2 involves the production of evanescent waves or propagative waves depending on the frequency because the content of the square root can be either positive or negative. If we rewrite p_2 with circular frequency term, we have the following

expression:

$$p_2 = \left(\frac{\rho h}{D}\right)^{\frac{1}{4}} \sqrt{\omega_n - \omega} \tag{3.14}$$

with:

$$\omega_n = \sqrt{\frac{D}{\rho h}}\, k_y^2 = \sqrt{\frac{D}{\rho h}} \left(\frac{n\pi}{W}\right)^2 \tag{3.15}$$

In terms of frequency we thus have:

$$\boxed{f_n = \frac{\omega_n}{2\pi} = \frac{\pi}{4\sqrt{3}} \frac{h}{W^2} \sqrt{\frac{E}{\rho(1-\nu^2)}}\, n^2} \tag{3.16}$$

Now, when the circular frequency verifies $\omega < \omega_n$, only evanescent waves are produced and the exponential term is a decreasing exponential e^{γ_n} with a decay constant:

$$\gamma_n = -p_2 = -\left(\frac{\rho h}{D}\right)^{\frac{1}{4}} \sqrt{\omega_n - \omega} \quad \text{with } \omega < \omega_n \tag{3.17}$$

The circular frequency ω_n is therefore a cut-off frequency that marks the transition between propagative and evanescent behavior of the given mode index n.

The homogeneous solution of (3.1) for a semi-infinite plate with its longer edge simply supported are therefore in the form:

$$u(x > 0, y, \omega) = \sqrt{\frac{2}{W}} \sum_n \sin(k_y y) \left[\alpha_n^+ e^{-p_1 x} + \beta_n^+ e^{-p_2 x}\right] \tag{3.18}$$

$$u(x < 0, y, \omega) = \sqrt{\frac{2}{W}} \sum_n \sin(k_y y) \left[\alpha_n^- e^{p_1 x} + \beta_n^- e^{p_2 x}\right] \tag{3.19}$$

In our case, we aim to produce a local vibration field around the excitation point. Such a situation occurs when all modes are evanescent, that is for all frequencies lower than the first cut-off frequency f_1:

$$f_1 = \frac{\pi}{4\sqrt{3}} \frac{h}{W^2} \sqrt{\frac{E}{\rho(1-\nu^2)}} \tag{3.20}$$

We can see here that the cut-off frequency depends on the plate material properties $\sqrt{\frac{E}{\rho(1-\nu^2)}}$ and more importantly on its geometric characteristics W and h.

Green function

The Green function g is of the same form as the solutions found before:

$$g(x,y,t) = G(x,y,\omega)\mathrm{e}^{-\mathrm{j}\omega t} = \sum_n \Psi(x)\Phi_n(y)\mathrm{e}^{-\mathrm{j}\omega t} \tag{3.21}$$

and is the solution of the wave equation in thin plates for a point force at (x_s, y_s), i.e:

$$-\rho\omega^2 G(x,y,\omega) + D\nabla^4 G(x,y,\omega) = \delta(x-x_s)\delta(y-y_s) \tag{3.22}$$

Putting (3.22) in (3.21), multiplying by Φ_m on both sides and integrating the expression on the width of the plate gives us:

$$\begin{aligned}\int_0^W \left[-\rho\omega^2 \sum_n \Psi(x)\Phi_n(y) + D\nabla^4 \sum_n \Psi(x)\Phi_n(y)\right] \\ \times \Phi_m(y)\,\mathrm{d}y = \int_0^W \delta(x-x_s)\delta(y-y_s)\Phi_m(y)\,\mathrm{d}y\end{aligned} \tag{3.23}$$

The definition of the dirac function allows us to write:

$$\int_0^W \delta(y-y_s)\Phi_m(y)\,\mathrm{d}y = \Phi_m(y_s) \tag{3.24}$$

The right side of (3.23) becomes:

$$\int_0^W \delta(x-x_s)\delta(y-y_s)\Phi_m(y)\,\mathrm{d}y = \delta(x-x_s)\Phi_m(y_s) \tag{3.25}$$

In addition, the orthogonality of the eigenmodes and their normalization leads to:

$$\begin{aligned}\int_0^W \Phi_n(y)\Phi_m(y)\,\mathrm{d}y &= \delta(n-m) \times \int_0^W \Phi_n^2(y)\,\mathrm{d}y \\ &= \delta(n-m)\end{aligned} \tag{3.26}$$

Thus the left side becomes:

$$\begin{aligned}&\int_0^W \left[-\rho\omega^2 \sum_n \Psi\Phi_n + D\nabla^4 \sum_n \Psi\Phi_n\right]\Phi_m\,\mathrm{d}y \\ &= -\rho\omega^2 \sum_n \Psi\delta(n-m) + D\int_0^W \sum_n \nabla^4\left[\Psi\Phi_n\right]\Phi_m(y)\,\mathrm{d}y \\ &= \sum_n \left(D\left[\Psi^{(4)} - 2k_y^2\Psi^{(2)} + \left(k_y^4 - \frac{\rho}{D}\omega^2\right)\Psi\right]\delta(n-m)\right)\end{aligned} \tag{3.27}$$

The dirac delta function gives 1 if $n = m$ and 0 if $n \neq m$ thus giving the following equation:

$$\Psi^{(4)} - 2k_y^2\Psi^{(2)} + \left[k_y^4 - \frac{\rho}{D}\omega^2\right]\Psi = \frac{1}{D}\delta(x - x_s)\Phi_m(y_s) \tag{3.28}$$

The solutions are of the previously found form :

$$\begin{aligned} \Psi(x) &= \alpha_n^+ e^{-p_1 x} + \beta_n^+ e^{-p_2 x} \quad \text{if } x > 0 \\ \Psi(x) &= \alpha_n^- e^{p_1 x} + \beta_n^- e^{p_2 x} \quad \text{if } x < 0 \end{aligned} \tag{3.29}$$

The unknowns are therefore the terms α_n^+, α_n^-, β_n^+, β_n^-. At $x = x_s$, the derivatives of order 0, 1 and 2 are continuous but the presence of the right-hand term requires a jump to the derivative of order 3. The conditions of continuity are therefore written:

$$\begin{aligned} \Psi(x = x_s^-) &= \Psi(x = x_s^+) \\ \frac{\partial\Psi}{\partial x}(x = x_s^-) &= \frac{\partial\Psi}{\partial x}(x = x_s^+) \\ \frac{\partial^2\Psi}{\partial x^2}(x = x_s^-) &= \frac{\partial^2\Psi}{\partial x^2}(x = x_s^+) \\ \frac{\partial^3\Psi}{\partial x^3}(x = x_s^-) &= \frac{\partial^3\Psi}{\partial x^3}(x = x_s^+) + \frac{1}{D}\Phi_m(y_s) \end{aligned}$$

Applying previous continuity conditions to (3.29), we obtain:

$$\begin{aligned} \alpha_n^- e^{p_1 x} + \beta_n^- e^{p_2 x} - \alpha_n^+ e^{-p_1 x} - \beta_n^+ e^{-p_2 x} &= 0 \\ p_1\alpha_n^- e^{p_1 x} + p_2\beta_n^- e^{p_2 x} + p_1\alpha_n^+ e^{-p_1 x} + p_2\beta_n^+ e^{-p_2 x} &= 0 \\ p_1^2\alpha_n^- e^{p_1 x} + p_2^2\beta_n^- e^{p_2 x} - p_1^2\alpha_n^+ e^{-p_1 x} - p_2^2\beta_n^+ e^{-p_2 x} &= 0 \\ p_1^3\alpha_n^- e^{p_1 x} + p_2^3\beta_n^- e^{p_2 x} + p_1^3\alpha_n^+ e^{-p_1 x} + p_2^3\beta_n^+ e^{-p_2 x} &= \Phi_m(y_s)/D \end{aligned}$$

which translate to the following matrix form:

$$\begin{bmatrix} -1 & -1 & 1 & 1 \\ p_1 & p_2 & p_1 & p_2 \\ -p_1^2 & -p_2^2 & p_1^2 & p_2^2 \\ p_1^3 & p_2^3 & p_1^3 & p_2^3 \end{bmatrix} \begin{bmatrix} \alpha^+ \\ \beta^+ \\ \alpha^- \\ \beta^- \end{bmatrix} = \begin{bmatrix} 0 \\ 0 \\ 0 \\ \frac{1}{D}\Phi_m(y_s) \end{bmatrix} \tag{3.30}$$

which is reversed to find the values of the coefficients α_n^+, α_n^-, β_n^+, β_n^-:

$$\alpha^+ = \alpha^- = -\frac{\Phi_m(y_s)}{2D(p_2^2 - p_1^2)p_1} = \frac{\Phi_m(y_s)}{4Dk^2\sqrt{k_y^2 + k^2}} \tag{3.31}$$

$$\beta^+ = \beta^- = \frac{\Phi_m(y_s)}{2D(p_2^2 - p_1^2)p_2} = \frac{-\Phi_m(y_s)}{4Dk^2\sqrt{k_y^2 - k^2}} \tag{3.32}$$

knowing Φ_n from the previous section as:

$$\Phi_n(y) = \pm\sqrt{\frac{2}{W}}\sin(k_y y), \quad \text{with } k_y = n\pi/W \tag{3.33}$$

the Green's function is therefore written:

$$G(x,y,\omega) = \frac{1}{2W}\sum_n \frac{\sin(k_y y)\sin(k_y y_s)}{Dk^2}\left[\frac{e^{-p_1|x-x_s|}}{p_1} - \frac{e^{-p_2|x-x_s|}}{p_2}\right]$$
$$\text{with } k_y = \frac{n\pi}{W},\ k^2 = \sqrt{\frac{\rho h}{D}}\omega,\ p_1 = \sqrt{k_y^2 + k^2},\ p_2 = \sqrt{k_y^2 - k^2}. \tag{3.34}$$

3.2.2. CUT-OFF FREQUENCY f_1 AND BOUNDARY CONDITIONS

Theory showed an analytic solution for a plate with infinite length on the x-axis and simply supported boundary conditions on the y-axis at $y = 0$ and $y = W$. Different boundary conditions do not provide a full analytic solution of the out of plane displacement of the plate but we can still estimate k_{y_1} leading to the value of the first cut-off frequency f_1. Based on [29][Chapter 4], we extract frequency equations for different couples of boundary conditions which gives us Table 3.1 (the letters: S, C and F refer respectively to Simply Supported, Clamped and Free boundary conditions).

Taking a plate of thickness $h = 0.4$ mm and aluminum properties ($\nu = 0.346$, $E = 69$ GPa, $\rho = 2700$ kg/m^3), we can plot cut-off frequencies relative to the width of the plate (Figure 3.1). We can see that for a value of W, the C-C conditions provide a higher cut-off frequency than S-S conditions. This difference will later be seen with the values obtained experimentally (Section 3.3). Figure 3.1 also shows us that the cut-off frequency decreases with the plate width, which implies an important characteristic of our method: the plate must be narrow for the low-frequency band-gap to exist.

Boundary Conditions	k_{y_1}
S - S	π / W
C - C	α_1 / W with $\tan(\alpha_n/2) + \tanh(\alpha_n/2) = 0$
F - F	0
C - F	α_0 / W with $\cos(\alpha_n)\cosh(\alpha_n) + 1 = 0$
C - S	$\alpha_1 / (2W)$ with $\tan(\alpha_n/2) - \tanh(\alpha_n/2) = 0$
F - S	0

Table 3.1: Expression of k_{y_1} depending on boundary conditions.

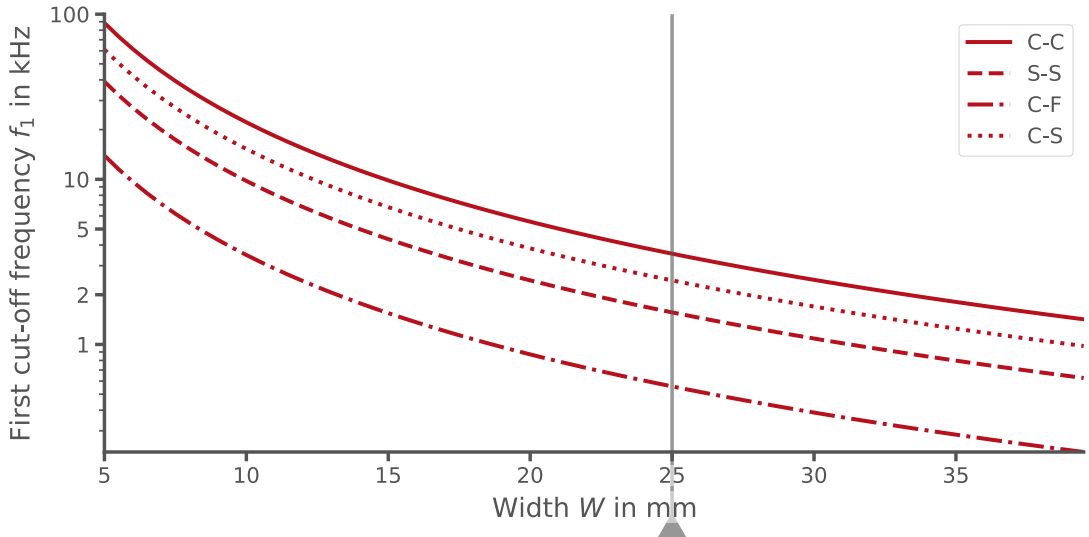

W = 25 mm	Boundaries	C - C	S - S	C - S	C - F
	f_1 in kHz	3.5	1.6	2.4	0.5

Figure 3.1: Cut-off frequency value depending on the width of the plate and the boundary conditions.

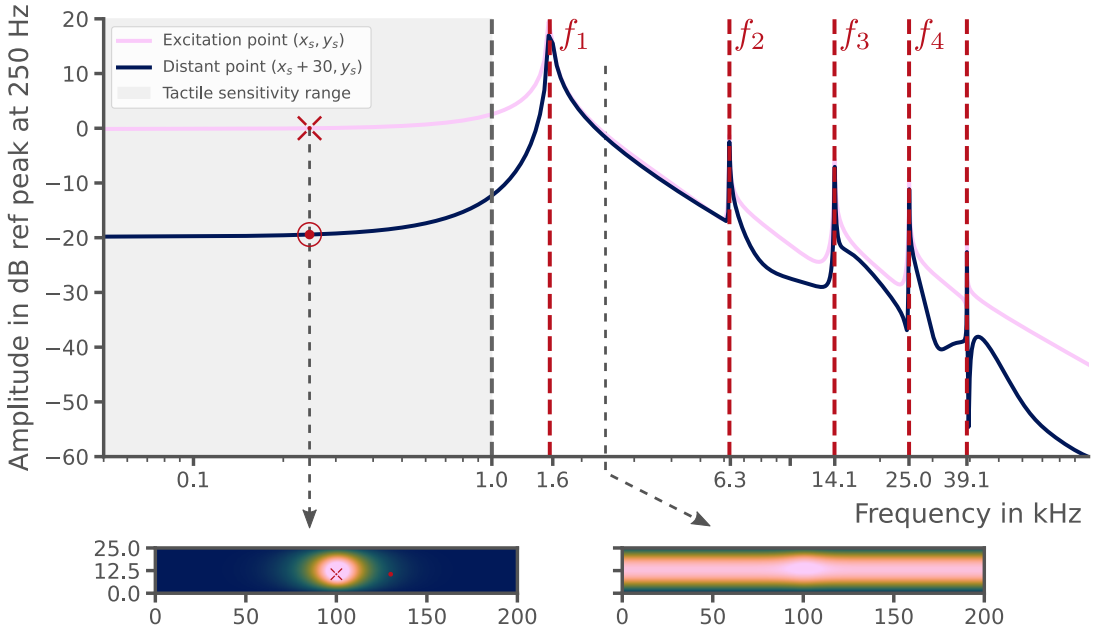

Figure 3.2: Numerical solutions of equation (3.34) in the frequency domain at the excitation point ($x_s = 100$ mm, $y_s = 3W/7$) (light pink) and at a point 30 mm away on the x-axis (dark blue). Frequencies from 0 to 1.6 kHz are said to be non-propagative. At these frequencies, amplitudes at the center of the actuator are theoretically higher than elsewhere on the plate. After the first cut-off frequency f_1, modes begin to propagate.

3.2.3. EQUATION SIMULATION

Taking equation (3.34) with a plate of width $W = 25$ mm, thickness $h = 0.4$ mm and aluminum properties ($\nu = 0.346$, $E = 69$ GPa, $\rho = 2700$ kg/m^3) and an excitation point at ($x_s = 100$ mm, $y_s = 3W/7$) gives us the frequency response function in Figure 3.2. The activation of the first mode at 1.6 kHz leaves a band-gap from 0 to 1.6 kHz. In other words, the geometry of the waveguide implies only evanescent waves until the 1.6 kHz cut-off frequency. Those evanescent waves, which amplitudes decrease exponentially with the source distance, can be used to give a localized vibrotactile feedback in the actuated region of the surface. After that cut-off frequency, modes begin to spread and the localized effect is lost.

3.3. EXPERIMENTAL VALIDATION

3.3.1. MEASUREMENT PROCESS

The following experiments aim to verify the previous theory on an aluminum plate clamped on its longer sides to a rigid frame and submitted to different actuator excitations. All measurements were assured by a Doppler vibrometer OFV-505/OFV-5000 mounted on a motorized 3 axis platform.

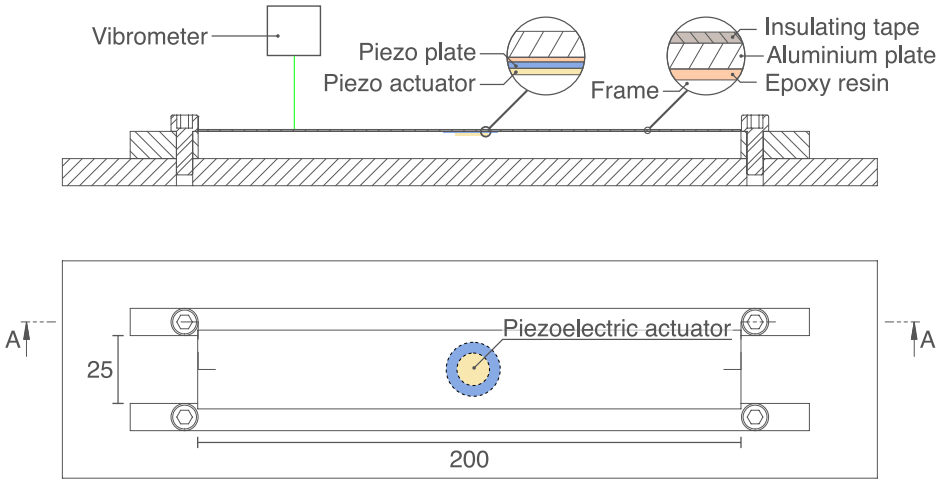

Figure 3.3: Experimental setup. Top: A piezoelectric actuator is glued to the bottom side of an aluminum plate. The laser vibrometer measures the surfaces out of plane displacement. Bottom: plate dimensions and actuator position.

3.3.2. SINGLE PIEZOELECTRIC ACTUATOR

In order to validate the theory introduced in Section 3.2, an aluminum plate with a piezoelectric actuator glued to the center of its bottom side was prepared (Figure 3.3). The actuator (muRata 7BB-20-3), of circular geometry, is composed of two parts: a plate of diameter 20 mm and a thickness of 0.1 mm; and a piezoelectric transducer of diameter 12.8 mm and a thickness of 0.11 mm. When bounded, this actuator produces radial forces that are equivalent to compression forces and bending moments which give birth to longitudinal compression waves and transverse flexural waves [30, Chapter 10]. The simply supported conditions being quite difficult to achieve, the plate, measuring $200 \times 30 \times 0.4$ mm^3, was rather clamped on its longer sides to a rigid frame via epoxy resin (DP490 Scotch-Weld) and left free on both ends. The 2.5 mm clamping width on each side produced an effective plate width of 25 mm. This leads to several differences compared to the simply supported case. With clamped conditions: the shape of the deformation along the y-axis of the plate changes; the amplitude of vibration is less important; and the cut-off frequency is higher. The actuator was driven by an analog signal sent with an NI-USB-6363 acquisition card and amplified (Elbatech T-500 series).

FREQUENCY RESPONSE FUNCTION (FRF)

We measured the frequency response function or FRF (ratio of the displacement at a given point to the voltage applied to an actuator in the frequency domain) by sending an exponential sweep signal of 2 V amplitude going from 1 Hz to 100 kHz sampled at 200 kHz. Figure 3.4 shows the the averaged FRF inside and outside the actuated area. The FRFs are normalized by the amplitude at 250 Hz at the center of the actuator. At

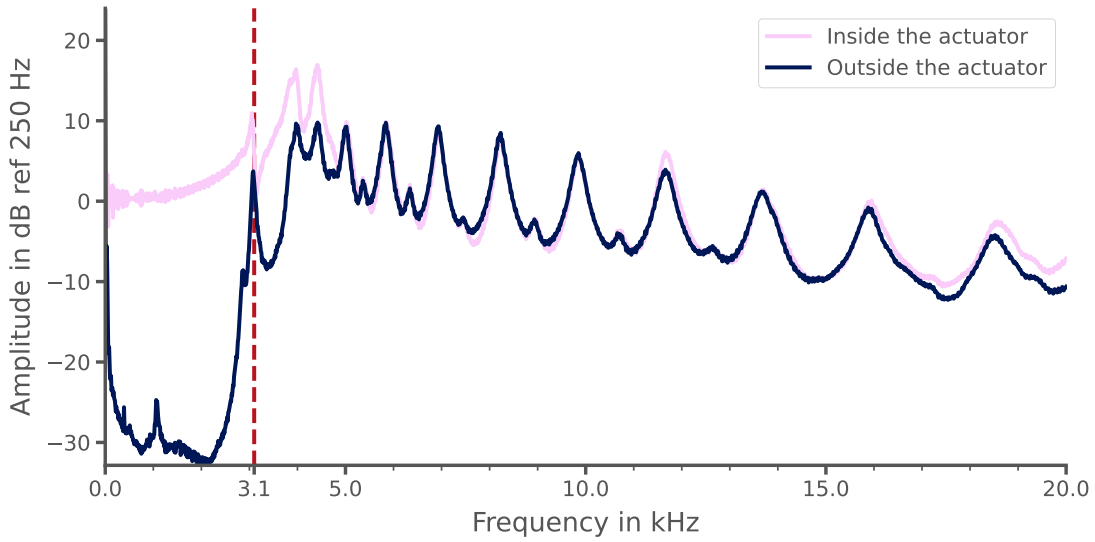

Figure 3.4: Averaged measured frequency response function (FRF) $H_{dB} = 20\log_{10}|H|$ inside and outside the activated actuator. The frequencies between 0 and 3.1 kHz are non-propagative. Within this range, amplitudes at the center of the actuator are about 30 dB larger than elsewhere on the plate.

low frequency, these amplitudes exhibit a frequency evolution very similar to those obtained with the analytic model in Section 3.2.3. A low frequency band-gap appears in the FRF between DC and 3.2 kHz (value of the same order as what was found in Figure 3.1 for C-C boundaries). In this range, the displacement at the center of the actuator is about 30 dB higher in average than at any points outside the actuator.

Sine signal

To check the actual confinement of vibration and amplitudes in play in the frequency band-gap, we submitted the plate to a 250 Hz harmonic excitation of 100 V amplitude (200 V peak-to-peak). Figure 3.5 show the resulting plate displacement. The chosen frequency is below the cut-off frequency, as such, a localized effect corresponding to the non-propagation of modes can be seen. Some points of interest can be highlighted. On Figure 3.5, we can discern three areas: the inner surface of the actuator, the outer area near the edge of the actuator, and the rest. Before the cut-off frequency, the spatial deformation inside the actuator depends exclusively on its geometry and nature. The exponentially decreasing shape found in the outer area near the edge of the actuator corresponds to the non-propagative behavior of the plate before its first cut-off frequency.

Button signal

The first part of a click signal (pushing phase) based on [31] was implemented to show the robustness of this method to dynamic signals. Figure 3.6.a recreates each phase within a button pushing interaction and contains the following in order: a grain sig-

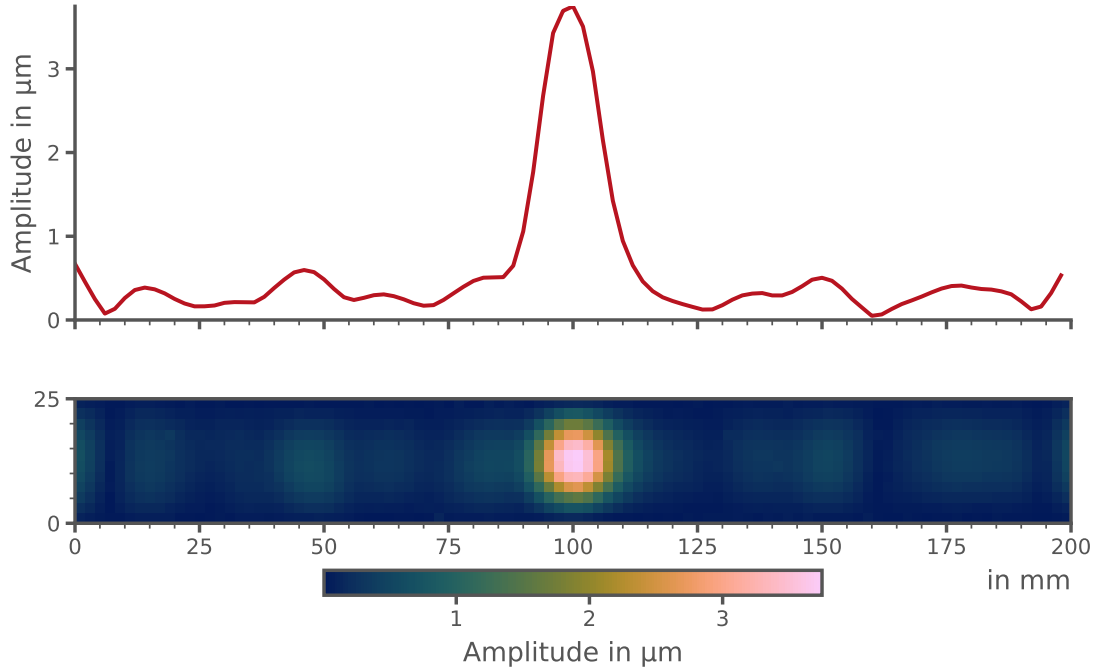

Figure 3.5: Quadratic mean of the measured displacement across the plate ($200 \times 25 \times 0.4$ mm^3) under a 250 Hz harmonic excitation of 100 V amplitude. The area above the piezoelectric actuator has an amplitude of 4.6 μm whereas the rest of the plate stays at a negligible amplitude.

nal emulating compliance; a jump feedback occurring when a sudden displacement of the finger occurs; and a bottom-out feedback which simulates the end point of the button press operation.

Figure 3.6.b shows the quadratic mean of the resulting signal throughout the plate. The energy distribution is confined to the activated area. Indeed, as long as the frequency content of the signal is within the band-gap, dynamic signals can be confined and can provide a localized custom interaction. We can also observe in Figure 3.6.a the high fidelity and responsiveness provided by the piezoelectric actuator reaching a normalized correlation of 97 %.

The following sections aim to verify that the non-propagative behavior of the plate is still relevant when we use multiple actuators and different types of actuators.

3.3.3. SIMULTANEOUS PIEZOELECTRIC ACTUATORS

This section demonstrates, the possibility to produce multiple located vibrations at the same time thanks to multiple actuators.

On the same prototype as before, we added another actuator, identical to the previous one (muRata 7BB-20-3), arbitrarily placed around 7 cm away from the first actuator. We then drove both actuators with the same amplitude at a frequency inside

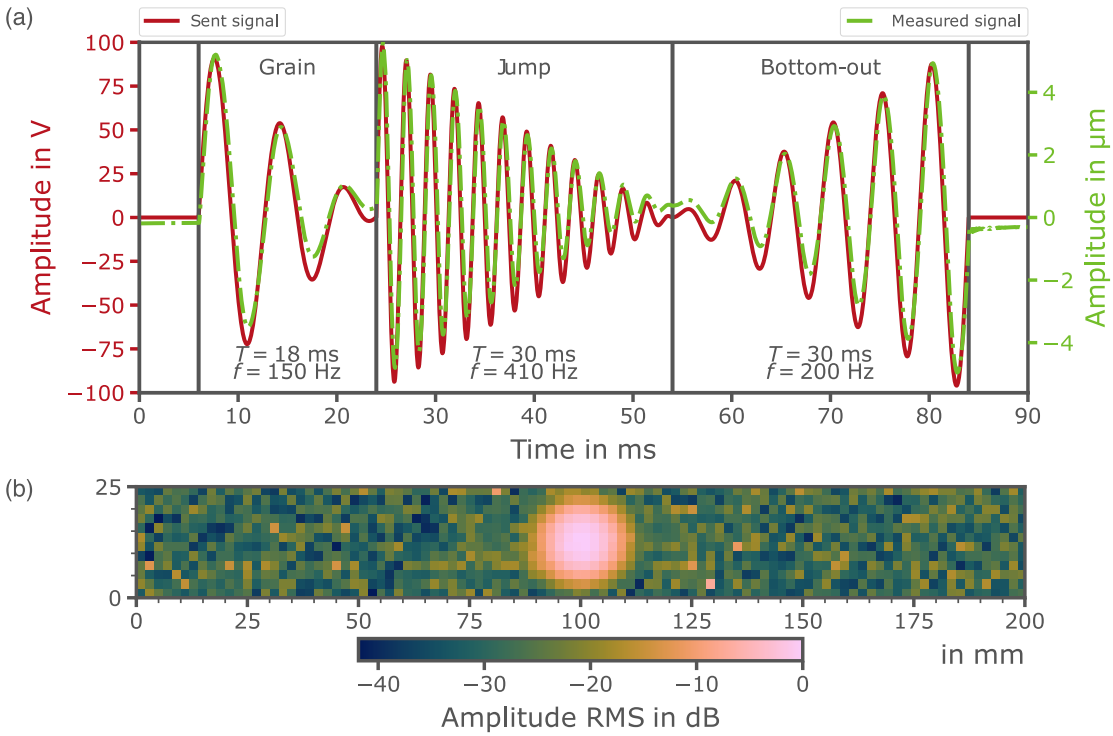

Figure 3.6: (a) Button pushing signal sent to the piezoelectric actuator (red solid line) and obtained displacement at its center (light green dashed line). Instantaneous response with high fidelity to the desired signal is obtained. (b) Quadratic mean of the measured out of plane displacement of the plate under the button pushing signal.

the tactile sensitivity range [1]. Since the low frequency band-gap spreads over several kHz, different frequency within this band were tested. We chose a burst signal of 100 V amplitude and of frequency 250 Hz with 6 cycles for both actuator in one case and also tested driving one of the two with a burst signal of 500 Hz frequency, 12 cycles and 100 V amplitude. The vibration field was measured over the plate by steps of 2 mm.

Figure 3.7 shows the localized effect for both cases where we can observe two distinct deformations above each actuated area. We can also notice that there is a difference of amplitude between localized areas even thought we sent the same voltage amplitude. As this difference occurs for both frequency used (500 Hz and 250 Hz), we assume that it is caused by differences in the bonding quality of the piezoelectric actuators (a little difference in the thickness of the bounding layer can result in important behavior differences [32, 33]). We can assume that in the case of perfectly bonded actuators, the displacement would be the same in both areas and amplitudes over 4 μm (2 μm rms) would be achievable. The obtained amplitudes are enough for tactile perception [1] (Section 3.5 also provide validation for this claim).

As a result, one can also imagine covering the plate with an array of piezoelectric actuators to obtain an interface allowing multiple localized haptic feedback. Adding

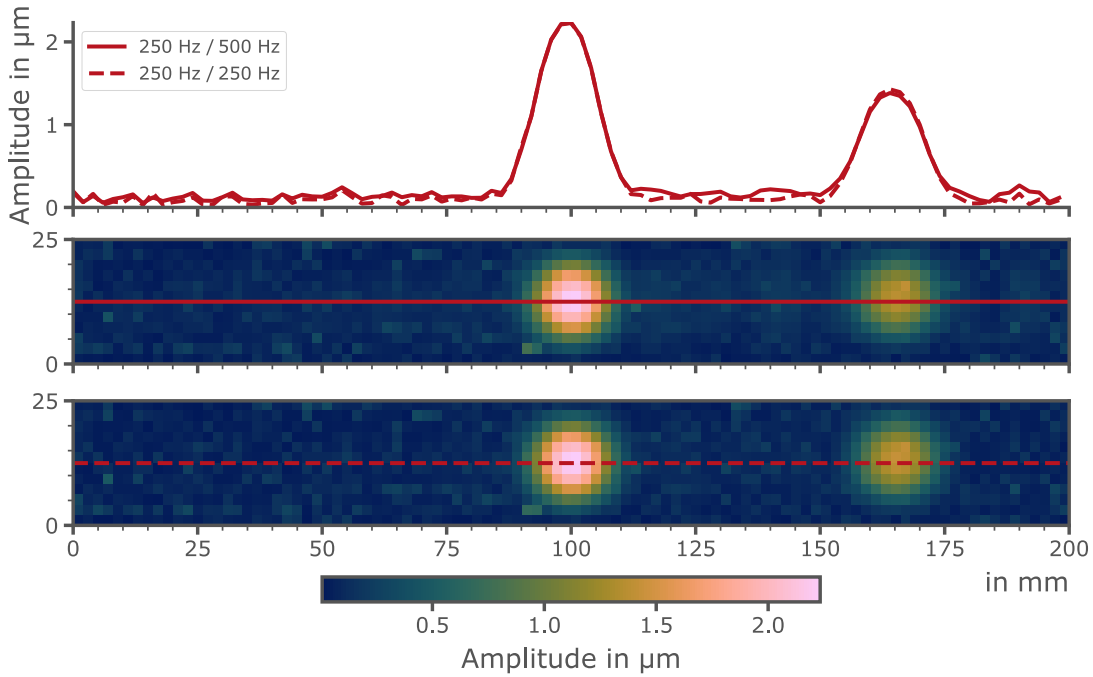

Figure 3.7: Quadratic mean of the measured displacement across the plate under two simultaneous burst signals at different frequency [250 Hz / 500 Hz (solid line)] and same frequency [250 Hz / 250 Hz (dashed line)] with an amplitude of ±100 V. Both vibration sources are localized while the rest of the plate stays at rest.

actuators would result in increased local stiffness to the plate, thus increasing the cut-off frequency value of the plate and decreasing the decay constant of the evanescent waves.

3.3.4. OTHER CONFIGURATIONS

In this section, we prove that the actuator geometry or the nature of the vibration source gives a localized effect as long as the excitation frequency is within the band-gap provided by the waveguide. We added to the previous setup three actuators: a square piezoelectric actuator (SMPL7W8T02412WL Steminc) with same working principle as the muRata actuators), a linear resonant actuator (LRA Model C10-100 Precision Microdrives TM) and an eccentric rotating mass vibration motor (ERM Model 306-109 Precision Microdrives TM). A representation of the modified setup and the actuators positions and dimension are presented on Figure 3.8.

The actuators were placed on the middle axis of the plate in order to get higher vibration amplitudes. The square piezoelectric actuator, of effective dimension $7 \times 7 \times 0.2$ mm^3, was glued with cyanoacrylate and powered with a 6 cycles burst signal of frequency 250 Hz at 100 V amplitude. The LRA was also fixed thanks to cyanoacrylate glue (rather than its self adhesive sheet backing) and driven with a 175 Hz harmonic signal of 2 V amplitude (manufacturer's values). Finally, the ERM vibration motor

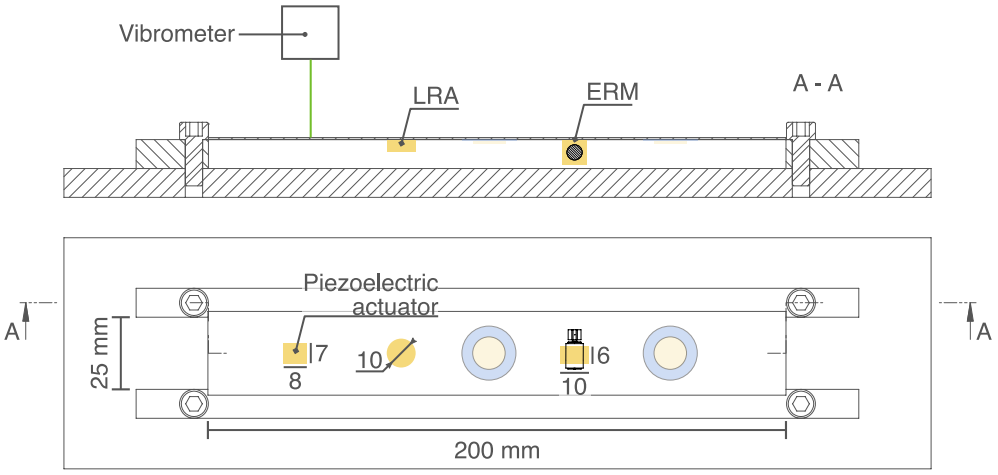

Figure 3.8: Upgraded experimental setup. Top: Three actuators are added to the bottom side of the previously used aluminum plate. The laser vibrometer measures the surface's out of plane displacement. Bottom: plate dimensions and actuator positions.

was first fixed to an intermediate plastic part then glued with cyanoacrylate to the plate. It was powered with a constant 2 V amplitude resulting in a frequency of 160 Hz (frequency found post-measurement with an FFT of the obtained displacement in Figure 3.11). A summary is provided in Table 3.2.

Actuator	Contact geometry	Frequency	Signal	Voltage
□ Piezo	7×7 mm^2	250 Hz	Burst (6 cycles / Hann window)	100 V
LRA	⌀10 mm	175 Hz	Sine	2 V
ERM	10×6 mm^2	~160 Hz	Constant	2 V

Table 3.2: Configurations acquisition specification.

For each actuator, we measured the displacement across the plate which are represented in Figure 3.9, 3.10 and 3.11.

SQUARE PIEZOELECTRIC ACTUATOR.

As with circular piezoelectric actuators, we observe the confinement of vibrations above the actuated area. It is interesting to notice the shape of the plate deformation. The actuator geometry gave a seemingly thinner form to the out plane displacement which could lead to a different feedback to the finger [1]. Also even if the y-dimension of the actuator is small compared to the width, the entire width of the plate is activated. This is to be expected because in equation (3.34) of Section 3.2, the y-component is modulated by a sine function. The rms amplitude is reduced compared to previous actuators (circular piezoelectric ⌀12.8 mm) as the size of the actuator is smaller.

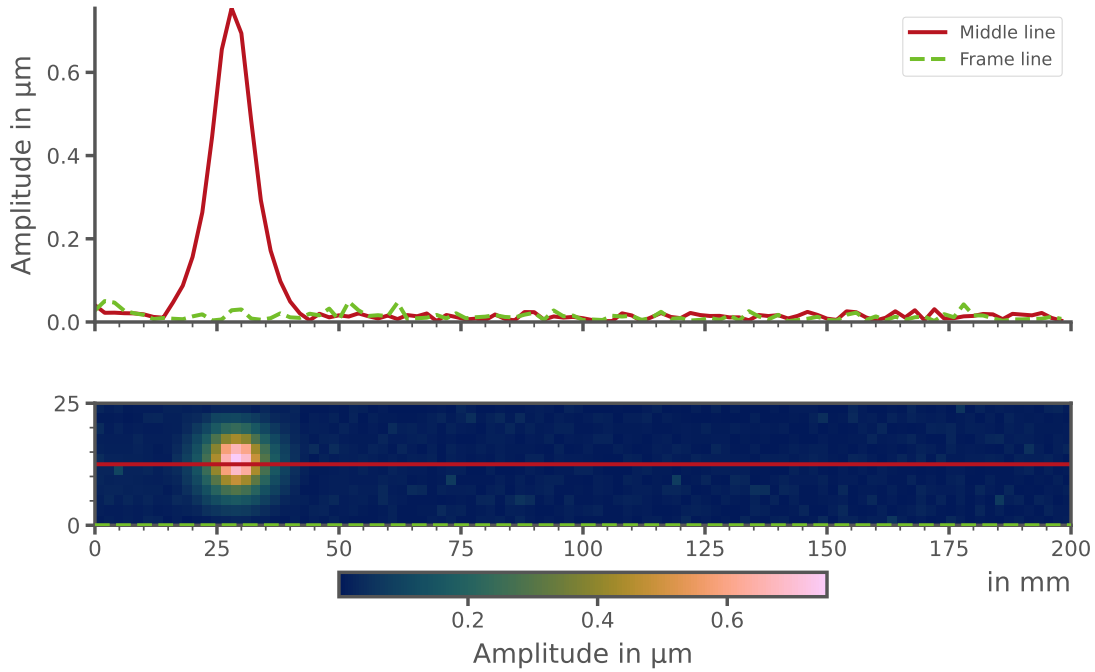

Figure 3.9: Quadratic mean of the measured displacement across the plate excited by a squared piezoelectric actuator (100 V/250 Hz) with a 7×7 mm^2 contact geometry. Vibrations are localized in the actuator region and reach a maximum RMS amplitude of 0.75 μm at the center of the actuator.

Linear resonant actuator (LRA).

The vibrations localization produced by the LRA is not as striking as with piezoelectric actuators. Although localization can be noticed, a rigid body motion is occurring throughout the plate (light green dashed line). The entire structure (waveguide + robot frame) is vibrating because of the inertia involved by the LRA (which is greater than the one involved by piezoelectric actuators).

Eccentric rotating mass vibration motor (ERM).

Like the LRA, the ERM rely on inertia to create vibrations. Thus Figure 3.11 also displays a rigid body motion but nonetheless present vibration localization. The out-of-plane displacement shows a deformation quite different from those obtained previously. Unlike the LRA or piezo actuators, the ERM does not produce a vibration only normal to the surface. Moreover, the ERM being in some way cantilevered with the intermediate part, the transmission of forces must involve additional torques on the plate leading to this peculiar deformation.

3.4. Finger Interaction

In most applications implying the use of vibration, the finger brings an added mechanical loading impedance to the plate which can reduce the amplitude of the

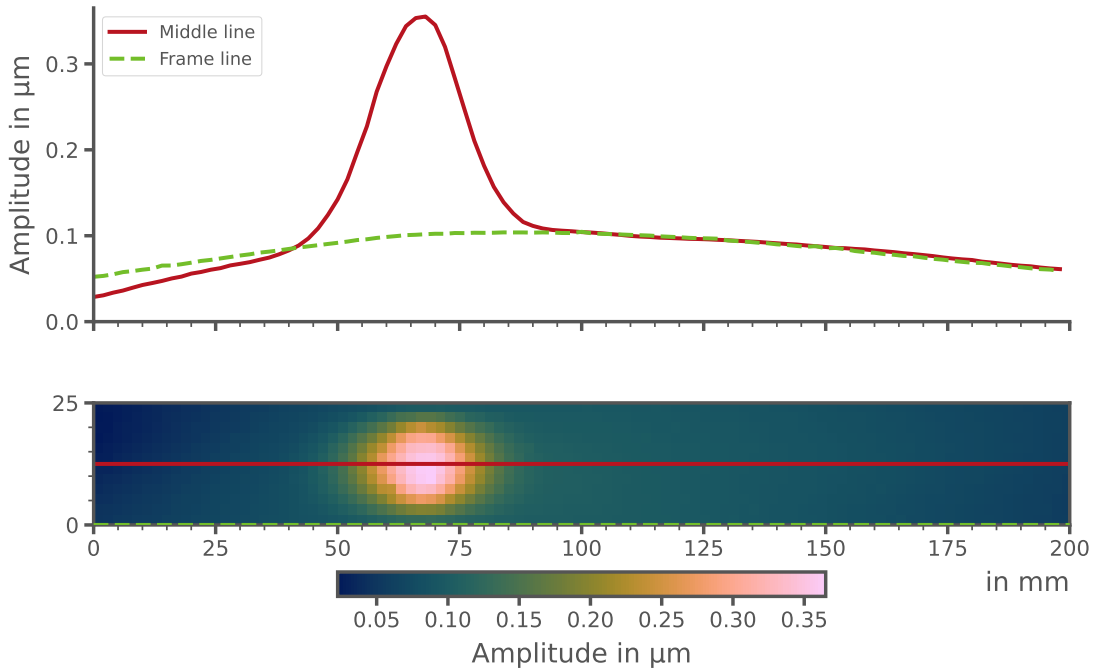

Figure 3.10: Quadratic mean of the measured displacement across the plate excited by a LRA (2 V/175 Hz) with a contact geometry consisting of a 10 mm diameter disk. The plate presents a rigid body motion implied by the structure vibration represented by the dashed line. Yet the localization effect is still present and shows a maximum RMS amplitude of 0.4 μm at the center of the actuator.

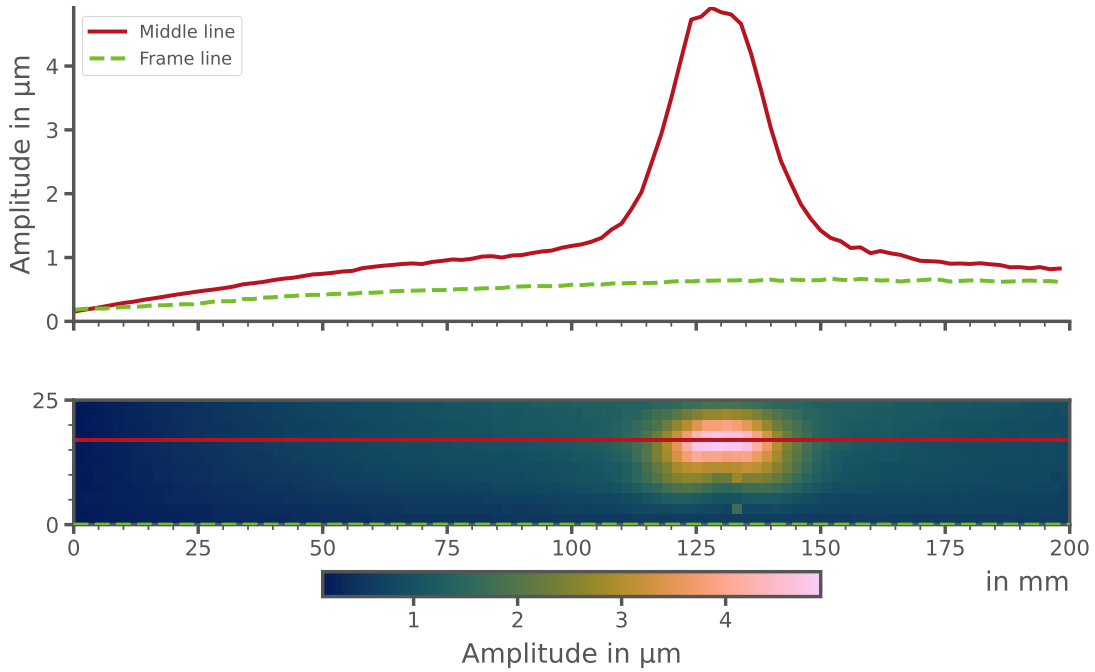

Figure 3.11: Quadratic mean of the measured displacement across the plate excited by an ERM with a contact geometry consisting of a 10×6 mm^2 rectangle. The plate presents a rigid body motion implied by the structure vibration which represented with a dashed line. Yet the localization effect is still present and shows a maximum rms amplitude of over 4 μm in average.

stimuli. In this section, we show theoretically and experimentally that the attenuation in the tactile frequency range (0 to 1 kHz [34]) brought by the finger depends on the first cut-off frequency and is negligible in our system.

3.4.1. MODEL

A harmonic force, $F(a,\omega)$, applied normally to the plate at a point a causes a displacement $U(a,\omega)$ such that $F(a,\omega) = j\omega Z_p(a,\omega)U(a,\omega)$, where $Z_p(a,\omega)$ is the plate impedance at point a. During interaction, if $Z_f(\omega)$ is an additional impedance due to the finger, then the resulting attenuation μ, ratio between the loaded displacement $\widetilde{U}$ relative to the free displacement U, is:

$$\mu = \frac{\widetilde{U}}{U} = \frac{Z_p}{Z_p + Z_f} \tag{3.35}$$

In our case, the plate impedance is given by the inverse of the green function of our semi-infinite model at point $a(x_a, y_a)$:

$$\begin{aligned} Z_{p_{\text{semi-inf}}} &= \frac{F(a,\omega)}{V_F(a,\omega)} = \frac{F(a,\omega)}{j\omega U_F(a,\omega)} = \frac{1}{j\omega}\frac{1}{G(x_a,y_a,\omega)} \\ &= \frac{2W}{j\omega}\sum_n \frac{Dk^2}{\sin^2(k_y y_a)}\left[\frac{\sqrt{k_y^4 - k^4}}{\sqrt{k_y^2 - k^2} - \sqrt{k_y^2 + k^2}}\right] \end{aligned}$$

We will also see the impedance behavior of a finite model for a rectangular plate simply supported on all its edges. The following Green expression is obtained following the same process used in Section 3.2.1:

$$G(x,y,\omega) = -\frac{4}{WL}\sum_{n,m}\frac{\sin(k_x x)\sin(k_y y)\sin(k_x x_a)\sin(k_y y_a)}{D\left(k^4 - (k_x^2 + k_y^2)^2\right)} \tag{3.36}$$

with $k_x = n\pi/L$ and $k_y = m\pi/W$. We then have the finite model impedance :

$$\begin{aligned} Z_{p_{\text{finite}}} &= \frac{F(a,\omega)}{V_F(a,\omega)} = \frac{F(a,\omega)}{j\omega U_F(a,\omega)} = \frac{1}{j\omega}\frac{1}{G(x_a,y_a,\omega)} \\ &= -\frac{WL}{4j\omega}\sum_{n,m}\frac{D\left(k^4 - (k_x^2 + k_y^2)^2\right)}{\sin(k_x x_a)^2\sin(k_y y_a)^2} \end{aligned}$$

For the finger impedance we chose a lumped element model based on [35] consisting of a mass-spring-damper system:

$$Z_f = b + j\left(m_f\omega - \frac{k_f}{\omega}\right) \tag{3.37}$$

where the viscosity b = 1.4 N.s/m, the moving mass m_f = 0.15 g, and the stiffness k_f = 1000 N/m. Those quantities are averages of the experimental values found in [35] for a normal force of 0.5 N applied by the finger.

3.4.2. IMPLEMENTATION

Taking each impedance expression and the attenuation expression with a plate of width W = 25 mm, thickness h = 0.4 mm and aluminum properties (ν = 0.346, E = 69 GPa, ρ = 2700 kg/m^3) gives us the frequency response function in Figure 3.12. In this figure, in the tactile sensitivity range, the plate impedance is more important than the finger impedance leading to almost no attenuation due to the finger interaction. The finger's impedance becomes larger than the plate impedance around the cut-off frequency and the resonance of the plate. This simulation highlights an important point that should be kept in mind when designing the system: if the first cut-off frequency of the system is to close to the tactile sensitivity range, attenuation will affect the desired feedback.

3.4.3. EXPERIMENTAL VALIDATION

In order to check the accuracy of the previous model and confirm our assumptions, we measured U and $\widetilde{U}$, the free and loaded displacements of the plate submitted to a linear frequency sweep thanks to a laser vibrometer (Polytec OFV-505/OFV-5000). Using the device of Section 3.3.2, the vibrometer laser beam was deflected by a mirror and reflected back on the bottom side of the piezoelectric actuator. The mechanical impedance of the fingertip varying with the pressing force [35, 36], we measured the force thanks to two load cells (HBM S2M) placed under our system as depicted in Figure 3.13.

We first measured the free displacement of the plate subjected to a linear sweep signal of 10 V amplitude, 25 ms duration. We then repeated the same experiment while a user pressed their finger onto the plate above the actuator area with a finger/plate angle around 30 degree during the full duration of the signal. This measurement was reproduced with two different forces around 1.5 N and 7.5 N (greater than usual interaction forces of 0.5 N [35])

The experimental attenuation curve is represented in Figure 3.14. A first peak at-

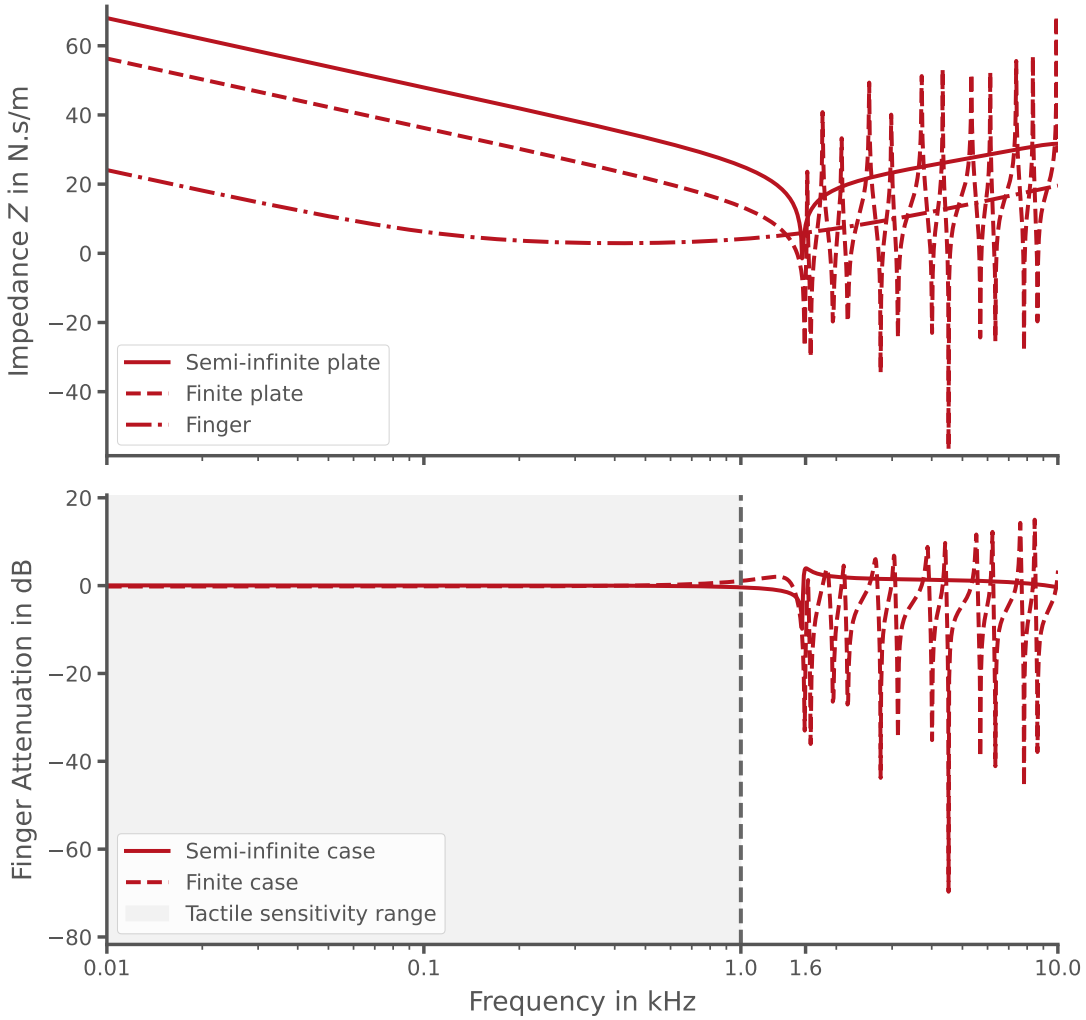

Figure 3.12: Theoretical attenuation curve $\mu_{dB} = 20\log_{10}|\mu|$ for semi-infinite plate (dotted line) and finite plate (solid line). On the tactile sensitivity range there's no attenuation due to the finger interaction. Mode activation causes a drop of the plate impedance implying important attenuation due to the finger.

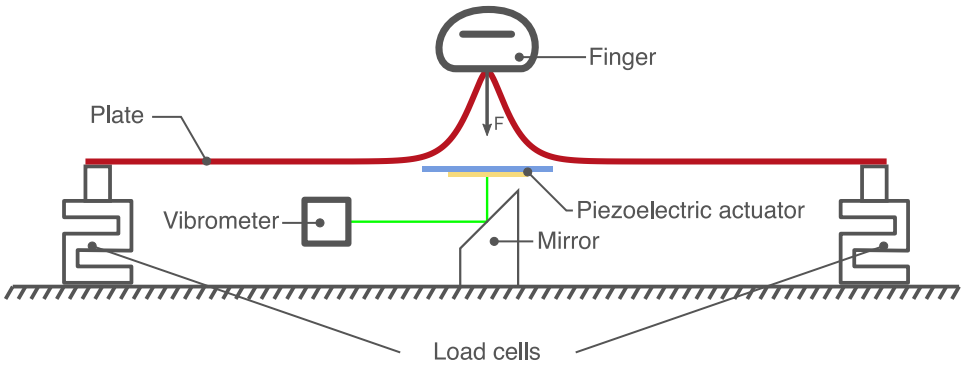

Figure 3.13: Setup for the measurement of the peak displacement attenuation in the center of the actuated area due to finger contact. The vibrometer laser beam was deflected by a mirror and reflected back on the bottom side of the piezoelectric actuator. Two load cells measured the force exerted by the finger.

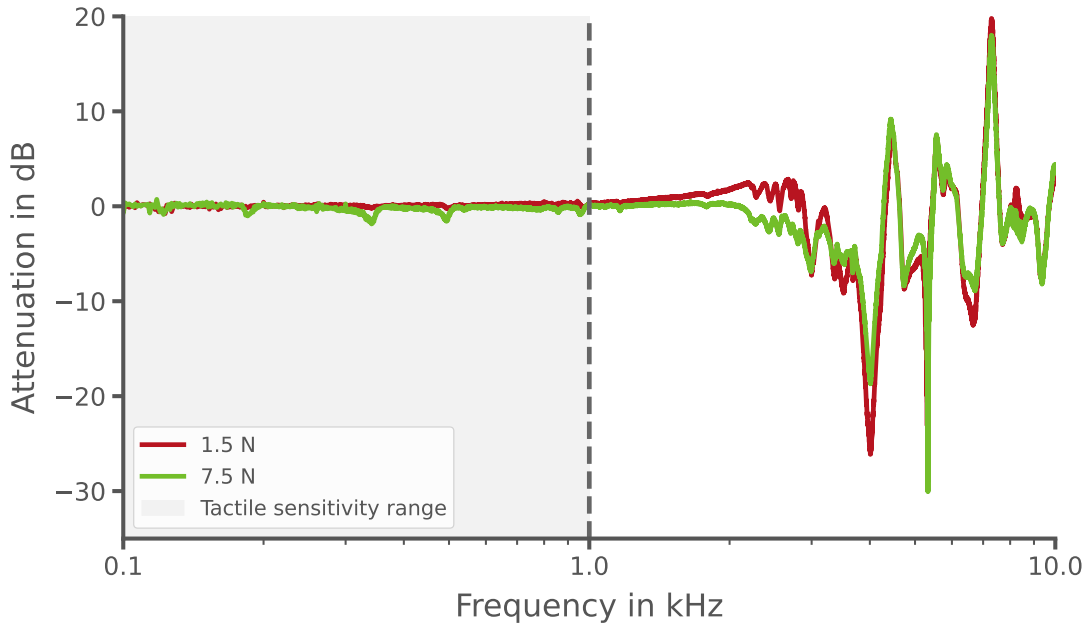

Figure 3.14: Experimental attenuation curve $\mu_{\text{dB}} = 20\log_{10}|\mu|$ obtain by realizing the ratio between loaded displacement $\widetilde{U}$ and free displacement U of the plate with different applied forces. As the model predicted, there's no attenuation due to the finger interaction on the tactile sensitivity range.

tenuation is attained around 3.2 kHz which corresponds to the first cut-off frequency of our system. The force has an effect on the attenuation but here its effect seems limited until 1 kHz. Before this frequency, the results show a low attenuation on the tactile sensitivity range which reaches a maximum of 2 dB. Hence, user interaction implies almost no attenuation on the system under 1 kHz and therefore we can say with confidence that amplitudes during interaction can be kept over 1 μm as shown in Section 3.3.2. This result is quite impressive because most touch surfaces are simply too stiff to generate sufficient vibration amplitude without the benefit of resonance. Strong attenuation implied by the drop of the impedance at those resonances are compensated with high amplitude provided at those same resonance. Here non-propagative, or evanescent, waves do not lead to an impedance drop like for the resonant case; meaning that the amplitude under the finger fully depends on the actuator capability and the properties of the plate and not the finger interaction. However, since we do not use resonance, we suspect a higher power consumption. Nevertheless, we can interact with the surface without changing its behavior in the tactile sensitivity range, which simplifies the possible control loops that could be implemented on such device in the future.

3.5. Perceptual Validation

A perceptual evaluation was carried out to demonstrate the ability of the device to produce noticeable and localized tactile feedback. This evaluation consisted in a detection task to determine whether the stimulation, with a dynamic signal with transitory and large frequency spectrum, could be felt only above the actuated area.

3.5.1. Stimuli, participants, and procedure

To demonstrate the wide band capability of our device, we used a one cycle burst sine at 500 Hz. This low number of cycles yields an excitation with a −3 dB bandwidth spreading from 200 Hz to 700 Hz. The amplitude was changed at every trial by selecting it randomly among five uniformly distributed values ranging from 60 V to 200 V peak-to-peak which corresponds to a plate peak-to-peak displacement amplitude ranging from 2.7 μm to 9 μm under the finger during the interaction (Section 3.4 justify that assumption). Five inexperienced volunteers, 1 female and 4 males, aged 20 to 26 participated in the study. Participants had to place both index fingers above each localized stimulation area 70 mm apart as depicted in Figure 3.15. Participants were asked to keep their fingers in contact with the surface during the whole experiment except during the 5-min break in the middle of the experiment. 75 stimuli were randomly presented at each finger, for a total of 150 stimuli. In addition to these 150, 5 catch trials consisting of exciting both fingers at the same time were added. Each participant had to answer left, right, both, or nothing. They wore isolating headphones playing pink noise during the duration of the task, and could not hear the stimuli.

3.5.2. Results and discussion

The correct answer ratio to a stimulus was calculated for each participant and each driving voltage amplitude. This ratio is, at a given stimuli amplitude, the ratio of the number of detected stimuli over the number of presented stimuli. Figure 3.16 shows the minimum, maximum and average ratio of correct answers over all participants.

As expected, the correct answer ratio increased with the driving voltage amplitude. It reached up to 1 for several participants, indicating a high rate of correct answer. Finally, 24 out of the 25 catch trials sent were noticed. The data also shows that 82% of the wrong answers were non-responses, meaning that users did not feel the stimulus. The remaining 18% are split between finger inversion errors (9%) and "both" responses when only one finger was excited (9%). The users admitted they got mixed up a few times because the task was repetitive. In addition, some responded

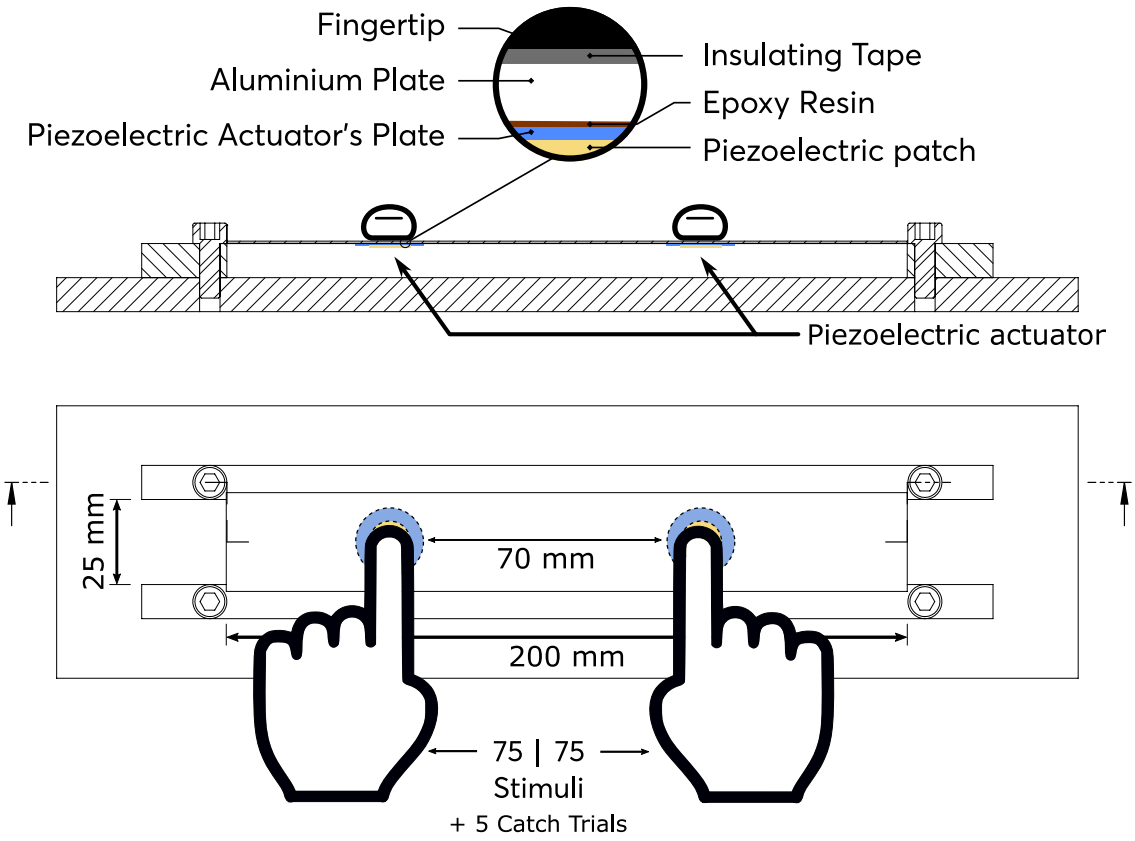

Figure 3.15: Perceptual validation setup. Both index fingers were placed above actuated areas and subjected to a series of stimuli consisting of a one cycle burst sine at 500 Hz at different amplitudes

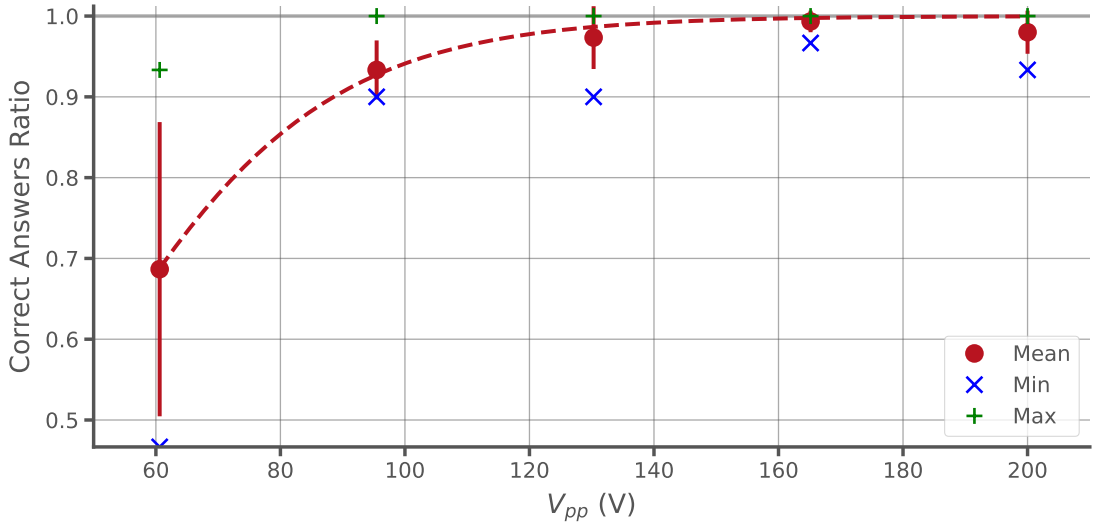

Figure 3.16: Correct answer ratio over all participants for each amplitude value. The ratio increase with the driving voltage amplitude. A high rate of correct answer (> 90%) is attained from V_{pp} = 95 V (around 4 μm peak-to-peak).

"both" when they were not sure if they felt the stimulus.

If the same procedure was to be conducted on a device with a cut-off frequency equal to 0, by changing the boundary conditions to F-F for instance, the whole plate would move and we assume that participants would not have been able to distinguish the stimuli between left or right. Also, the stimuli used in this evaluation consisting in a 1 cycle burst at 500 Hz is not the most suitable for tactile perception. 5 cycles at 250 Hz would have given us better results for low amplitudes stimuli. This configuration was not chosen as we wanted to test a highly dynamic stimuli with multiple frequency components inside the tactile sensitivity range (10-1000 Hz [1]). This short validation shows that dynamic stimuli with large frequency spectrum can be felt and distinguished, thus asserting the capability of our device for haptic applications.

3.6. Demonstration Prototype

For demonstration purposes in the World Haptics Conference 2019 we set up a prototype based on our findings. Through this prototype we wanted to demonstrate the localization and the multi-point feedback allowed with our approach. To do so, we followed several specifications regarding: geometry, haptics, interaction and safety.

3.6.1. Hardware and software

As this prototype was to be a "haptic" prototype i.e. meant to be touched, we used glass and plastic to assure the electric isolation of the user fingers regarding the actuators. We formed a thin stripped-shaped glass plate bounded on its longer edge to a rigid plastic frame and left free on both ends. On the bottom side of the plate, we applied an array of piezoelectric actuators. Keeping the user in mind, we decided to adapt the hardware dimensions according to the average user hands and fingers. We chose to arrange eight piezoelectric actuators (muRata 7BB-20-3) diametrically distinct of 25 mm each on a $25 \times 200 \times 1$ mm^3 plate (reduced to an effective width of 21 mm after bounded to the supports). The user was thus able to put on each area the index, middle, ring, and little finger of each hands. Taking the following properties for the Borofloat 33 glass: $E = 64$ GPa, $\rho = 2230$ kg/m^3 and $\nu = 0.2$, we can establish the sizing map for the glass plate shown in Figure 3.17. Displayed values for amplitude and cut-off frequency are purely theoretical and were used here just to have an idea of what to expect and not to predict exactly the outcome of our system. We chose 1 mm for the thickness to ensure robustness to travel and interaction. The width was then chosen in order to obtain sufficient amplitude (above 1 μm) and a high cut-off

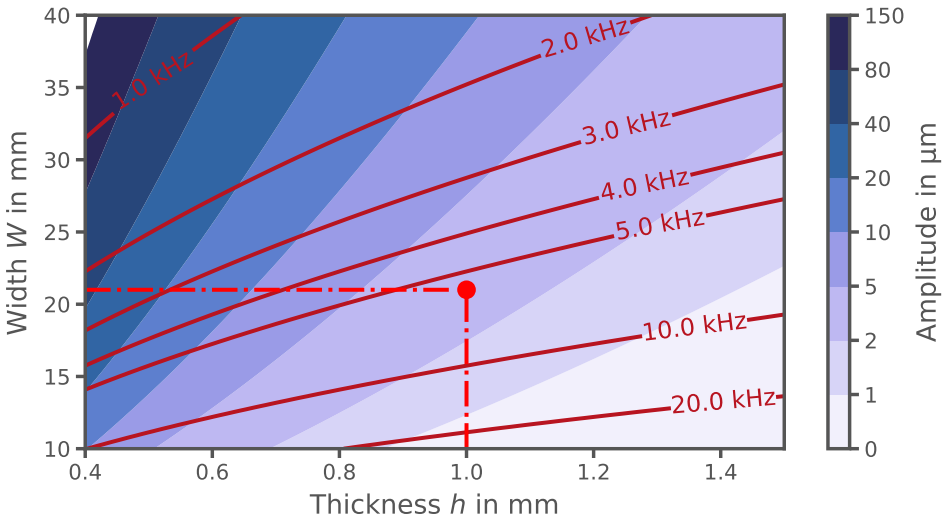

Figure 3.17: Analytic sizing map of a glass waveguide. A waveguide of width 21 mm and thickness 1 mm was chosen as it assured safety (for travel and during user interaction) as well as sufficient amplitude around 3 μm and a high cut-off frequency around 6 kHz.

frequency (above 1 kHz). Figure 3.18 shows the system assembly. The predicted first cut-off frequency of our system was around 8 kHz and measurements at the center of each actuator showed 2 μm of displacement in average at 250 Hz. The amplitude and cut-off frequency are thus sufficient to produce a localized and perceptible vibrotactile feedback [1]. In order to drive each actuator, we used eight Piezo Haptics Driver DRV8662 from Texas Instrument integrated in a custom-made lookalike circuit of the of the DRV8662 evaluation module. A voltage output module NI-9264 was used to send requested analog signals to each driver for amplification. Using Qt, we programmed an interface (Figure 3.19) allowing the control and design of signals on a touchpad. Users could chose the frequency, time and modulation window of the signal as well activating one or more actuators of their choosing.

3.6.2. AUDIENCE FEEDBACK AND DISCUSSION

The prototype received good reviews and all users were impressed that we could produce localized feedback this easily. The two main questions were:

- Is it possible to have feedbacks between two actuators ?
- How can we extend this in larger surfaces ?

Those two questions clearly draw the limits of this first work. The first question can be resolved in three ways. The easiest solution would be augmenting the density of actuators so that we can provide a feedback everywhere on the plate. If we want

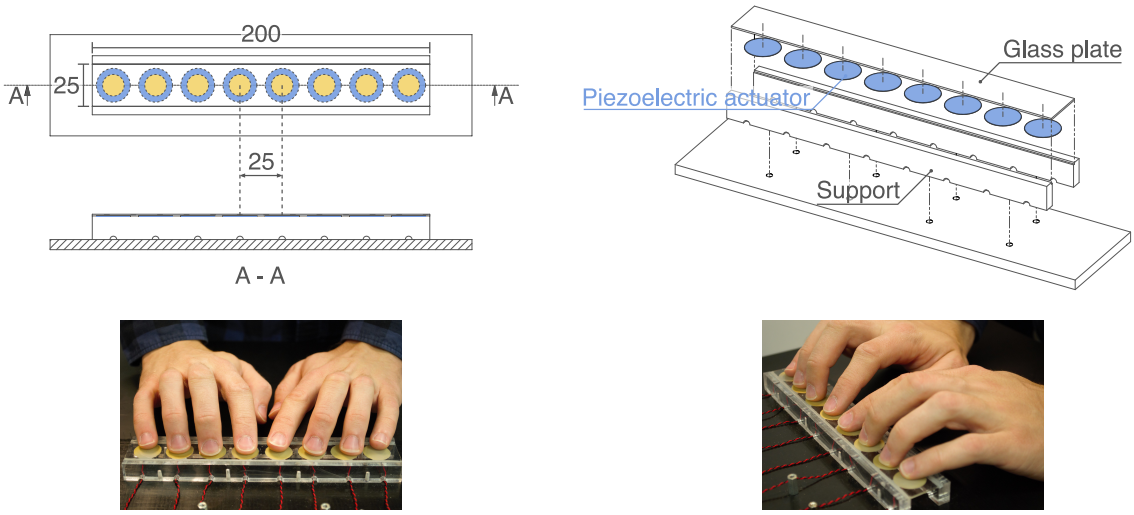

Figure 3.18: Demonstration prototype. A glass plate 25 × 200 × 1 mm^3 is bounded on its longer edges on a rigid frame and a set of 8 piezoelectric actuators distant of 25 mm is applied on its bottom side.

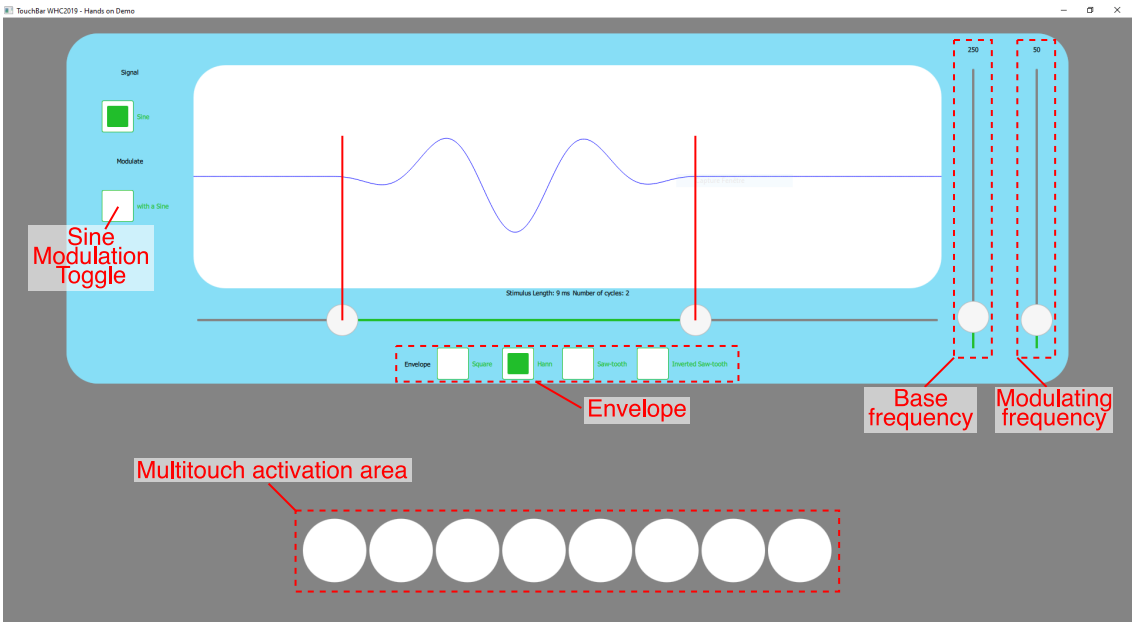

Figure 3.19: Demonstration interface. Upper side widgets allows for the design of the signal to be sent. Lower side area allow for the activation of one or more actuators with designed signal.

to avoid using too much actuators we can play with the spatial decay constant and calculate the optimal distance between actuators in order to provide a certain amplitude between the two when both are activated. The last solution is trickier as it use the funneling effect. The funneling effect is a haptic illusion allowing the creation of phamtom sensation between two excitation point on the skin. The effect can also be an "out of body" sensation i.e. between two fingers. In our case, for the out of body funneling effect to take place we need to have two fingers on two distinct vibration area [37].

The second question about the '2D' extension of our findings cannot be answered simply with the waveguide geometry. As a matter of fact, a wider waveguide would not provide a localized vibrotactile spot as we have seen before because the localization effect is only present on the length of the waveguide and not the width (next chapter provide more insight about that).

3.7. Discussion

This confinement technique is based solely on the geometry of the waveguide, which makes it very simple to implement. In the case of a piezoelectric array, it is sufficient to send the desired signals to obtain the desired effect. Different actuators were tested and showed a localized effect. The use of piezoelectric actuators should be preferred as the LRA and by extension all actuators relying on inertia to create vibrations (like ERM vibration motors), by there nature, can easily induce rigid-body motion to the structure. This rigid-body motion may be prevented by making the bounding structure more rigid or heavier. Also, localization effect is only present along the length of the waveguide and even narrow actuators cannot yield localized vibrations in the width of the waveguide. Wide actuators covering the whole width should thus be preferred in order to get higher vibration amplitude. The spatial resolution along the waveguide axis is given by both the actuator width and the attenuation rate of the plate. An array of piezoelectric actuators covering the entire surface would allow localized rendering of clicks by applying custom low frequency signals like Kim and Lee [31]. Such applications are possible because of the wide range of frequencies we can work in. Dynamic signals such as clicks can imply several frequencies, however, as long as those frequencies do not go beyond the cut-off frequency, the generated wave will be confined.

Also Kim et al. [3] showed that if two fingers are subjected to excitation with an amplitude difference of 20 dB, then a masking effect takes place and a stimulation will only be perceived at the finger subjected to the highest vibration. In our setup, we indeed verified that when two fingers are side by side, a stimulus is felt only on

the finger right on top of the actuated area. With the exponential decay, a distance as low as 1 cm is enough to reach the attenuation of 20 dB required for masking effects on two different hands to take place. This masking effect actually improves the localization of the vibrotactile feedback.

If we compare to other localization techniques [9–16] this method is simple. There is no active control nor heavy calculation to be made; what you send is what you get. Which also implies that latency can be kept to a minimum even with highly dynamic signal with large frequency spectrum. Also, because this method is independent from temperature, does not require any calibration and is not impacted by the user's touch, this method is therefore robust compared to other approaches relying on vibration control. This method is also compatible with different materials and can also be applied on curved surfaces as long as you keep a waveguide form and assure proper boundary conditions. We can also assume that, if you use piezoelectric actuators, current consumption can be kept at a minimum because we are working at low frequencies. However with all these advantages come some drawbacks. The method can only be used on narrow thin plates. Moreover, the localization is only in the actuator area, which makes it a discrete technology (like pin-arrays). As the actuators are not transparent, the method is limited to interactive surfaces where transparency is not necessary. And finally, since we do not use resonance, we have lower amplitudes leading to higher voltage requirement in the case of piezoelectric actuators.

3.8. CONCLUSION

THE presented non-propagative phenomenon at low frequency allows for the creation of local vibration fields above actuators. By driving the actuators at frequencies in the waveguide band-gap, we can produce local vibrotactile feedback to a set of small regions on the actuated surface directly above the actuator array. Hence, we can provide vibrotactile feedback at different frequencies and amplitudes to multiple fingers at the same time. The waveguide geometry cannot offer localization solutions to wide surfaces in its current state but it brought us the idea of "frequency band gaps" and inspired us to explore what kind of geometry could provide those for haptic applications.

NOMENCLATURE

ABBREVIATIONS

Abbreviation	Definition
ERM	Eccentric Rotating Mass
LRA	Linear Resonant Actuator
FRF	Frequency Response Function
FFT	Fast Fourier Transform
C-C	Clamped-Clamped boundary conditions
S-S	Simply supported-Simply supported boundary conditions
C-S	Clamped-Simply supported boundary conditions
C-F	Clamped-Free boundary conditions
rms	Root-Mean-Square (power measurement)

SYMBOLS

Symbol	Definition	Unit
b	Finger pulp viscosity	N.s/m
D	Bending stiffness	N.m
E	Young's modulus	GPa
f_1	First cut-off frequency	Hz
f_n	Cut-off frequency of the nth mode	Hz
$F(a)$	Harmonic force applied at point a	N
h	Thickness	m
H	Average transfer function	m/V
H_{ref}	Reference H transfer function value	m/V
H_{dB}	Average transfert function	dB
k	Wave number	rad/m
k_f	Finger pulp rigidity	N/m
k_x	Wave number along x	rad/m
k_y	Wave number along y	rad/m
L	Plate length	m
m	Mass	kg
m_f	Finger pulp moving mass	kg
n	Mode index	~
p	Wave number along x	rad/m
q	Wave number along y	rad/m
u	Transverse motion	m
U	Free displacement	m
$\widetilde{U}$	Loaded displacement	m
U_F	Displacement at point of excitation	m
V_F	Velocity at point of excitation	m/s
V_{pp}	Peak-to-Peak amplitude voltage	V
W	Plate width	m

Symbol	Definition	Unit
(x, y)	Space coordinates	m
(x_a, y_a)	Point a coordinates	m
(x_s, y_s)	Point force or excitation point coordinates	m
Z_p	Plate impedance	N.s/m
Z_f	Finger impedance	N.s/m
$Z_{p_{\text{semi-inf}}}$	Semi-infinite plate impedance	N.s/m
$Z_{p_{\text{finite}}}$	Finite plate impedance	N.s/m
γ_n	Spatial decay constant of mode n	rad/m
∇^4	Biharmonic operator	m^{-4}
μ	Attenuation brought by the finger to the plate	~
μ_{dB}	Attenuation brought by the finger to the plate	dB
ν	Poisson's ratio	~
ρ	Density	kg/m^3
ω	Circular frequency	rad/s
ω_n	Circular cut-off frequency	rad/s
$\delta(x)$	Dirac delta function	m^{-1}
$G(x, y, \omega)$	Green function	m/N
$\Psi(x)$	Displacement function along x	~
$\Phi(y)$	Displacement function along y	~
$\Theta(t)$	Time function	~

REFERENCES

[1] Ronald T. Verrillo. Psychophysics of vibrotactile stimulation. *The Journal of the Acoustical Society of America*, 77(1):225–232, January 1985. ISSN 0001-4966. doi: 10.1121/1.392263. URL https://asa.scitation.org/doi/abs/10.1121/1.392263.

[2] Masaaki Fukumoto and Toshiaki Sugimura. Active Click: Tactile Feedback for Touch Panels. In *CHI '01 Extended Abstracts on Human Factors in Computing Systems*, CHI EA '01, pages 121–122, New York, NY, USA, 2001. ACM. ISBN 978-1-58113-340-0. doi: 10.1145/634067.634141. URL http://doi.acm.org/10.1145/634067.634141. event-place: Seattle, Washington.

[3] Jin Ryong Kim, Xiaowei Dai, Xiang Cao, Carl Picciotto, Desney Tan, and Hong Z. Tan. A Masking Study of Key-Click Feedback Signals on a Virtual Keyboard. In Poika Isokoski and Jukka Springare, editors, *Haptics: Perception, Devices, Mobility, and Communication*, Lecture Notes in Computer Science, pages 247–257. Springer Berlin Heidelberg, 2012. ISBN 978-3-642-31401-8.

[4] Mélisande Biet, Frédéric Giraud, and Betty Lemaire-Semail. Squeeze film effect for the design of an ultrasonic tactile plate. *IEEE Transactions on Ultrasonics, Ferroelectrics, and Frequency Control*, 54(12):2678–2688, December 2007. ISSN 1525-8955. doi: 10.1109/TUFFC.2007.596. Conference Name: IEEE Transactions on Ultrasonics, Ferroelectrics, and Frequency Control.

[5] Corentin Bernard, Jocelyn Monnoyer, and Michaël Wiertlewski. Harmonious Textures: The Perceptual Dimensions of Synthetic Sinusoidal Gratings. In Domenico Prattichizzo, Hiroyuki Shinoda, Hong Z. Tan, Emanuele Ruffaldi, and Antonio Frisoli, editors, *Haptics: Science, Technology, and Applications*, Lecture Notes in Computer Science, pages 685–695, Cham, 2018. Springer International Publishing. ISBN 978-3-319-93399-3. doi: 10.1007/978-3-319-93399-3_58.

[6] Johan Kildal. 3D-press: haptic illusion of compliance when pressing on a rigid surface. In *International Conference on Multimodal Interfaces and the Workshop on Machine Learning for Multimodal Interaction on - ICMI-MLMI '10*, page 1, Beijing, China, 2010. ACM Press. ISBN 978-1-4503-0414-6. doi: 10.1145/1891903.1891931. URL http://portal.acm.org/citation.cfm?doid=1891903.1891931.

[7] Yon Visell, Bruno L. Giordano, Guillaume Millet, and Jeremy R. Cooperstock. Vibration Influences Haptic Perception of Surface Compliance During Walking. *PLOS ONE*, 6(3):e17697, March 2011. ISSN 1932-6203. doi: 10.1371/journal.pone.0017697. URL https://journals.plos.org/plosone/article?id=10.1371/journal.pone.0017697.

[8] Eric Vezzoli, Thomas Sednaoui, Michel Amberg, Frédéric Giraud, and Betty Lemaire-Semail. Texture Rendering Strategies with a High Fidelity - Capacitive Visual-Haptic Friction Control Device. In Fernando Bello, Hiroyuki Kajimoto, and Yon Visell, editors, *Haptics: Perception, Devices, Control, and Applications*,

Lecture Notes in Computer Science, pages 251–260. Springer International Publishing, 2016. ISBN 978-3-319-42321-0.

[9] Mingsian R. Bai and Yao Kun Tsai. Impact localization combined with haptic feedback for touch panel applications based on the time-reversal approach. *The Journal of the Acoustical Society of America*, 129(3):1297–1305, March 2011. ISSN 0001-4966. doi: 10.1121/1.3533725. URL https://asa.scitation.org/doi/10.1121/1.3533725.

[10] C. Hudin, J. Lozada, and V. Hayward. Localized Tactile Feedback on a Transparent Surface through Time-Reversal Wave Focusing. *IEEE Transactions on Haptics*, 8(2):188–198, April 2015. ISSN 1939-1412. doi: 10.1109/TOH.2015.2411267.

[11] S. Wöckel, U. Steinmann, and H. Arndt. Haptics by time reversal of elastic waves. In *2016 IEEE International Ultrasonics Symposium (IUS)*, pages 1–3, September 2016. doi: 10.1109/ULTSYM.2016.7728754. ISSN: 1948-5727.

[12] L. Pantera and C. Hudin. Sparse Actuator Array Combined with Inverse Filter for Multitouch Vibrotactile Stimulation. In *2019 IEEE World Haptics Conference (WHC)*, pages 19–24, July 2019. doi: 10.1109/WHC.2019.8816107.

[13] Charles Hudin and Sabrina Panëels. Localisation of Vibrotactile Stimuli with Spatio-Temporal Inverse Filtering. In Domenico Prattichizzo, Hiroyuki Shinoda, Hong Z. Tan, Emanuele Ruffaldi, and Antonio Frisoli, editors, *Haptics: Science, Technology, and Applications*, Lecture Notes in Computer Science, pages 338–350. Springer International Publishing, 2018. ISBN 978-3-319-93399-3.

[14] M. Tanter, J.-F. Aubry, J. Gerber, J.-L. Thomas, and M. Fink. Optimal focusing by spatio-temporal inverse filter. I. Basic principles. *The Journal of the Acoustical Society of America*, 110(1):37–47, July 2001. ISSN 0001-4966. doi: 10.1121/1.1377051. URL http://asa.scitation.org/doi/10.1121/1.1377051.

[15] Karl Katumu and Jenna L. Gorlewicz. Using modal superposition for generating localized tactile effects on variable friction touchscreens. In *2016 IEEE Haptics Symposium (HAPTICS)*, pages 211–216, April 2016. doi: 10.1109/HAPTICS.2016.7463179. ISSN: 2324-7355.

[16] Ehsan Enferad, Christophe Giraud-Audine, Frédéric Giraud, Michel Amberg, and Betty Lemaire Semail. Generating controlled localized stimulations on haptic displays by modal superimposition. *Journal of Sound and Vibration*, 449:196–213, June 2019. ISSN 0022-460X. doi: 10.1016/j.jsv.2019.02.039. URL http://www.sciencedirect.com/science/article/pii/S0022460X19301476.

[17] Takayuki Hoshi and Hiroyuki Shinoda. Airborne Ultrasound Tactile Display. In Hiroyuki Kajimoto, Satoshi Saga, and Masashi Konyo, editors, *Pervasive Haptics: Science, Design, and Application*, pages 121–138. Springer Japan, Tokyo, 2016. ISBN 978-4-431-55772-2. doi: 10.1007/978-4-431-55772-2_8. URL https://doi.org/10.1007/978-4-431-55772-2_8.

[18] C. Hudin. Local friction modulation using non-radiating ultrasonic vibrations. In *2017 IEEE World Haptics Conference (WHC)*, pages 19–24, June 2017. doi: 10.1109/WHC.2017.7989850.

[19] V. V. Krylov and F. J. B. S. Tilman. Acoustic 'black holes' for flexural waves as effective vibration dampers. *Journal of Sound and Vibration*, 274(3):605–619, July 2004. ISSN 0022-460X. doi: 10.1016/j.jsv.2003.05.010. URL http://www.sciencedirect.com/science/article/pii/S0022460X03009490.

[20] Stefano Papetti, Sébastien Schiesser, and Martin Fröhlich. Multi-Point Vibrotactile Feedback for an Expressive Musical Interface. In *Proceedings of the International Conference on New Interfaces for Musical Expression*, NIME 2015, pages 235–240, Baton Rouge, Louisiana, USA, 2015. The School of Music and the Center for Computation and Technology (CCT), Louisiana State University. ISBN 978-0-692-49547-6. URL http://dl.acm.org/citation.cfm?id=2993778.2993839. event-place: Baton Rouge, Louisiana, USA.

[21] T. Nara, Teruta Maeda, Yasuyuki Yanagida, and Susumu Tachi. Tactile display using ultrasonic elastic waves in a metal tapered membrane. In *1999 ASME International Mechanical Engineering Congress and Exposition, Haptic Interfaces for Virtual Environment and Teleoperator Systems Symposium*, volume 67, pages 283–288, Nashville, U.S.A, January 1999.

[22] Michaël Wiertlewski, Rebecca Fenton Friesen, and J. Edward Colgate. Partial squeeze film levitation modulates fingertip friction. *Proceedings of the National Academy of Sciences*, 113(33):9210–9215, August 2016. ISSN 0027-8424, 1091-6490. doi: 10.1073/pnas.1603908113. URL https://www.pnas.org/content/113/33/9210. Publisher: National Academy of Sciences Section: Physical Sciences.

[23] Richard Feynman. *The Feynman Lectures on Physics, vol.2*. Addison-Wesley, Boston, 1963. URL https://www.feynmanlectures.caltech.edu/II_24.html.

[24] Stan Gibilisco and Neil Sclater. *Encyclopedia of Electronics*. Tab Professional & Reference, Blue Ridge Summit, PA, subsequent edition edition, January 1985. ISBN 978-0-8306-3389-0.

[25] Allan W. Snyder and John D. Love. *Optical Waveguide Theory*. Springer US, Boston, MA, 1984. ISBN 978-0-412-24250-2 978-1-4613-2813-1. doi: 10.1007/978-1-4613-2813-1. URL http://link.springer.com/10.1007/978-1-4613-2813-1.

[26] Leonid A. Belov, Sergey M. Smolskiy, and Victor N. Kochemasov. *Handbook of RF, Microwave, and Millimeter-Wave Components*. Artech House, 1er édition edition, September 2012.

[27] Ian Hunter. *Theory and Design of Microwave Filters*. IET, The Institution of Engineering and Technology, Michael Faraday House, Six Hills Way, Stevenage SG1

2AY, UK, January 2001. ISBN 978-0-85296-777-5. doi: 10.1049/PBEW048E. URL https://digital-library.theiet.org/content/books/ew/pbew048e.

[28] Karl F Graff. *Wave motion in elastic solids*. Dover Publications, New York, 1991. ISBN 978-0-486-13957-9 978-1-62198-646-1. URL http://www.freading.com/ebooks/details/r:download/ZnJlYWQ6OTc4MDQ4NjEzOTU3OTpl. OCLC: 829198880.

[29] A. W. Leissa. *Vibration Of Plates*, volume NASA SP-160 of *NASA SP-160*. NASA, Ohio State University Columbus, Ohio, 1969.

[30] Victor Giurgiutiu. Chapter 8 - Coupling of PWAS Transducers to the Monitored Structure. In Victor Giurgiutiu, editor, *Structural Health Monitoring with Piezoelectric Wafer Active Sensors (Second Edition)*, pages 395–443. Academic Press, Oxford, January 2014. ISBN 978-0-12-418691-0. doi: 10.1016/B978-0-12-418691-0.00008-3. URL https://www.sciencedirect.com/science/article/pii/B9780124186910000083.

[31] Sunjun Kim and Geehyuk Lee. Haptic Feedback Design for a Virtual Button Along Force-displacement Curves. In *Proceedings of the 26th Annual ACM Symposium on User Interface Software and Technology*, UIST '13, pages 91–96, New York, NY, USA, 2013. ACM. ISBN 978-1-4503-2268-3. doi: 10.1145/2501988.2502041. URL http://doi.acm.org/10.1145/2501988.2502041.

[32] Heinsten Frederich Leal dos Santos, Bryan Willy Gonçalves, and Guilherme Silva Prado. UNCERTAINTIES ON ADHESIVE LAYER FOR A CANTILEVER BEAM: PASSIVE CONTROL. In *Procceedings of the 24th ABCM International Congress of Mechanicl Engineering*. ABCM, 2017. doi: 10.26678/ABCM.COBEM2017.COB17-2008. URL http://abcm.org.br/anais-de-eventos/COB17/2008.

[33] Hamid Asadi Dereshgi, Huseyin Dal, and Mehmet Emin Sayan. Analytical analysis of a circular unimorph piezoelectric actuator in the range of low voltages and pressures. *Microsystem Technologies*, 26(8):2453–2464, August 2020. ISSN 1432-1858. doi: 10.1007/s00542-020-04786-w. URL https://doi.org/10.1007/s00542-020-04786-w.

[34] Lynette A. Jones and Susan J. Lederman. *Human Hand Function*. Oxford University Press, Oxford, New York, May 2006. ISBN 978-0-19-517315-4.

[35] Michael Wiertlewski and Vincent Hayward. Mechanical behavior of the fingertip in the range of frequencies and displacements relevant to touch. *Journal of Biomechanics*, 45(11):1869–1874, July 2012. ISSN 0021-9290. doi: 10.1016/j.jbiomech.2012.05.045. URL http://www.sciencedirect.com/science/article/pii/S0021929012003260.

[36] A. Z. Hajian and R. D. Howe. Identification of the Mechanical Impedance at the Human Finger Tip. *Journal of Biomechanical Engineering*, 119(1):109–114, February 1997. ISSN 0148-0731. doi: 10.1115/1.2796052. URL https:

//asmedigitalcollection.asme.org/biomechanical/article/119/1/109/398500/Identification-of-the-Mechanical-Impedance-at-the.

[37] Mathilde Jeannin, Ayoub Ben Dhiab, Lucie Pantera, Charles Hudin, and Sabrina Panëels. The Funneling Illusion Using the Confinement of Vibrotactile Stimuli in Narrow Plates. In *2021 IEEE World Haptics Conference (WHC)*, pages 1147–1147, July 2021. doi: 10.1109/WHC49131.2021.9517236.

4

Confinement of Vibrotactile Stimuli on Wider Surfaces

For multi-touch and multi-user interactions on a touch surface, providing a local vibrotactile feedback is essential. Usually, vibration propagation impedes this localization. Previous work showed that narrow strip-shaped plates could allow the confinement of vibrotactile stimuli to the actuated area. Adding to this principle, periodically supported plates also provide a non-propagative effect at low frequencies. Using both geometrical properties, we provide a device allowing a multi-touch interaction through an array of piezoelectric actuator. Experimental validation show that vibrations are well confined on top of actuated areas with vibration amplitude over two micrometers.

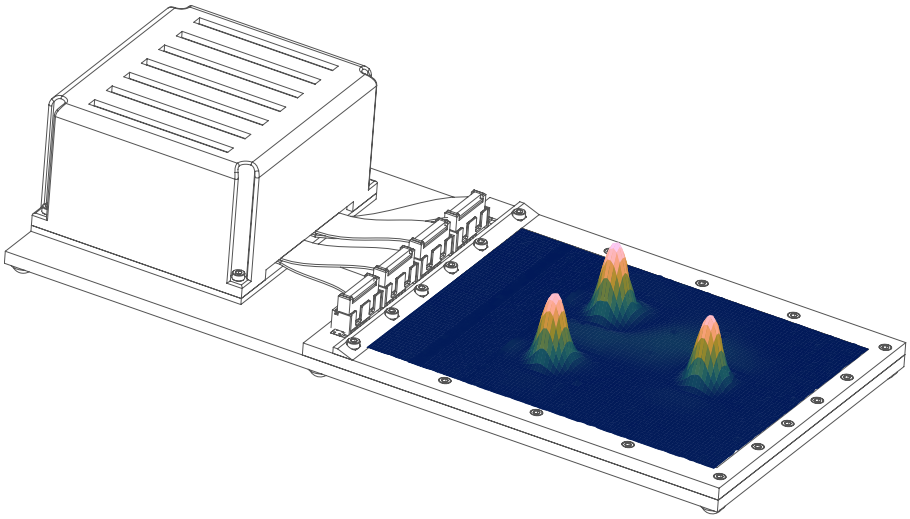

Parts of this chapter have been published in A. Ben Dhiab et C. Hudin, « Confinement of Vibrotactile Stimuli in Periodically Supported Plates », in Haptics: Science, Technology, Applications, Cham, 2020, p. 334-342. doi: 10.1007/978-3-030-58147-3_37.

4

Outline

4.1. INTRODUCTION

In chapter 3 we have shown that it is possible to obtain localized deformations above the actuated regions for low frequency signals in narrow thin plates (1D). A particularity of this technique is that it allows the spatial localization of low-frequency stimuli i.e. a local deformation of the plate even if we use low-frequencies with long wavelength. In addition, finger interaction does not attenuate low-frequency evanescent waves. No matter the surface in contact, i.e. finger, hand, arm, foot⋯the behavior of the vibrating plate is not impacted and a localized stimuli can be provided. Although interesting, this approach is limited to narrow plates. However, for a rich multi-touch interaction, extending this approach to an arbitrary 2D plate becomes necessary and is the focus of this chapter. Because waves tend to directly propagate in 2D plates, their confinement isn't trivial.

As discussed in chapter 2, for spatial localization of vibrations, i.e. the creation of local deformation at a point or area of the plate, there are two techniques: *Time-Reversal* [1] and *Modal Superimposition* [2]. For these two techniques, the wavelength of the vibrations to obtain a local deformation at the centimeter or millimeter scale necessarily involves high frequencies. The *Time-Reversal Wave Focusing* technique uses the propagation of elastic waves to generate constructive interference at a given time and position on the plate. The acceleration peak created by the focusing of the waves causes the ejection of a static or moving finger-pulp, giving a haptic feedback smaller than the fingertip. However, this approach needs a calibration procedure and is subjected to external parameters (e.g. temperature, finger interaction), which can impede the tactile stimulation. As for *Modal Superimposition*, it uses a truncated modal decomposition to focus a deformation shape and control its position. The high frequencies produced by an array of piezoelectric actuators allow for the appearance of a tactile lubrication phenomenon, i.e. a variation in friction that is only felt when the finger is moved [3]. Both techniques rely on propagation of high frequency waves. During user interaction, the non-linear behavior of the finger significantly modifies the vibrational behavior of the plate. Such modifications are particularly striking for high frequencies thus leading to many complications (incl. flexural waves scattering, mode damping, mode translation).

In order to avoid these limitations and provide a haptic feedback both to static and moving fingers, the *Inverse-Filter* approach [4] proposes to dynamically control low-frequency waves, which are less impacted by finger interaction, to provide the user with the desired stimuli only at the contact points. Nonetheless, this technique is based on computation, signal processing and calibration procedures. As this technique uses waves within the tactile frequency range (10-1000 Hz), it induces a global

movement of the plate and therefore limits the interaction on a number of control points. Generally, all the previously mentioned methods depend on wave propagation and thus, are in need of calculations and signal processing in order to achieve localization.

This thesis looks into other methods relying on boundary conditions, geometry and material that could overcome such requirements. In this chapter, we investigate how frequency band-gaps can be obtained using periodic structures.

4.2. LATE MODE ACTIVATION

WAVEGUIDES and their cut-off frequencies introduced us to a more general view related to late mode activation. What are the conditions in which late mode activation can take place? Let's take the case of a squared 2D-plate of dimension $a \times a \times h$ simply-supported on all its edges. In this case the natural frequencies can be expressed analytically by:

$$\omega_n = \sqrt{\frac{D}{\rho h}} \frac{\pi^2}{a^2} \left(2n^2\right) \tag{4.1}$$

The first mode to appear is for $n = 1$, thus giving:

$$\omega_1 = 2\sqrt{\frac{D}{\rho h}} \frac{\pi^2}{a^2} = 2\sqrt{\frac{Eh^2}{12(1-\nu^2)\rho}} \frac{\pi^2}{a^2} \tag{4.2}$$

We are searching to maximize ω_1. To this end, a first solution is to tinker with the plate dimensions to maximize the ratio h/a^2. The thickness having an important impact on amplitudes (essential in our applications) we can only change the size a which would have to be small (see Figure 4.2.a).

For example, taking a glass plate ($E = 64$ GPa, $\rho = 2230$ kg/m^3 and $\nu = 0.2$) of $75 \times 75 \times 0.7$ mm^3, we simulate the frequency behavior under the excitation of a squared piezoelectric of size $10 \times 10 \times 0.5$ mm^3. Figure 4.1 shows the frequency response function (FRF). The plots of the average response inside and outside the actuator shows the first resonance of our system being around 580 Hz. By representing mappings at frequencies before and after the first resonance, we can properly see: evanescence with a decay constant related to the expression (3.17) found in chapter 3 and propagation respectively. To have a high localization contrast, we would have to reduce a leading to the case treated in chapter 3. We could also play on boundary conditions to get a higher frequency for the activation of the first mode. As we did in 3.2.2, by using the expressions in [5][Chapter 4], we can find for the same plate that

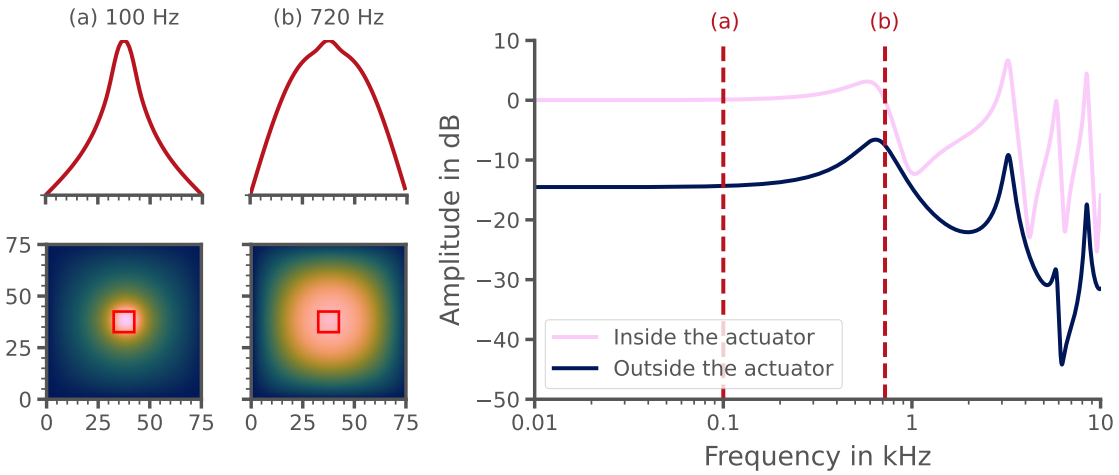

Figure 4.1: Simulation of a $75 \times 75 \times 0.7$ mm^3 glass plate excited with a square piezoelectric actuator in its center. The first resonance is around 580 Hz. (a) Before the first resonance, we have an evanescent behavior. (b) After the first mode, propagation occurs and we have a uniform distribution of vibration energy across the surface.

ω_1 of a clamped plate is around 3 times higher than for a simply supported plate.

An other solution would be to choose a material with the ratio $E/(1-\nu)\rho$ the higher possible. Figure 4.2b. shows the location of several material in regard to their cut-off frequency in the case of a plate of dimension $75 \times 75 \times 0.7$ mm^3. (We rounded the Poisson's ratio of all material to 0.3 for representation purposes as it does not heavily influence obtained ω_1.) We can see that it is difficult to obtain the first mode activation over 1 kHz, if not impossible, because homogeneous materials displaying both high stiffness ($E \nearrow$) and lightness ($\rho \searrow$) do not exist. Thus researchers came up with composite material like carbon fiber reinforced plastic which stands out from homogeneous materials in Figure 4.2.b. Unfortunately using composite materials for haptic application or everyday touch screen do not seem to be feasible as we would have to find a composite material with a high cut off-frequency, transparent (to see the screen behind it) and pleasant to the touch.

Another way than composite material to get high stiffness while maintaining low weight would be the use of stiffeners or ribs like in aeronautical structures. Such structures display peculiar properties regarding wave propagation. In particular, periodically stiffened structures present frequency band-gaps where stiffeners confine vibrations. This can be seen for example in the article by Ege et al. [6][p.22] studying piano soundboards. Next section will discuss the use of periodically placed supports for the localization of low frequency stimuli.

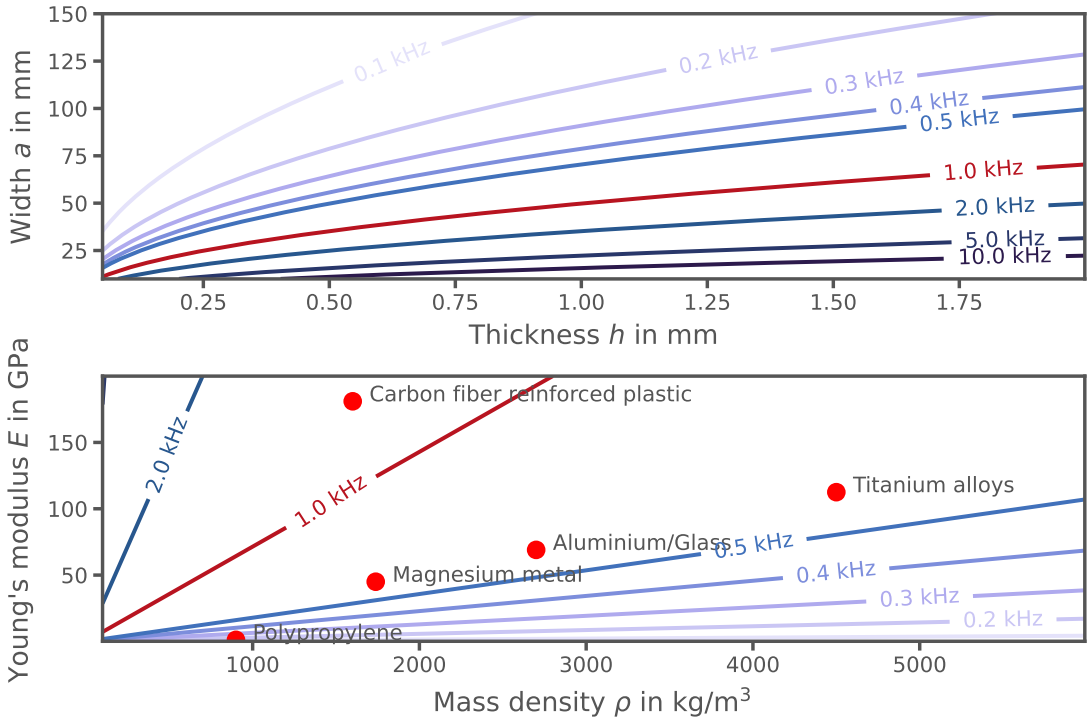

Figure 4.2: Abacus. Upper: First mode frequency abacus of a glass plate depending on its geometrical properties. Lower: First mode frequency abacus of a $75 \times 75 \times 0.7$ mm^3 plate depending on its material properties ($\nu = 0.3$).

4.3. Wave Propagation in Periodic Structures

Periodic structures consists in the connection in an identical manner of a number of identical elements to one another. One can construct a periodic structure by assembling together similar elements or by dividing a uniform structure in identical elements. Our case is the latter as we consider a uniform medium which is rendered periodic by the application of regularly spaced supports.

Taking advantage of the spatially periodic property of such structure, it is possible to predict in simple cases the structure behavior by considering just one of the periodic element together with the boundary conditions. Through Mead's research [7], we know that the amplitude of any point in one element is e^{μ} times the amplitude of the corresponding point in the previous element. Thus :

$$u(x + L_x) = u(x)e^{\mu}, \text{ with } \mu = \mu_r + j\mu_i \tag{4.3}$$

μ is an attenuation constant that depends on frequency and spatial resolution of the supports. In following sections we express μ for periodic rigid simple supports. To do so, it is interesting to consider that periodic supports/constraints are imposing forces or moments at regular intervals. Considering this "phased array" of forces and/or

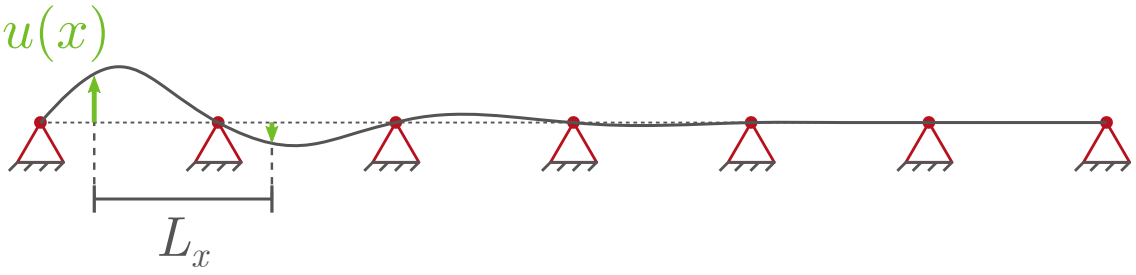

Figure 4.3: Mead's assumption on the propagation of waves in periodically supported mediums.

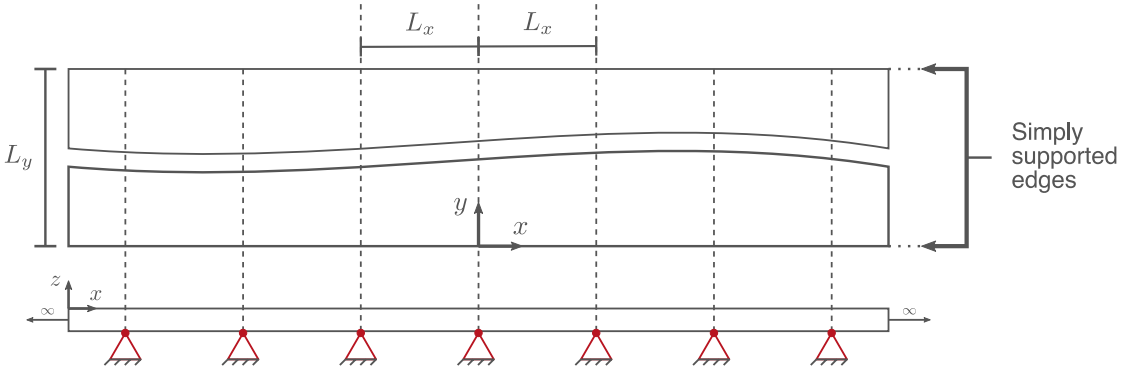

Figure 4.4: Plate bounded to a set of equispaced identical supports in the y-direction and simply-supported on its x-wise edges.

moments, the attenuation constant μ can be expressed to find frequency band-gaps in our structure.

4.3.1. PROPAGATION CONSTANT μ

When free wave motion occurs in a medium with periodic rigid simple supports, they exert only a phased array of forces on the plate. This implies that μ must satisfy the condition that the displacement at each simple support is null thus leading to the following expression [7]:

$$\cosh(\mu) = \frac{a_1 \sinh(k_1 W)\cosh(k_2 W) + a_2 \sinh(k_2 W)\cosh(k_1 W)}{a_1 \sinh(k_1 W) + a_2 \sinh(k_2 W)} \tag{4.4}$$

k_1 and k_2 are wave numbers of the uninterrupted uniform medium and depends on the medium considered i.e. an Euler-Bernoulli beam or a Kirchhoff plate. a_1, a_2 are terms depending on the medium, types of supports and boundary conditions.

4.3.2. Case of an infinite plate with simply-supported edges and periodic structure

Formulation

Following Figure 4.4, we have now a semi-infinite plate with a width L_y simply-supported on x-wise edges. Identical supports/constraint equidistant of L_x are applied in the y-direction forming the periodic structure. This case have already been treated by [8, Appendix B]. Spatial symmetry and periodicity allowed to reduce the problem from a two-dimensional system to a one-dimensional structure theory. By supposing that supports/contraints submit the plate to a harmonic force displacement across the plate at $x = 0$, Mead expresses terms of interest as:

$$a_1 = -\frac{1}{2Dk_{x_1}\left(k_{x_1}^2 - k_{x_2}^2\right)}, \quad a_2 = \frac{1}{2Dk_{x_2}\left(k_{x_1}^2 - k_{x_2}^2\right)} \tag{4.5}$$

with:

$$k_{x_1} = \sqrt{k_y^2 + \sqrt{\frac{\rho h}{D}}\omega}, \quad k_{x_2} = \sqrt{k_y^2 - \sqrt{\frac{\rho h}{D}}\omega}, \quad k_y = \frac{n\pi}{L_y} \tag{4.6}$$

Which forms the following displacement expression:

$$u(x,y,t) = \left(P_0 a_1 \mathrm{e}^{-k_{x_1}x} + P_0 a_2 \mathrm{e}^{-k_{x_2}x}\right)\sin(k_y y)\mathrm{e}^{i\omega t} \tag{4.7}$$

where P_0 is the force amplitude applied to the plate by the supports.

Propagation constant simulation

Taking the expressions of a_1, a_2, k_{x_1} and k_{x_2} we can calculate μ with equation (4.4). Figure 4.5 represent the evolution of the propagation constant μ over an extended frequency range. We can notice two types of regions: one where the imaginary part of the propagation constant μ_i is constant while the real part μ_r is non-zero, and the other where the imaginary part is varying and the real part is zero and constant. Both regions corresponds to attenuation and propagation zones respectively. As the evolution of waves depends on e^{μ} between each junctions, when μ_i is constant all wave motions decay, and when μ_i varies propagation occurs. We thus have a succession of attenuating zones (band-gaps) and propagating zones (pass-bands). This frequency feature can be observed in all periodic structures. Natural frequencies as well as maximum vibration amplitudes are usually found inside the propagation zones and depends significantly on the phase constant within these bands.

In our case we are interested in the first attenuation zone. Its range depends on the lower bounding frequency of the following propagation zone which is identical

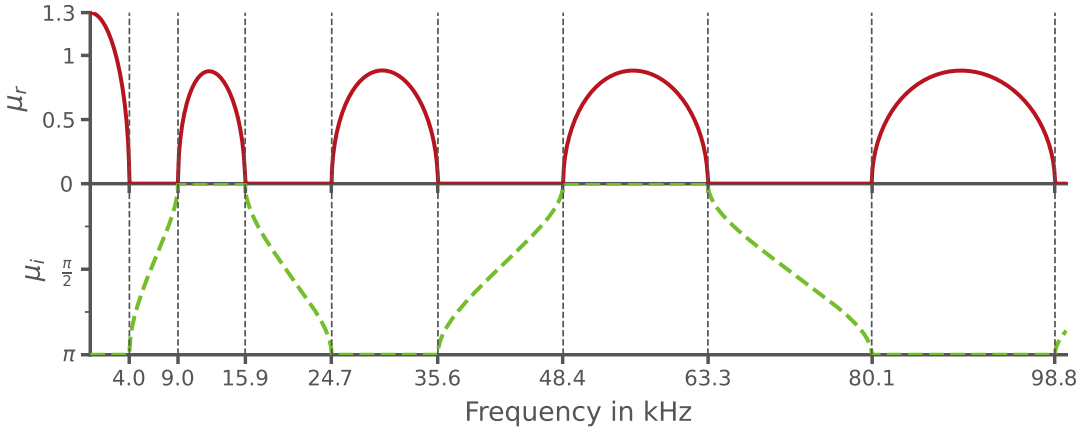

Figure 4.5: Representation of the real part (solid red line) and imaginary part (dashed green line) of the propagation constant μ for a simply-supported semi-infinite plate of width $L_y = 175$ mm on periodic rigid simple supports equispaced of $L_x = 21.2$ mm. When μ is real we have attenuation between each beam sections. When μ is purely imaginary we have propagation. The alternation between real and imaginary part forms a set of propagation and attenuation band-gaps.

with the fundamental natural frequency of one junction element. In other words, the cut-off frequency of a junction in the y-direction corresponds to the upper bounding frequency of our first attenuation zone found in the x-direction. Thus, a plate with periodic supports is defined by a cut-off frequency under which vibrations will be confined to the actuated area.

4.3.3. Experimental validation

Apparatus

To verify the spatial localization of low-frequency waves provided by our method, we have set up a system designed to allow a user to freely explore a surface. The size of the device thus corresponds to the size of an adult hand, and the number of areas formed corresponds to the number of fingers. The only requirement associated with the implementation of this method is having a plate correctly bounded periodically to a rigid frame. If each created area have a waveguide geometry, late mode activation occurs and a localized vibration can be obtained in both axis.

Mechanical components. The apparatus consists in a glass plate, measuring 150 × 130 × 0.5 mm^3, bounded on a set of 6 equidistant supports of width 4 mm forming 5 areas. In order to provide haptic feedbacks, piezoelectric actuators (muRata 7BB-20-3) of circular geometry, composed of two parts: a plate of diameter 20 mm, thickness of 0.1 mm; and a piezoelectric transducer of diameter 12.8 mm, thickness of 0.11 mm, were glued on the bottom side of the plate between each supports. The out of plane

displacement of the surface is measured by a laser vibrometer (OFV-505/OFV-5000) mounted on a motorized 3 axis platform. This setup is illustrated on Figure 4.6.

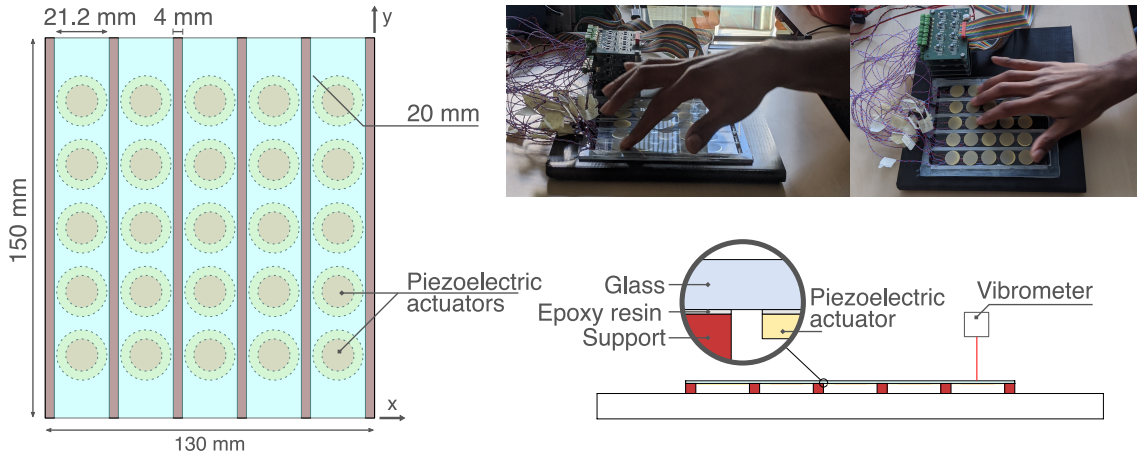

Figure 4.6: Experimental setup. A glass plate is bounded onto a set of 6 equidistant supports with epoxy resin. The actuators are glued to the bottom of the plate, 5 per area between each rib, for a total of 25 actuators.

Driving components. Because vibration localization is induced by the propagation medium geometry, no specific calculation nor wave control implementation are needed. Signal amplification for each actuators was assured by a Piezo Haptics Driver DRV8662 from Texas Instrument. A voltage output module NI-9264 was used to send requested analog signals to each driver for amplification. Communication with the NI-9264 voltage output module and signal design was made with Python using the PyDAQmx package [9].

System frequency response function (FRF)

The frequency response function or FRF (ratio of the displacement at a given point to the voltage applied to an actuator in the frequency domain) for the actuator was measured by sending a linear sweep signal of 40 V amplitude going from 0 Hz to 5 kHz sampled at 10 kHz. All measurements were assured by a Doppler vibrometer OFV-505/OFV-5000 mounted on a motorized 3 axis platform. Figure 4.7 displays FRFs at the center of the actuator (light pink) and outside the actuator in the same junction (light green) and in the adjacent junction (dark blue). A noticeable difference of 20 dB in average spreading from 0 to 1 kHz can be observed between inside and outside the actuator. In this frequency band gap, elastic waves do not propagate throughout the plate. The FRFs at other points were also measured and show the same behavior, though with some differences. Unfortunately, proper clamping conditions were not assured during the mounting process thus leading to different cut-off frequencies at other points. The boundary condition being made with epoxy resin we can assume

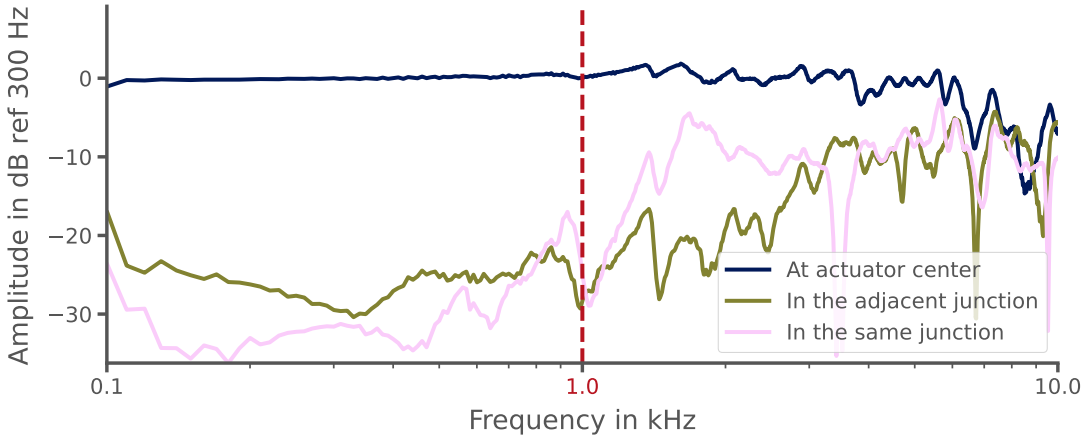

Figure 4.7: Experimental system frequency response function (FRF) $H_{\mathrm{dB}} = 20\log_{10}|H|$ at the center of the activated actuator and outside in two points outside the actuator located in the adjacent junction and same junction to the actuator.

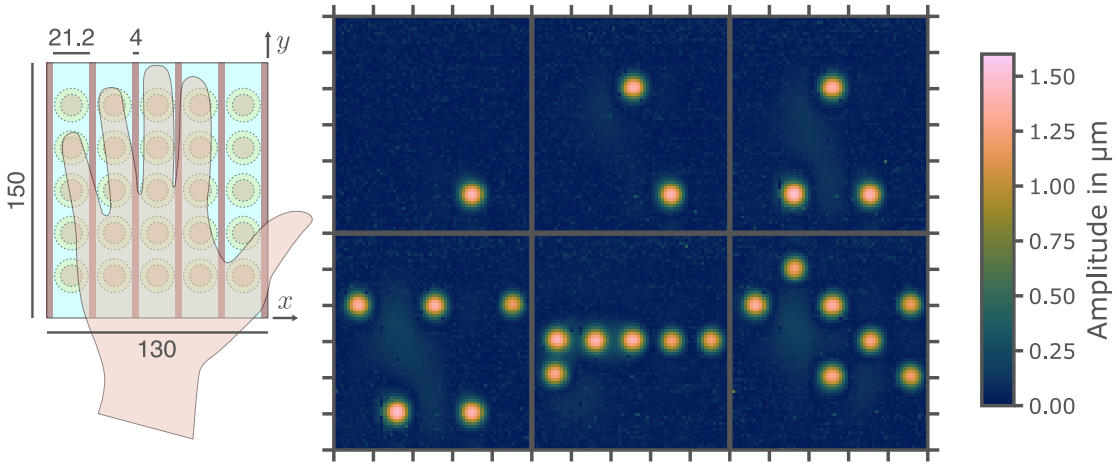

Figure 4.8: Quadratic mean of the out of plane displacement of the plate for 1, 2, 3, 5, 6 and 7 actuators activated at same time. Vibration sources are localized and reach a vibration rms amplitude above 1.6 μm while most of the un-actuated area of the plate stays at rest.

that eventual air bubbles or gaps could have been left and implying behavior differences between each area and locally within each area. This observation becomes clearer in the following sections.

STIMULI CONFINEMENT

To illustrate the spatial localization of vibrotactile stimuli allowed by the device, we mapped the out of plane displacement of the plate submitted to signals sent with multiple piezoelectric actuators. We chose a 250 Hz (tactile sensitivity peak [10]) 5 cycles burst excitation and a driving voltage amplitude of a 100 V for every actuator used. Figure 4.8 shows the maximum displacement throughout the plate when using 1, 2, 3, 5, 6 and 7 actuators at the same time. We can notice that waves are confined

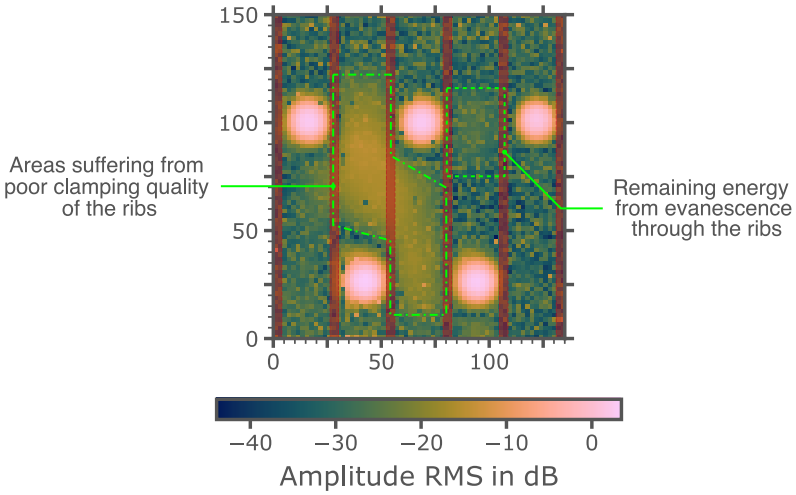

Figure 4.9: Quadratic mean with a logarithmic scale of the plate submitted to 5 activated actuators. Most of the energy is localized above each piezoelectric actuator but leaks due to poor bounding conditions can be noticed.

above activated actuators with RMS amplitudes reaching 1.5 μm inside the actuator area. Outside the actuated area, waves propagating along the y-axis are evanescent and die exponentially. Along the x-axis, we also have evanescence but this time due to the periodical supports. The energy representation with a logarithmic scale of Figure 4.9 shows certain areas of interest. Apart from the localized energy above each actuated area, we can note leaks (light green dash-dot frame) with a 15 dB amplitude difference between vibrations inside actuated areas and leaked vibrations while other areas present a 30 dB difference. This leak is actually due to clamping imperfection caused during the prototype assembly. Another area which is less visible (light green dashed frame), asses the evanescent behavior along the x-axis due to the set of supports. This important loss of energy (around 25 dB loss) comes from the evanescence behavior and the width of the supports which, by providing strong bending moments, reduce the transmitted energy. The use of thinner supports would also provide a localized effect as long as their stiffness (in both translation and rotation) are guarantied.

4.4. Demonstration Prototype

For the EuroHaptics 2020 we prepared a prototype for demonstration purpose. In the same way as Section 3.6, we wanted to show the spatial localization of vibrotactile stimuli as well as the possibility of multi-point feedback and the exploration freedom provided by this approach.

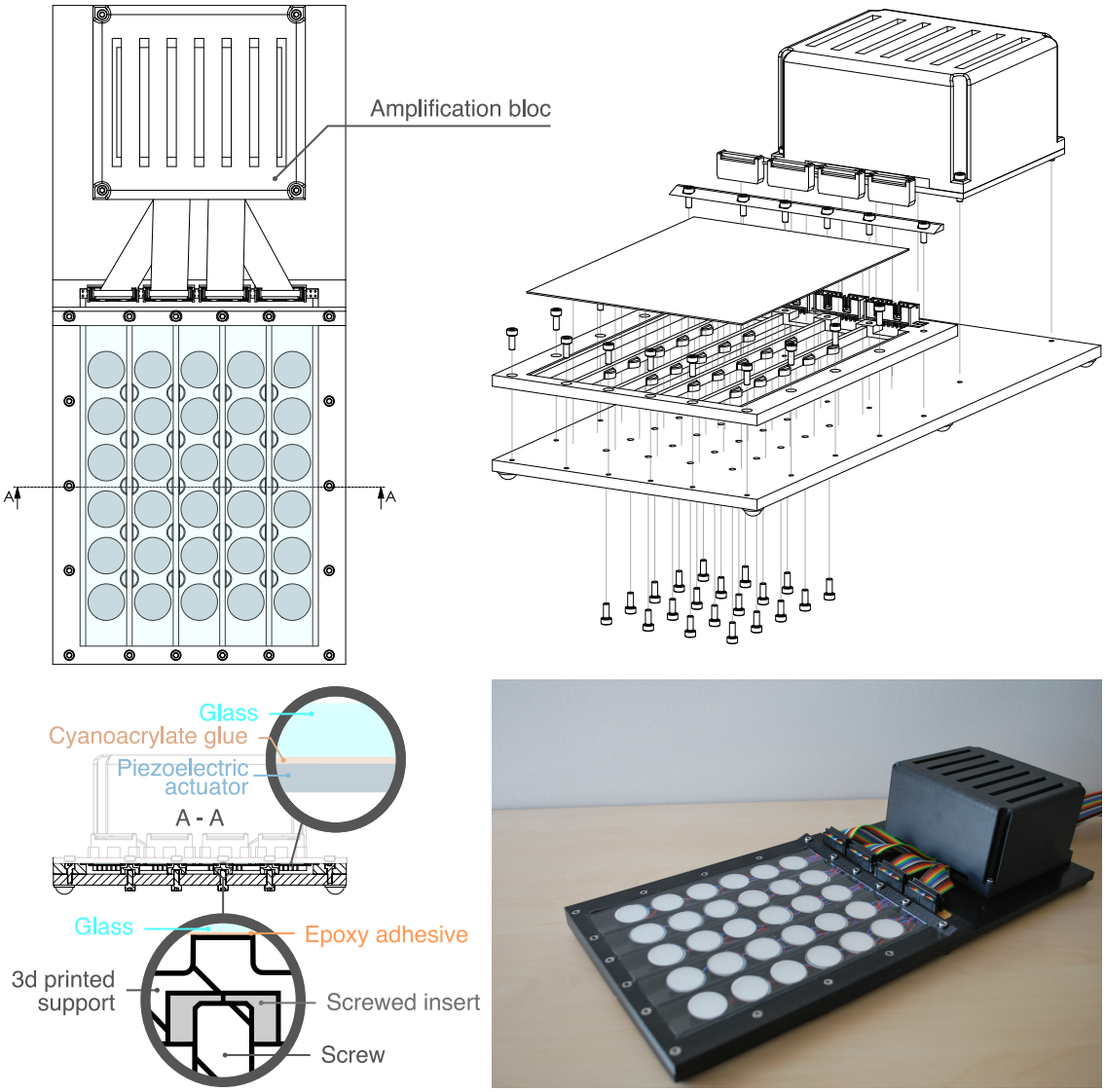

Figure 4.10: Demonstration prototype. A glass plate 175 × 130 × 0.7 mm^3 is bounded to periodic rigid supports forming 5 sub-areas with a waveguide form. In each 5 sections 6 piezoelectric actuators were applied thus forming an array of 30 actuators with a spatial resolution of 25 mm.

4.4.1. HARDWARE AND SOFTWARE

This haptic prototype was designed thinking that users would want to explore the surface with their whole hand. The size of the interaction area 175 × 130 × 0.7 mm^3 thus corresponds to the size of an adult hand. The spacing of the periodic supports 21.2 mm was chosen by experience because it allowed a cut-off frequency above 1 kHz and sufficient amplitudes for haptic applications, coincidentally it also allowed to form 5 areas (1 area for each fingers in the case of a static hand resting on the device). We applied 6 actuators per area, thus forming a matrix of 30 actuators equispaced of 25 mm in both direction (Figure 4.10). Measurements showed that amplitudes reached 4 μm (8 μm peak-to-peak). In order to drive each actuator, we used 30

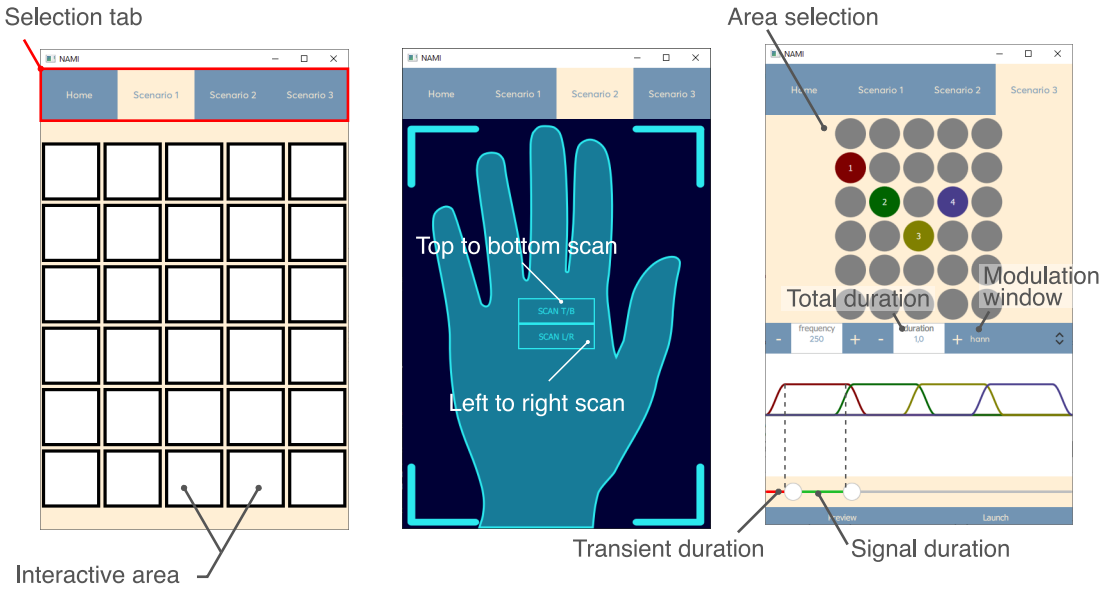

Figure 4.11: Qt interface consisting of three scenarios.

Piezo Haptics Driver DRV8662 from Texas Instrument integrated in a custom-made lookalike circuit of the of the DRV8662 evaluation module. Two voltage output modules NI-9264 were used to send requested analog signals to each driver for amplification.

Using Qt, we programmed an interface on a touchpad offering 3 scenarios (Figure 4.11). The first one allowed the user to activate one or more of the 30 areas available. The second one was using apparent movement to give the illusion of a continuous wave traveling throughout the hand from one side to another. The last one gave the possibility to the user to create a spatial pattern by selecting the areas to be activated as well as the activation timing and window thus allowing static (simultaneous activation) or dynamic (i.e. phantom illusions) patterns.

4.4.2. ADDITIONAL MEASUREMENTS

The last apparatus presented some assembly defects which limited us on its frequency analysis. With this new prototype we tried to extend our analysis to higher frequencies. Unfortunately, analyzing the system in terms of wave numbers did not lead to any usable results and did not allow us to highlight the notion of propagation constant mentioned earlier. However, by observing the frequency spectrum in space we can still distinguish certain behaviors. In Figure 4.12, we can see that localization is still present at frequencies as high as 2.6 kHz. Going further in frequency, even-though the plate is strongly bonded to the frame through the ribs, energy spreads throughout the plate with some particularities. Again, we cannot draw clear boundaries and define propagation and attenuation zones but we can observe that de-

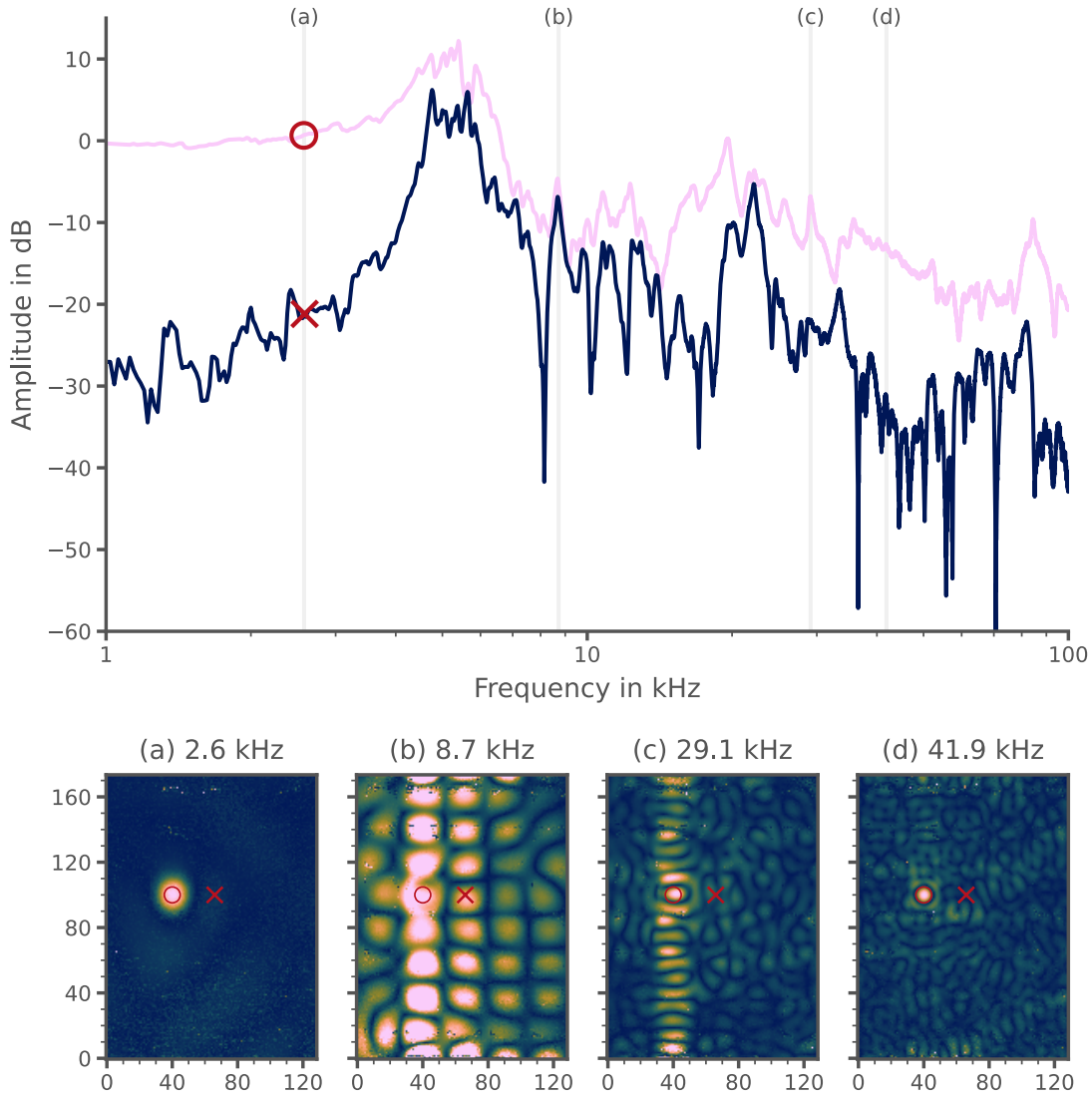

Figure 4.12: Top: System frequency response function (FRF) $H_{\text{dB}} = 20\log_{10}|H|$ inside and outside the activated zone. Bottom: Plate behavior at different frequency.

pending on the frequency the energy can easily spread throughout the plate (Figure 4.12(b)) or is strongly attenuated and confined to its region of origin (Figure 4.12(c)). The last case depicted in Figure 4.12(d) is not exclusive to plates with periodic structures and comes from an interference phenomenon produced by the nature of the piezoelectric actuation. This "feature" of piezoelectric actuation was used in previous research by Hudin [11] and is further discussed in chapter 5.

4.4.3. AUDIENCE FEEDBACK AND DISCUSSION

Due to the Covid-19 outbreak the setup was not presented during the EHC2020 in Leiden, Netherlands. But fortunately we were still able to present it during a presenta-

tion at the ISIR laboratory of Sorbonne University. Like our first prototype presented in chapter 3, people were surprised that we could easily produce local feedback and produce apparent movement throughout the hand. Most questions were about the resolution of such device and the integration capability in tactile devices.

The haptic resolution depends on two things, the number of actuators and the number of periodical supports. Increasing the number of actuators would be really interesting and beneficial but the apparatus would have to be made with proper procedures for applying piezoelectric array and supports. As a matter of fact, we saw previously that this localization technique depends almost entirely, if not entirely, on the quality of bonding procedures. Low quality bounding directly lead to energy leakage and loss of localization and contrast. Increasing the number of supports while keeping the same plate dimensions would lead to lower amplitudes and a wider low frequency band gap. We also have to keep in mind that supports have a certain geometry and stiffness which define the frequency evolution of the propagation constant μ. With thin supports, chances are that the rigidity in translation and rotation would imply pairs of solutions for μ at each frequency thus leading to some propagation in attenuation zones.

4.5. Discussion and Perspective

The presented method can provide localized vibrotactile feedback in several areas of a continuous plate. The confinement is achieved along both axis by low frequency evanescence phenomenon: one based on the geometry of the propagation medium; the other based on the periodically placed supports. This system is particularly unique and there is to our knowledge no setup with such capabilities and we believe that our device offers new possibilities for studying the tactile perception and to develop new interactions. The interface is simple and robust, i.e. it does not require any special signal processing or computation to work and is not impacted by user interaction. However, since evanescent waves are used, the localization of stimuli is only done in the area of each actuator. In order to increase the resolution of such a device, the number of actuators must be multiplied as well as the number of supports. It raises questions about the control electronics, the power consumption and the available amplitude (sufficient amplitudes cannot be guaranteed with small actuators).

Another point that can also be addressed is concerning possible use case of such device. We believe that the method in question is easily applicable to medium to large surfaces such as car dashboards. Breitschaft et al. [12] indicates that in the automotive domain four tasks must be performed by tactile interiors: exploration,

detection, identification and usage. These tasks are already achievable as is if the method is applied to a thin touch screen (< 2 mm). The user can explore the surface freely with one or more fingers or by sliding or tapping or even by placing his hand entirely on the surface without changing its behavior. The detection of the localized stimulus and its identification is ensured by the shape and frequency content of the signal used, which can also be varied according to the position of the fingers if one wants to create areas with different vibratory behaviors. Finally the confirmation action is done by the selected zone by sending a signal with a strong frequency dynamic to simulate a button (this function can be improved by adding a force sensor).

We believe that interesting effects throughout the hand (like apparent motion [13] or funneling illusion [14, 15]) can also be studied thanks to this method. By placing the user's hand on the device we can create localized vibrotactile stimuli in multiple places of the hand at the same time or with a time delay. Playing on the time delay and stimuli waveform we can create compelling feelings on the user's hand.

This prototype can also be compared to pin-array interfaces and could realize, to some extent, the same task as the HaptiComm [16]. The HaptiComm is a promising device improving the communication of deafblind people. The user's hand is laying on a custom-made 3D-printed imprint of their hand. An array of electromagnetic actuators which can emulate tapping, place-and-hold and swipping of a finger on the hand with great fidelity is placed facing the hand. With those three basic interaction the device can recreate several deafblind tactile fingerspelling. One of the first comparison we can make with the HaptiComm and pin-arrays interfaces in general is related to the actuators. The electromagnetic actuators constituting them can provide important amplitude, force and skin deformation on small areas of the hand (5 mm^2) whereas our device can only produce noticeable stimuli on large area (fingertip scale). On the other side, piezoelectric actuators are less cumbersome than pin-arrays and have less power-consumption which is suitable for tactile screen applications. Smaller vibrotactile spots would be achievable by reducing the distance between each support but will result in reduced amplitudes. Optimizing material properties could prevent to some extent the amplitude loss but would change the first cut-off frequency of the system. Keeping a balance between each variable depending on the application is thus essential and the implementation of optimization schemes with finite element simulation would be of great interest. The Hapticomm also ensures to the user a comfortable rest of the hand while in the case of a plate the contact with the palm is guaranteed only by adopting a certain position which can, for long duration of interactions, become uncomfortable. In our knowledge, the method presented in this chapter is not limited to flat medium. We can thus imag-

ine 3D-printing a continuous medium adapted to the user's hand where we would conveniently apply periodic rigid supports and piezoelectric actuators in areas of interest.

4.6. Conclusion

Periodically supported plates allow for the localization of vibrotactile stimuli. A piezoelectric actuator bounded to such medium mostly produce evanescent waves which are confined to the actuator covered area as long as the driving frequency is lower than the first cut-off frequency of our system. No control strategies nor signal processing are needed, directly sending the desired signal to the desired actuator suffice in order to obtain a localized vibrotactile stimuli. Multi-touch and multi-user interactions can therefore be implemented with ease. Application such as tactile finger-spelling [16], tactile keyboard [17, 18], tactile memory games [19] and experimentation on subitizing [20, 21] and saliency [22] of vibrotactile spots on tactile surfaces can be implemented. Although the presence of actuators underneath the plate limits applications to surfaces where transparency is not necessary, recent breakthroughs shows that transparent piezoelectric actuators are at hand [23] making our technology compatible with screen surfaces.

NOMENCLATURE

ABBREVIATIONS

Abbreviation	Definition
FRF	Frequency Response Function
rms	Root-Mean-Square (power measurement)

SYMBOLS

Symbol	Definition	Unit
a	Width	m
(a_1, a_2)	Geometry dependent terms	~
D	Bending stiffness	N.m
E	Young's modulus	GPa
h	Thickness	m
H	Average transfer function	m/V
H_{ref}	Reference H transfer function value	m/V
H_{dB}	Average transfer function	dB
(k_1, k_2)	Wave numbers	m^{-1}
L_x	Section width	m
L_y	Section length	m
P_0	Force applied by the supports	N
W	Plate width	m
(x, y)	Space coordinates	m
μ	Propagation constant	~
μ_r	Reel part of the propagation constant	~
μ_i	Imaginary part of the propagation constant	~
ν	Poisson's ratio	~
ρ	Density	kg/m^3
ω	Circular frequency	rad/s
ω_n	Circular cut-off frequency	rad/s

REFERENCES

[1] C. Hudin, J. Lozada, and V. Hayward. Localized Tactile Feedback on a Transparent Surface through Time-Reversal Wave Focusing. *IEEE Transactions on Haptics*, 8(2):188–198, April 2015. ISSN 1939-1412. doi: 10.1109/TOH.2015.2411267.

[2] Ehsan Enferad, Christophe Giraud-Audine, Frédéric Giraud, Michel Amberg, and Betty Lemaire Semail. Generating controlled localized stimulations on haptic displays by modal superimposition. *Journal of Sound and Vibration*, 449: 196–213, June 2019. ISSN 0022-460X. doi: 10.1016/j.jsv.2019.02.039. URL http://www.sciencedirect.com/science/article/pii/S0022460X19301476.

[3] Michaël Wiertlewski, Rebecca Fenton Friesen, and J. Edward Colgate. Partial squeeze film levitation modulates fingertip friction. *Proceedings of the National Academy of Sciences*, 113(33):9210–9215, August 2016. ISSN 0027-8424, 1091-6490. doi: 10.1073/pnas.1603908113. URL https://www.pnas.org/content/113/33/9210. Publisher: National Academy of Sciences Section: Physical Sciences.

[4] Lucie Pantera and Charles Hudin. Multitouch Vibrotactile Feedback on a Tactile Screen by the Inverse Filter Technique: Vibration Amplitude and Spatial Resolution. *IEEE Transactions on Haptics*, pages 1–1, 2020. ISSN 2329-4051. doi: 10.1109/TOH.2020.2981307.

[5] A. W. Leissa. *Vibration Of Plates*, volume NASA SP-160 of *NASA SP-160*. NASA, Ohio State University Columbus, Ohio, 1969.

[6] Kerem Ege, Xavier Boutillon, and Marc Rébillat. Vibroacoustics of the piano soundboard: (Non)linearity and modal properties in the low- and mid-frequency ranges. *Journal of Sound and Vibration*, 332(5):1288–1305, March 2013. ISSN 0022-460X. doi: 10.1016/j.jsv.2012.10.012. URL https://www.sciencedirect.com/science/article/pii/S0022460X12007936.

[7] D. M. Mead. Wave Propagation in Continuous Periodic Structures: Research Contibution from Southampton, 1964–1995. *Journal of Sound and Vibration*, 190(3):495–524, February 1996. ISSN 0022-460X. doi: 10.1006/jsvi.1996.0076. URL https://www.sciencedirect.com/science/article/pii/S0022460X96900760.

[8] D. J. Mead. A new method of analyzing wave propagation in periodic structures; Applications to periodic timoshenko beams and stiffened plates. *Journal of Sound and Vibration*, 104(1):9–27, January 1986. ISSN 0022-460X. doi: 10.1016/S0022-460X(86)80128-6. URL https://www.sciencedirect.com/science/article/pii/S0022460X86801286.

[9] Pierre Cladé. PyDAQmx : a Python interface to the National Instruments DAQmx driver., 2010. URL http://pythonhosted.org/PyDAQmx/.

[10] Ronald T. Verrillo. Psychophysics of vibrotactile stimulation. *The Journal of the Acoustical Society of America*, 77(1):225–232, January 1985. ISSN 0001-4966. doi:

10.1121/1.392263. URL https://asa.scitation.org/doi/abs/10.1121/1.392263.

[11] C. Hudin. Local friction modulation using non-radiating ultrasonic vibrations. In *2017 IEEE World Haptics Conference (WHC)*, pages 19–24, June 2017. doi: 10.1109/WHC.2017.7989850.

[12] Stefan Josef Breitschaft, Stella Clarke, and Claus-Christian Carbon. A Theoretical Framework of Haptic Processing in Automotive User Interfaces and Its Implications on Design and Engineering. *Frontiers in Psychology*, 10, 2019. ISSN 1664-1078. doi: 10.3389/fpsyg.2019.01470. URL https://www.frontiersin.org/articles/10.3389/fpsyg.2019.01470/full.

[13] Carl E. Sherrick and Ronald Rogers. Apparent haptic movement. *Perception & Psychophysics*, 1(6):175–180, June 1966. ISSN 0031-5117, 1532-5962. doi: 10.3758/BF03215780. URL http://link.springer.com/10.3758/BF03215780.

[14] Mathilde Jeannin, Ayoub Ben Dhiab, Lucie Pantera, Charles Hudin, and Sabrina Panëels. The Funneling Illusion Using the Confinement of Vibrotactile Stimuli in Narrow Plates. In *2021 IEEE World Haptics Conference (WHC)*, pages 1147–1147, July 2021. doi: 10.1109/WHC49131.2021.9517236.

[15] Payal Patel, Rahul Kumar Ray, and Muniyandi Manivannan. Power Law Based "Out of Body" Tactile Funneling for Mobile Haptics. *IEEE Transactions on Haptics*, 12(3):307–318, July 2019. ISSN 2329-4051. doi: 10.1109/TOH.2019.2933822. Conference Name: IEEE Transactions on Haptics.

[16] Basil Duvernoy, Ildar Farkhatdinov, Sven Topp, and Vincent Hayward. Electromagnetic Actuator for Tactile Communication. In Domenico Prattichizzo, Hiroyuki Shinoda, Hong Z. Tan, Emanuele Ruffaldi, and Antonio Frisoli, editors, *Haptics: Science, Technology, and Applications*, Lecture Notes in Computer Science, pages 14–24, Cham, 2018. Springer International Publishing. ISBN 978-3-319-93399-3. doi: 10.1007/978-3-319-93399-3_2.

[17] Seokhee Jeon, Hongchae Lee, Jiyoung Jung, and Jin Ryong Kim. User-Adaptive Key Click Vibration on Virtual Keyboard. *Mobile Information Systems*, 2018: e6126140, October 2018. ISSN 1574-017X. doi: 10.1155/2018/6126140. URL https://www.hindawi.com/journals/misy/2018/6126140/. Publisher: Hindawi.

[18] Chia-Hsuan Kung, Tzu-Chieh Hsieh, and Shana Smith. Usability study of multiple vibrotactile feedback stimuli in an entire virtual keyboard input. *Applied Ergonomics*, 90:103270, January 2021. ISSN 0003-6870. doi: 10.1016/j.apergo.2020.103270. URL https://www.sciencedirect.com/science/article/pii/S0003687020302192.

[19] Qi Wang, Vincent Levesque, Jerome Pasquero, and Vincent Hayward. A haptic memory game using the STRESS ^{2} tactile display. In *CHI '06 extended abstracts on Human factors in computing systems - CHI EA '06*, page 271,

Montréal, Québec, Canada, 2006. ACM Press. ISBN 978-1-59593-298-3. doi: 10.1145/1125451.1125510. URL http://dl.acm.org/citation.cfm?doid=1125451.1125510.

[20] Myrthe A. Plaisier, Wouter M. Bergmann Tiest, and Astrid M. L. Kappers. Haptic pop-out in a hand sweep. *Acta Psychologica*, 128(2):368–377, June 2008. ISSN 0001-6918. doi: 10.1016/j.actpsy.2008.03.011. URL https://www.sciencedirect.com/science/article/pii/S0001691808000486.

[21] Myrthe A. Plaisier and Jeroen B. J. Smeets. Haptic subitizing across the fingers. *Attention, Perception, & Psychophysics*, 73(5):1579, April 2011. ISSN 1943-393X. doi: 10.3758/s13414-011-0124-8. URL https://doi.org/10.3758/s13414-011-0124-8.

[22] Astrid M. L. Kappers and Wouter M. Bergmann Tiest. Haptic saliency. *Scholarpedia*, 10(4):32734, April 2015. ISSN 1941-6016. doi: 10.4249/scholarpedia.32734. URL http://www.scholarpedia.org/article/Haptic_saliency.

[23] Chaorui Qiu, Bo Wang, Nan Zhang, Shujun Zhang, Jinfeng Liu, David Walker, Yu Wang, Hao Tian, Thomas R. Shrout, Zhuo Xu, Long-Qing Chen, and Fei Li. Transparent ferroelectric crystals with ultrahigh piezoelectricity. *Nature*, 577(7790):350–354, January 2020. ISSN 1476-4687. doi: 10.1038/s41586-019-1891-y. URL https://doi.org/10.1038/s41586-019-1891-y.

5

Non-Radiating Frequencies for Local Friction Modulation

Ultrasonic friction modulation can elicit texture sensations on a smooth surface but is currently limited to single touch exploration. This chapter develops a technique introduced in 2017 by C. Hudin that locally modulates tactile friction on a surface to allow for a multi-touch exploration. Using this technique, the friction modulation effect is co-located with the actuator through the use of specific non-radiating frequencies. Because waves do not propagate in the surface at these specific frequencies, the vibration amplitude is controlled locally with a simple harmonic excitation of the actuators. The existence of such frequencies is explained through a semi-analytic model of piezoelectric actuation. The ability to locally control the vibration field and to modulate the friction is demonstrated experimentally on a thin glass plate. Extension to a matrix of piezoelectric actuators is also explored and applications were proven possible on an OLED screen.

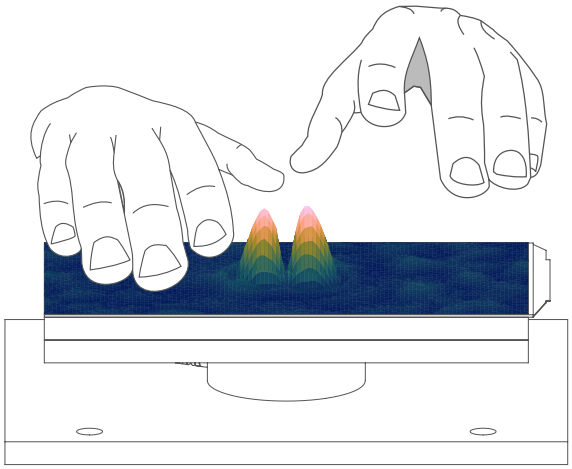

Outline

5.1. INTRODUCTION

UNTIL this point, we searched for ways to localize stimuli with a frequency spectrum in the tactile perception range (10 to 1000 Hz [1]). We adjusted the propagation medium geometry and boundary conditions to create an attenuation bandgap in frequencies of interest with waveguides in chapter 3 (1D approach) and periodic supports in chapter 4 (2D approach).

Like most products that use haptic stimuli (smartphones, gamepads...) to share information, we used low frequency vibrations in our configurations to produce normal forces not across the entire surface, as it is systematically the case in existing technologies, but spatially localized, allowing the user to benefit from haptic feedback on discrete contact areas. The use of normal forces is not the only way to produce haptic feedback. We can also produce tactile effects by modulating the force in the tangential plane. Following Basdogan et al. taxonomy [2], we can distinguish three categories of actuation methods generating forces in the tangential plane: lateral vibration, net tangential force and friction modulation. The latter is the most studied and there are already startups pushing this technology onto the market. By using ultrasonic waves, one can generate a squeeze film of air and intermittent contact between a surface and a sliding finger [3]. Both mechanisms contribute to the friction reduction phenomena which is called active lubrication [4]. To create ultrasonic waves, piezoelectric actuator are glued to a surface and powered with a sine signal at a plate resonance above 20 kHz. As such, the whole plate vibrates reducing the user interaction to a single finger exploration. Natural haptic exploration necessarily involves multiple fingers [5] and even more during blind exploration e.g. interactions with car dashboards during driving. Thus we believe that providing feedback to multiple fingers can communicate more information and guide the user in complex tasks.

In this chapter, we aim to localize ultrasonic waves to create local friction modulation and allow for multi-finger and multi-user interaction on a surface. In the continuity of past research [6] on non-radiating frequencies, we propose in this chapter a semi-analitic 2d model, extend the technique to an hexagonal meshed actuator matrix and demonstrate its feasibility on an OLED screen.

5.2. LOCALIZED ULTRASONIC LUBRICATION

5.2.1. PRINCIPLE

A thin piezoelectric actuator perfectly bonded to a plate produces punctual radial forces at its outer edge [7, p. 515] (Figure 5.1.a). On the plate neutral plane, these

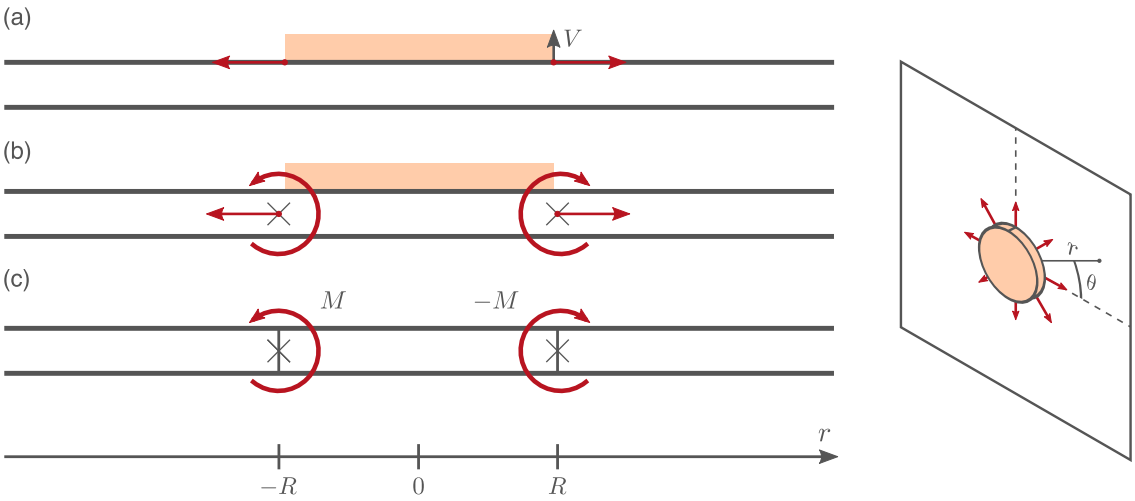

Figure 5.1: Pin force model of piezoelectric actuation. (a) A perfectly bounded piezoelectric patch (in yellow) produces two tangential forces at the plate surface localized at the actuator boundary in $x = \pm R$. (b) These tangential forces produce compression forces and bending moments in the plate. (c) For bending waves, the patch actuation resumes to two bending moments and an increased stiffness and density in the actuator-covered area.

radial forces are equivalent to compression forces and bending moments that give birth to longitudinal compression waves and transverse flexural waves respectively (Figure 5.1.b). Thus, we can examine piezoelectric generation of flexural waves in a plate by considering punctual bending moments M applied on the plate and an increased bending stiffness D and mass density ρ in the area covered by the actuator (Figure 5.1.c). The waves produced by a circular actuator are said to be circular-crested waves. Meaning that the waves generated from the actuator are propagating in a concentric circular pattern. To analyze these waves we will use cylindrical coordinates (r, θ, z). The equation governing the transverse motion $u(r,\theta,t)$ in a plate has the following general form [8, p. 233]:

$$\rho h \frac{\partial^2 u}{\partial t^2} + D\nabla^4 u = 0 \tag{5.1}$$

with m the mass per surface unit, D the bending stiffness and ∇^4 the biharmonic operator. The bending stiffness D is expressed as:

$$D = \int \frac{E}{1-\nu^2} z^2 dz \tag{5.2}$$

The plate bending stiffness is therefore :

$$D(r > R) = D_e = \frac{E_p}{1-\nu_p^2} \int_{-h_p/2}^{h_p/2} z^2 dz = \frac{E_p}{12\left(1-\nu_p^2\right)} h_p^3 \tag{5.3}$$

While the actuator stiffness is :

$$D_a = \frac{E_a}{1-\nu_a^2}\int_{-h_p/2-h_a}^{-h_p/2} z^2 dz = \frac{E_a}{12\left(1-\nu_a^2\right)}\left(3h_p^2 h_a + 6h_p h_a^2 + 4h_a^3\right) \tag{5.4}$$

Giving the overall stiffness :

$$D(r<R) = D_i = \frac{E_p}{12\left(1-\nu_p^2\right)}h_p^3 + \frac{E_a}{12\left(1-\nu_a^2\right)}\left(3h_p^2 h_a + 6h_p h_a^2 + 4h_a^3\right) \tag{5.5}$$

where h_p, h_a, E_p, E_a and ν_p, ν_a are the thickness, Young's modulus and Poisson's ratio of the plate and the actuator respectively. For the mass per surface unit we have:

$$m(r>R) = m_e = \rho_p h_p, \quad m(r<R) = m_i = \rho_p h_p + \rho_a h_a \tag{5.6}$$

Also, the biharmonic operator ∇^4 is in circular coordinates:

$$\nabla^4 = \nabla^2\nabla^2 = \left(\frac{\partial^2}{\partial r^2} + \frac{1}{r}\frac{\partial}{\partial r} + \frac{1}{r^2}\frac{\partial^2}{\partial\theta^2}\right)\left(\frac{\partial^2}{\partial r^2} + \frac{1}{r}\frac{\partial}{\partial r} + \frac{1}{r^2}\frac{\partial^2}{\partial\theta^2}\right) \tag{5.7}$$

In our case, the problem is θ-invariant and the biharmonic operator can be simplified as:

$$\nabla^4 = \left(\frac{\partial^2}{\partial r^2} + \frac{1}{r}\frac{\partial}{\partial r}\right)\left(\frac{\partial^2}{\partial r^2} + \frac{1}{r}\frac{\partial}{\partial r}\right) \tag{5.8}$$

$$= \frac{\partial^4}{\partial r^4} + \frac{2}{r}\frac{\partial^3}{\partial r^3} - \frac{1}{r^2}\frac{\partial^2}{\partial r^2} + \frac{1}{r^3}\frac{\partial}{\partial r} \tag{5.9}$$

Assuming harmonic motion with

$$u(r,t) = \hat{u}(r)e^{-i\omega t}$$

we can write :

$$D\nabla^4\hat{u} - m\omega^2\hat{u} = 0 \tag{5.10}$$

we can therefore define the wave number as:

$$k^4 = \frac{m}{D}\omega^2 \tag{5.11}$$

Leading to the following frequency relation:

$$(\nabla^2 - k^2)(\nabla^2 + k^2)\hat{u} = 0 \tag{5.12}$$

This equation is satisfied when:

$$(\nabla^2 - k^2)\,\hat{u} = 0 \quad \text{or} \quad (\nabla^2 + k^2)\,\hat{u} = 0$$

After multiplying by r^2 the previous relations, we form Bessel and modified Bessel equations of order 0 thus yielding the following general solution:

$$\hat{u} = AJ_0(kr) + BY_0(kr) + CI_0(kr) + DK_0(kr) \tag{5.13}$$

Inside the actuator boundary ($r < R$), we have finite solutions which excludes K and Y terms as they tend to infinity when $x \to 0$. Recalling that $I_0(kr) = J_0(ikr)$, we can express with Bessel functions of the first kind:

$$\hat{u}(r < R) = A_1 J_0(k_i r) + A_2 J_0(ik_i r) \tag{5.14}$$

Outside the actuator boundary ($r > R$), we have propagative solutions which we can express with Hankel functions of the first kind as:

$$\hat{u}(r > R) = A_3 H_0^{(1)}(k_e r) + A_4 H_0^{(1)}(ik_e r) \tag{5.15}$$

The term $H_0^{(1)}(kr)$ corresponds to an outward propagating wave and $H_0^{(1)}(ikr)$ is a rapidly attenuating evanescent wave.

As explained in the first paragraph of this section, we consider here a pin force model of piezoelectric coupling [7, p. 515] (Figure 5.1.a), the actuation by a ceramic coupled to a thin plate is reduced to a bending moment M_p exerted on the plate around the actuator in $r = R$. We also have continuity regarding displacement, its derivatives as well as continuity of torques and shearing forces leading to:

$$\begin{aligned}
\hat{u}(r = R^-) &= \hat{u}(r = R^+) \\
\frac{\partial \hat{u}}{\partial r}(r = R^-) &= \frac{\partial \hat{u}}{\partial r}(r = R^+) \\
M_r(r = R^-) &= M_r(r = R^+) + M_p \\
V_r(r = R^-) &= V_r(r = R^+)
\end{aligned} \tag{5.16}$$

with the bending moment M_r:

$$M_r = -D\left[\frac{\partial^2 \hat{u}}{\partial r^2} + \nu \frac{1}{r}\frac{\partial \hat{u}}{\partial r}\right] \tag{5.17}$$

and the shear stress V_r:

$$V_r = -D\frac{\partial}{\partial r}\nabla^2\hat{u} = -D\left[\frac{\partial^3\hat{u}}{\partial r^3} + \frac{1}{r}\frac{\partial^2\hat{u}}{\partial r^2} - \frac{1}{r^2}\frac{\partial\hat{u}}{\partial r}\right] \tag{5.18}$$

And M_p the bending moment exerted on the plate along the circumference of the actuator at $r = R$ and given by [9, p.408] as:

$$\begin{aligned} M_p = F\frac{h_p}{2} = \frac{h_p}{2}R\tau &= \frac{h_pR}{2}\frac{\psi}{\alpha+\psi}\frac{h_a}{R}E_a\epsilon \\ &= \frac{h_pR}{2}\frac{\frac{E_ph_p}{E_ah_a}}{4+\frac{E_ph_p}{E_ah_a}}\frac{h_a}{R}E_a\frac{-d_{31}V}{h_a} \\ &= -\frac{E_ph_p}{4+\frac{E_ph_p}{E_ah_a}}\frac{h_p}{h_a}\frac{d_{31}V}{2} \end{aligned}$$

where V is the voltage introduced in the piezoelectric actuator and d_{31} the piezoelectric coefficient. The set of equations (5.16), together with the expressions of displacements given in (5.14) and (5.15) provide, for each frequency, a set of four linear equations:

$$\mathbb{G}\mathbb{A} = \mathbb{F} \tag{5.19}$$

with $\mathbb{A} = \left[A_1, A_2, A_3, A_4\right]^T$ and $\mathbb{F} = \left[0, 0, M_p, 0\right]^T$. This can be solved by matrix inversion to obtain the complex amplitude of the waves produced by the piezoelectric actuator. The vibration amplitude at the center of the actuator is then given by $|\hat{u}(r^- = 0)| = |A_1 + A_2|$ and the amplitude of outward propagating waves is $|\hat{u}(r >> R)| = |A_3|$.

For localization purposes we seek frequencies where the amplitude of outward propagating waves $|A_3|$ becomes zero. To do so, we can use adjugate matrices and write:

$$A_3 = M_p\frac{\det\left(\mathbb{G}\downarrow_{3,3}\right)}{\det(\mathbb{G})} \tag{5.20}$$

with $\mathbb{G}\downarrow_{3,3}$ the sub-matrix of $\mathbb{G}$ without its 3rd line and column. Thus we seek solutions where $\det\left(\mathbb{G}\downarrow_{3,3}\right) = 0$. After derivation and simplification we can write $\mathbb{G}\downarrow_{3,3}$:

$$\mathbb{G}\downarrow_{3,3} = \begin{bmatrix} J_0(Rk_i) & I_0(Rk_i) & -H_0^{(1)}(iRk_e) \\ -k_iJ_1(Rk_i) & k_iI_1(Rk_i) & ik_eH_1^{(1)}(iRk_e) \\ -D_ik_i^3J_1(Rk_i) & -D_ik_i^3I_1(Rk_i) & -iD_ek_e^3H_1^{(1)}(iRk_e) \end{bmatrix} \tag{5.21}$$

By assuming that mass and rigidity of the piezoelectric actuator are negligible, we

can write that $k_i = k_e = k$. Thus leading to the following expression:

$$\det\left(\mathbb{G}\downarrow_{3,3}\right) = \frac{4iDk^3}{\pi R} J_1(Rk) = 0 \tag{5.22}$$

with $m_i = m_e = m$ and $D_i = D_e = D$.
Thus $\det\left(\mathbb{G}\downarrow_{3,3}\right)$ is zero for wave number k verifying $J_1(Rk) = 0$. Taking α_n as solution of $J_1(x)$, giving $k_n = \alpha_n/R$, we can write using (5.11) that:

$$f_n = \frac{1}{2\pi}\sqrt{\frac{D}{m}}\left(\frac{\alpha_n}{R}\right)^2 \tag{5.23}$$

with $\alpha_n = 3.83, 7.02, 10.17, \ldots$
At those frequencies, which we will call non-radiating frequencies, the amplitude of outward propagating waves is theoretically null thus allowing localization of high frequency signals (for haptic applications such as friction modulation for example).

5.2.2. NUMERICAL IMPLEMENTATION

In Figure 5.2, we plot the constants which frequency evolution represents the behavior of the plate inside and outside the actuated area using dimensions and mechanical properties of the experimental setup described in the following section. We can notice that the amplitude of the propagating waves is canceled out around frequencies 58 kHz and 184 kHz, while the amplitude at the center of the actuator remains non-zero. At these frequencies the piezoelectric actuator is non-radiating and only evanescent waves are produced, except in the area covered by the actuator. In the case of local friction modulation, choosing one of these frequencies as the carrier frequency will ensure a localized displacement of the plate. The relation given in equation (5.23) gives us the first and second non-radiating frequency equal to 51.4 kHz and 172.4 kHz which are relatively close to the obtained values. Better precision can be achieved if $\det\left(\mathbb{G}\downarrow_{3,3}\right) = 0$ was numerically resolved without assuming that mass and rigidity of the piezoelectric are negligible.

5.2.3. EXPERIMENTAL VALIDATION

To asses our model we made a simple setup consisting of a piezoelectric actuator PIC255 ($R = 10$ mm, $h_a = 0.5$ mm, $\rho_a = 7800$ kg/m^3, $E_a = 62.1$ GPa, $\nu_a = 0.3$) glued on a borosilicate glass plate ($300 \times 200 \times 1.1$ mm^3, $\rho_p = 2200$ kg/m^3, $E_p = 64$ GPa, $\nu_p = 0.2$) which is fixed by a foam tape to a rigid frame. The frequency behavior mapping of part of the plate (80×80 mm^2 grid) was measured point by point with a laser vibrometer (Polytec OFV-534/2570) mounted on a motorized 3 axis platform. From

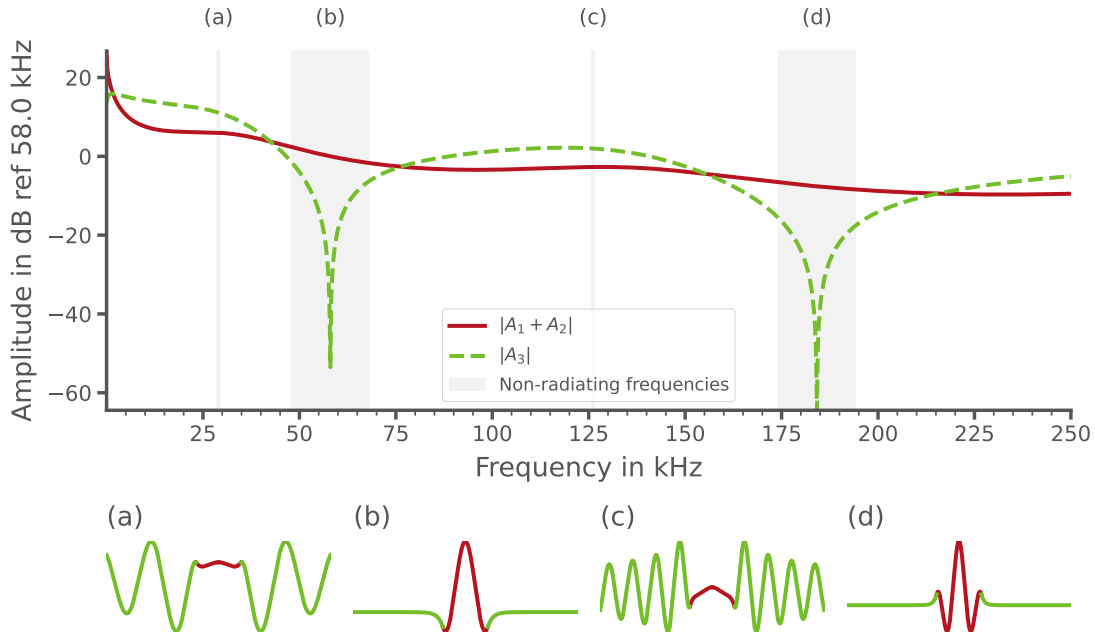

Figure 5.2: Top: Vibration amplitude at the center of the actuator (solid red line) and amplitude of the outward propagative wave (dashed green line) obtained with $h_a = 0.5$ mm, $h_p = 1.1$ mm, $R = 10$ mm, $E_a = 62.1$ GPa, $E_p = 64$ GPa, $\rho_a = 7800$ kg/m^3, $\rho_p = 2200$ kg/m^3, $\nu_a = 0.34$ and $\nu_p = 0.2$. Amplitudes are relative to the amplitude at the center of the actuator at $f = 58$ kHz and $f = 184$ kHz. Bottom: Plate deformation at different frequencies. In cases (b) and (d), only evanescent waves are produced outside of the actuated portion of the plate.

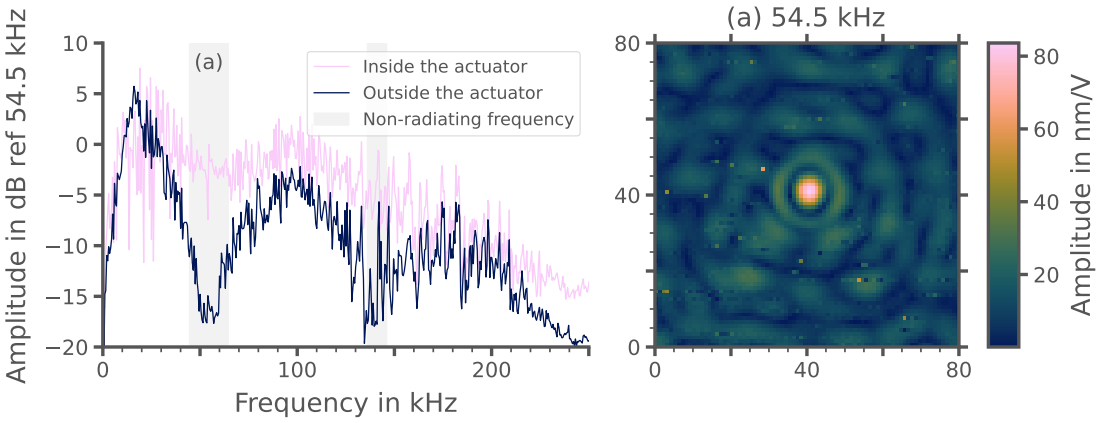

Figure 5.3: Averaged system frequency response function (FRF) $H_{\text{dB}} = 20\log_{10}|H|$ inside and outside the activated actuator. Around $f = 54.5$ kHz a first drop in amplitude of -15 dB can be observed, implying a higher amplitude in the center of the actuator than outside at this frequency. A second drop around 141 kHz seems to be happening but is polluted with resonances making it hard use.

this measurement we plot the averaged system frequency response inside and outside the actuator in order to check the presence of non-radiating frequencies. Figure 5.3 shows around 54.5 kHz a first drop of amplitudes reaching −15 dB in average outside the actuator. A second drop around 141 kHz seems to be happening but modal noise makes it unclear. We assume those drops of amplitude to be the non-radiating frequencies revealed in Section 5.2.2. The value of the first non-radiating frequency (54.5 kHz) is close to the one found with the semi-analytic model (58 kHz) which constitutes a good approximation knowing that there are uncertainties concerning the bonding of the actuator and the numerical values used in the simulation.

5.3. Extension to a Dense Array of Actuators

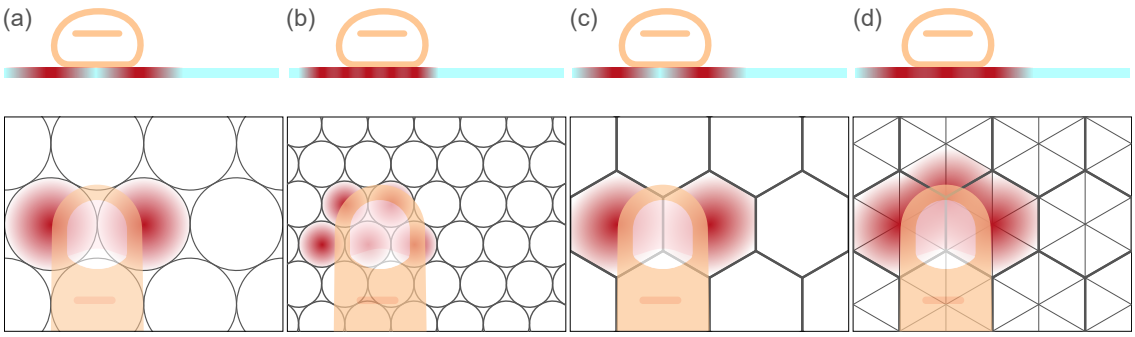

Figure 5.4: Piezoelectric distribution. a) Circular pattern. b) High density circular pattern. c) Hexagon pattern. d) Triangular pattern.

Previous section showed the existence of non-radiating frequencies in the case of a circular piezoelectric actuator. Now, as the localization provided by non-radiating frequencies is confined to the actuated region, using only circular actuators will lead to dead zones i.e. zones where controlling haptic feedbacks becomes impossible (Figure 5.4.a). In order to provide a continuous feedback under the finger throughout the surface, we could multiply the number of actuators by reducing their surface area (Figure 5.4.b), but smaller actuators means lower amplitudes hindering haptic applications and higher non-radiating frequencies (difficult to amplify). To maximize amplitudes, circular-shaped actuators are not optimal, using hexagons would allow us to fully use the available space (Figure 5.4.c). But yet again we would have to reduce the surface area to provide feedback continuity. To preserve amplitudes while multiplying the number of possible actuated area we have to mesh our actuator: from hexagons we propose using triangles (Figure 5.4.d). By activating six triangular electrodes, we form a hexagon whose shape is close enough to a circle, thus allowing for the apparition of non-radiating frequencies. In this section, we in-

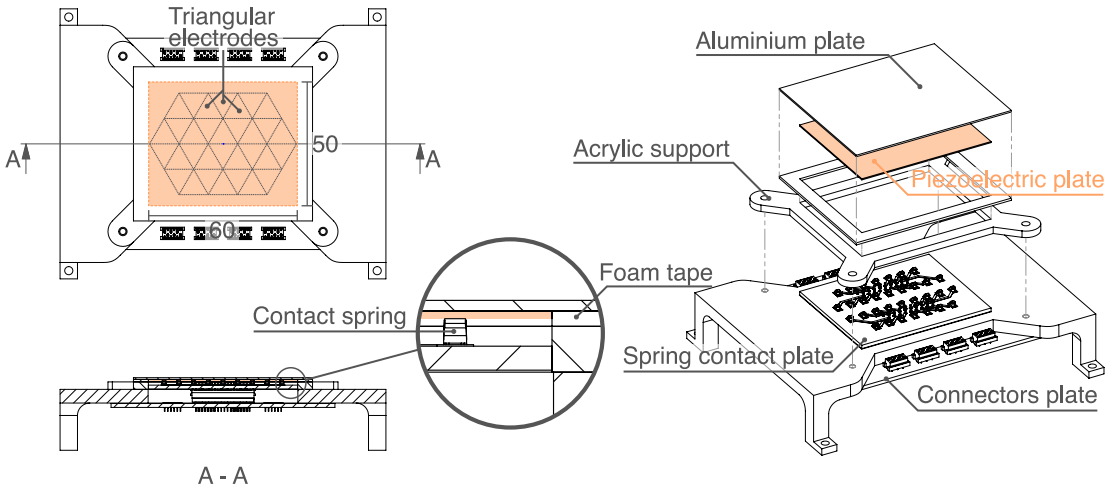

Figure 5.5: Experimental setup. A piezoelectric plate with a laserized triangular electrode pattern is glued to an aluminium plate. A plate with a set of spring assure the wiring of all 32 electrodes.

vestigate the feasibility of triangular pattern electrodes to create localized ultrasonic lubrification.

5.3.1. APPARATUS

To assess the possibilities offered by the triangular pattern and study non-radiating frequencies produced by an hexagon-shaped actuator, we prepared an apparatus consisting of a piezoelectric plate PIC151 with dimensions $50 \times 60 \times 0.5$ mm^3 with a laserized triangular electrode pattern glued to an aluminium plate of dimension $62 \times 72 \times 0.8$ mm^3. The pattern consisted of 32 equilateral electrodes with sides of around 11.8 mm. Six triangles formed an hexagon with an inscribed diameter of 20.5 mm. To avoid damaging the piezoelectric material through repeated soldering of the electrodes and bothersome cable management, we assured the electrical connection through contact springs. Powering was made with a custom-made amplification electronic which also managed signal supervision and buffer timing.

5.3.2. SYSTEM FREQUENCY RESPONSE FUNCTION (FRF)

SINGLE ACTIVATION AREA

In the same manner as Section 5.2.3, we measured the frequency behavior of our plate but this time by powering 6 triangular electrodes forming an hexagon. Figure 5.6 shows the average system frequency response inside and outside the actuator area and reveals an amplitude drop of 15 dB around $f = 25.6$ kHz. Figure 5.7 display the FRF at the non-radiating frequency. Vibrations are not perfectly localized above the actuated area and leaks can be observed. These discrepancies can be caused by several things. Firstly, the corners of an hexagon shaped piezoelectric actuator bring

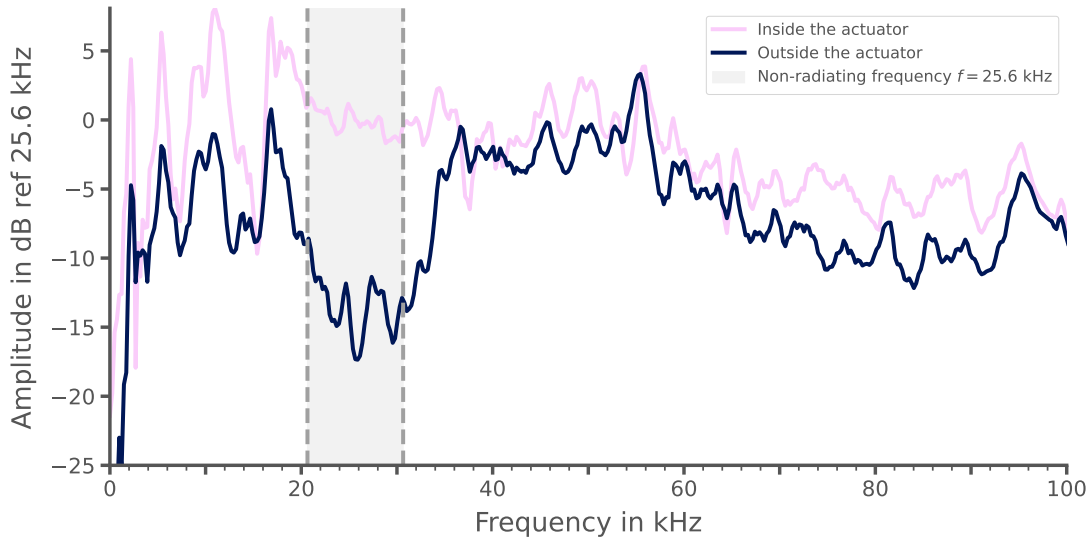

Figure 5.6: Averaged system frequency response function (FRF) $H_{\text{dB}} = 20\log_{10}|H|$ inside and outside the activated actuator. Around $f = 25.6$ kHz a drop in amplitude of 15 dB can be observed, implying a higher amplitude in the center of the actuator than outside at this frequency.

discontinuities regarding moment distributions on the actuator circumference, thus affecting the localization quality. Secondly, because the bonding of the piezo plate was done by hand, the actuator is not perfectly bonded to the plate and parallelism issues between the actuator plane and the plate can affect the moment distributions around the actuator circumference. Thirdly, the piezoelectric plate thickness is of the same order as the thickness of the plate while in the theory it is expected to be much smaller, this also clashes with the assumption that the neutral plane of our setup is the same as the neutral plane of the plate, thus leading to amplitude loss and further arbitrary behaviors. Finally, although the use of spring contacts is convenient, its effect on the plate behavior is unknown as it stresses the plate with a certain amount of force.

Activation of multiple hexagons

We also investigated if spatial patterns were achievable by activating several overlapping hexagons. We applied the principle of superposition and added in the overlapping region the signals corresponding to the two hexagons. We activated several areas with a sweep signal to extract the frequency behavior of our system under such powering configurations. Figure 5.8 shows the mapping of two overlapping hexagons which were powered with the same sweep signal, thus the triangles in the overlapped region are powered with twice the base tension. At the non-radiating frequency $f = 25.6$ kHz found previously with the single activation case, the plate displays a lot of leaks. Even though we can discern some localization in the activated

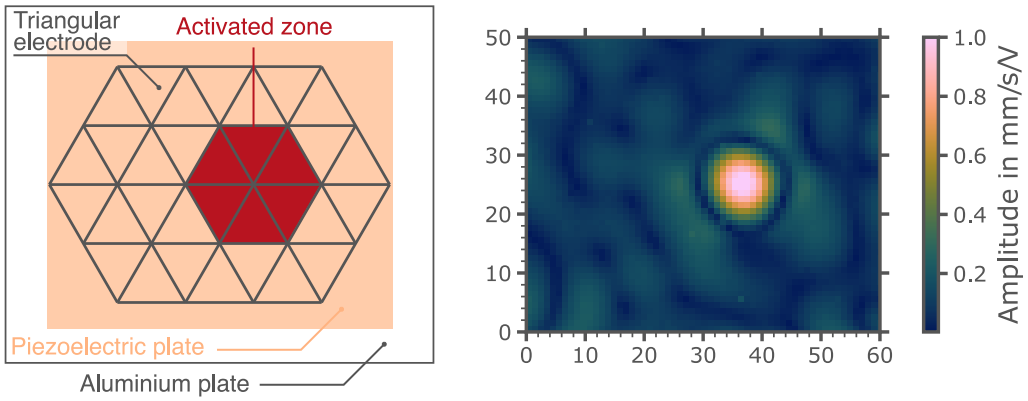

Figure 5.7: A group of 6 piezoelectric actuators forming an hexagon is powered by a sweep signal. The system frequency response function H is represented at the non-radiating frequency $f = 25.6$ kHz and a localized effect can be observed above the activated zone.

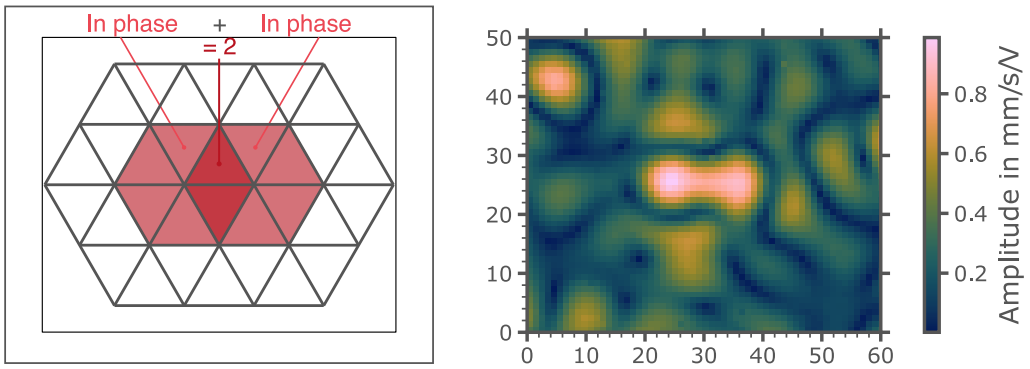

Figure 5.8: FRF mapping showing the behavior of the aluminium plate at the non-radiating frequency $f = 25.6$ kHz. Electrodes are activated in phase and overlapping zone are powered with twice the base tension.

region, it isn't significant enough. Figure 5.9 also shows mappings of several activated overlapping hexagons at $f = 25.6$ kHz but this time electrodes are activated in counter-phase, overlapping zones are therefore not supplied with any voltage. Contrary to the previous case, we have a nice localization of the waves with a satisfactory difference of amplitude between the actuated zone and the rest of the plate.

5.4. FRICTION REDUCTION APPLICATION ON AN OLED SCREEN

PREVIOUS section assessed the possibility of using piezoelectric actuator of hexagonal shape formed by a set of six triangular electrodes to create local friction modulation at specific non-radiating frequencies. In this section, we try to apply the same method in the same way as before to a different propagation medium i.e. an Organic Light-Emitting Diode (OLED) screen.

OLED screens are becoming more popular in smartphone technologies as they allow for high resolution display while being extremely thin. Localization techniques

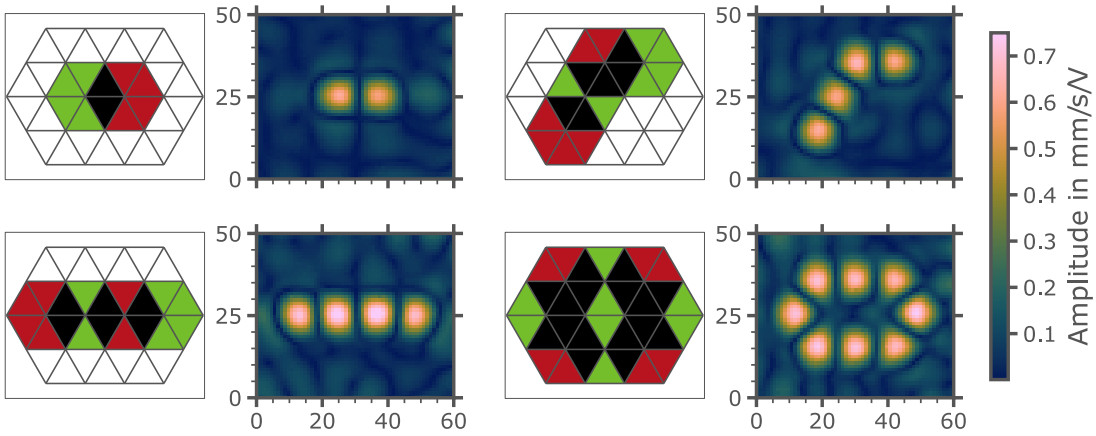

Figure 5.9: FRF mapping showing the behavior of the aluminium plate at the non-radiating frequency $f = 25.6$ kHz. Electrodes are activated in counter phase and overlapping zone are powered with no tension (in black).

introduced in this thesis imply the use of matrix of actuators which should be applied, in the case of a normal screen (i.e. LCD screens), directly between the screen and the interaction glass to assure sufficient amplitudes. This deprives us of the visual feedback provided by the screen. Thanks to the low thickness (0.6 to 0.8 mm) provided by the OLED technology we can directly apply our array of actuator to the OLED stack behind the screen and still get sufficient amplitudes for haptic feedbacks.

5.4.1. Apparatus

Reproducing the same triangular piezoelectric electrode pattern as in Section 5.3, we bonded the piezoelectric plate PIC151 ($50 \times 60 \times 0.5$ mm^3) to the OLED screen back glass. We did not use spring contact this time in order to avoid overstressing the screen. We thus only wired 10 electrodes out of the 32 available. Powering was made this time with analog signals sent with an NI-USB-6363 acquisition card and amplified by an Elbatech T-500. An ATI Mini40 6 axis F/T sensor was placed under our screen for the measurement of friction reduction during finger interaction. The out of plane displacement of the surface was measured by a laser vibrometer Polytec OFV-534/2500.

5.4.2. System frequency response function (FRF)

As usual, we measure the frequency behavior throughout the plate point by point and calculate the frequency response function H. Figure 5.11 displays the averaged system FRF inside and outside the activated actuator. A drop of amplitude of 20 dB is happening around $f = 17.76$ kHz implying a higher amplitude in the center of the actuator than outside at this frequency. Figure 5.12 shows the screen behavior at

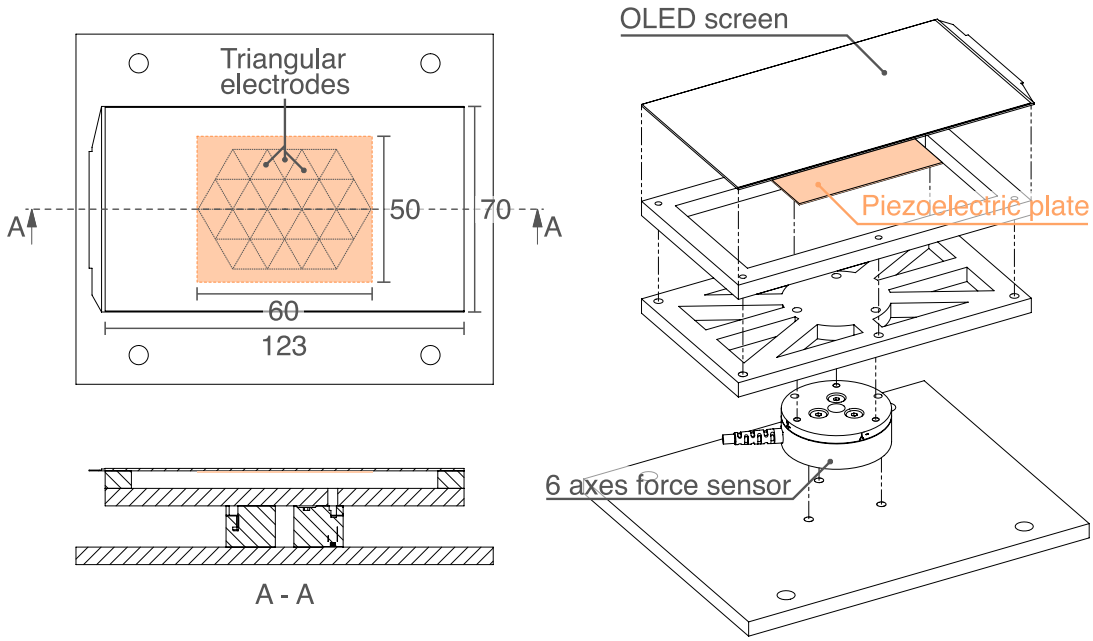

Figure 5.10: Experimental setup. A piezoelectric plate with a laserized triangular electrode pattern is glued to an OLED screen and mounted on a 6 axes force sensor.

this non-radiating frequency. The contrast between actuated area and the rest of the screen, although leaks are still present, is better than the aluminum apparatus of last section. We think that the damping provided by the screen stack is in a way helping the localization. We tried like before to actuate two overlapping hexagon actuators in phase and in counter-phase which resulted in the FRF mapping of Figure 5.13.

5.4.3. VIBRATION FIELD

Before proceeding with force measurements, we measured the vibration field throughout the screen under a modulated sine signal with a carrier frequency at 17.5 kHz and 250 Hz modulation. Figure 5.14 shows the vibration field map as well as amplitudes at the center of the actuated area and at a point 20 mm away. The representation reveals several information. First, an important amount of leaks is happening even though the previous FRFs (Figure 5.12) did not predicted so. We can also see amplitude differences between locations where we have [piezoelectric plate + OLED screen] and OLED screen alone. This explains by a difference in the flexural rigidity D between locations which shifts the non-radiating frequencies. Hence, application of this technique seems to be reduced to structures with constant properties. In other words, applied in our case, the interaction area should be covered with a piezoelectric layer for this localization technique to properly work. However, despite the large number of leaks, the amplitude difference inside and outside the actuated area is still significant and can lead to a localized haptic feedback.

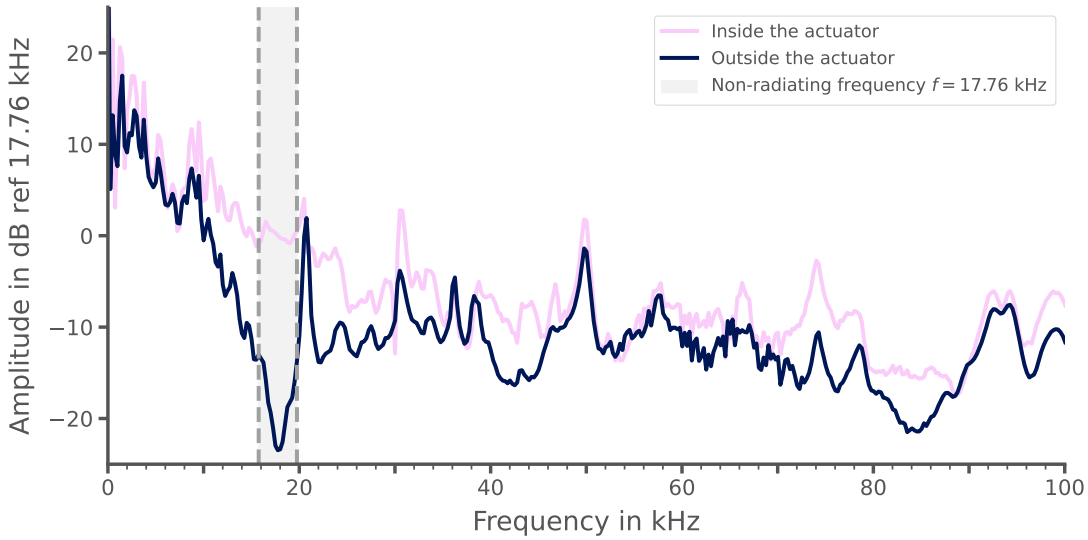

Figure 5.11: Averaged system frequency response function (FRF) $H_{\text{dB}} = 20\log_{10}|H|$ inside and outside the activated actuator. Around $f = 17.76$ kHz a drop in amplitude of -20 dB can be observed, implying a higher amplitude in the center of the actuator than outside at this frequency.

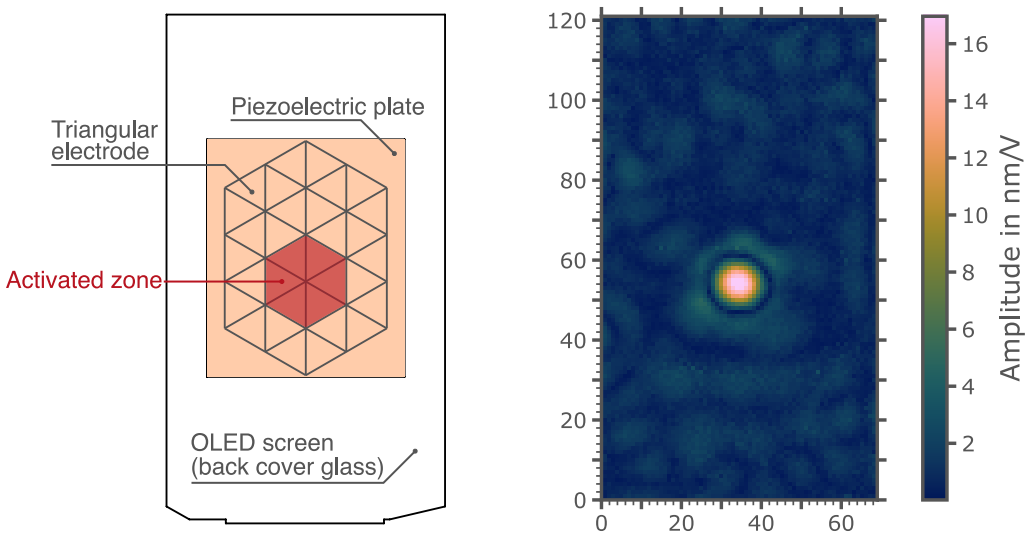

Figure 5.12: A group of 6 piezoelectric actuators forming an hexagon is powered by a sweep signal. The absolute value of the system frequency response function $|H|$ is represented at the non-radiating frequency $f = 17.76$ kHz and a localized effect can be observed above the activated zone.

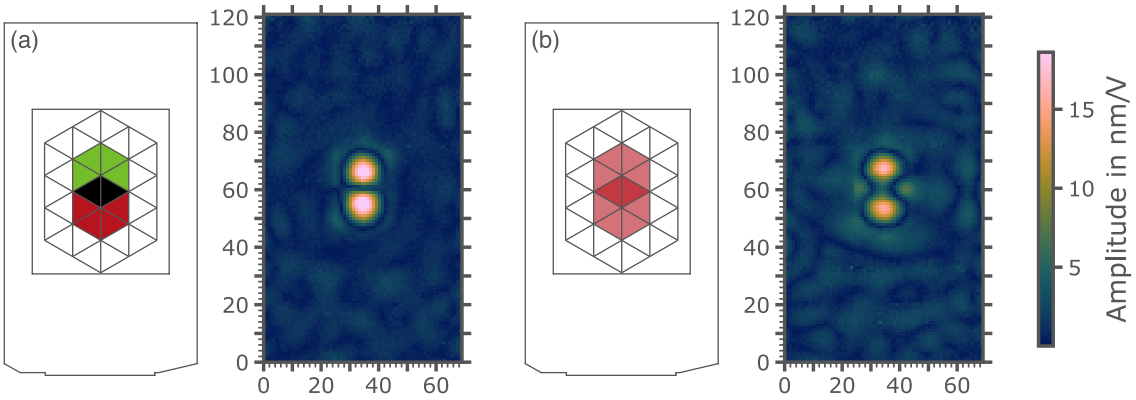

Figure 5.13: FRF mapping showing the behavior of an OLED screen at the non-radiating frequency $f = 17.76$ kHz. (a) Electrodes are activated in counter phase and overlapping zones are powered with no tension. (b) Activated electrodes are added so that overlapping zone are powered with twice the base tension.

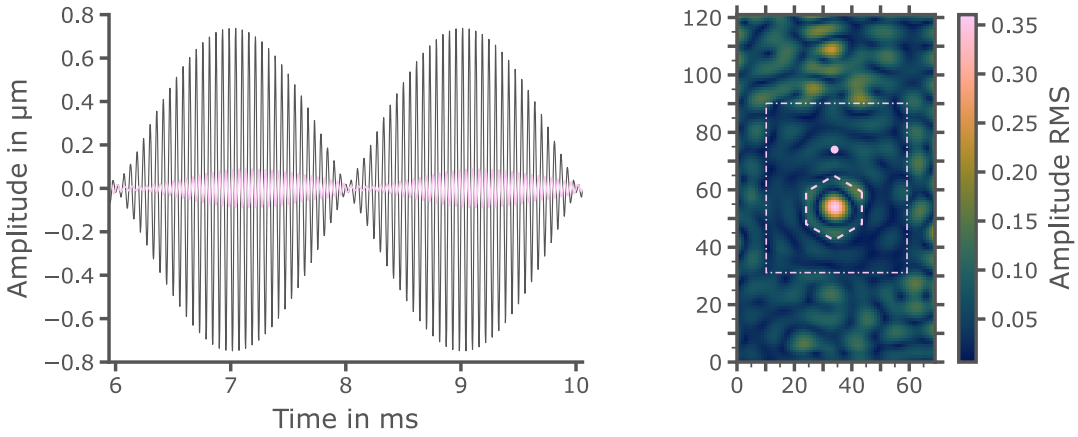

Figure 5.14: Left: vibration amplitude in the center of the actuated zone (black) and 20 mm away (light pink). Right: quadratic mean of the measured displacement across the plate under a modulated sine. The area covered by the actuators (dashed hexagon contour) vibrates with a much larger amplitude than other points on the plate. A difference in amplitude can also be seen inside the piezoelectric plate zone (point-dashed rectangular contour) and outside.

5.4.4. Tactile friction

To asses the localized friction reduction capability of our system, we used an ATI Mini40 6 axis F/T sensor to extract lateral forces during the swipe of a finger over the middle line of the screen. As friction reduction also depends on the exploration velocity, we tried as best as possible to keep it constant during the experimentation. Figure 5.15 shows in order: a spectrogram of the lateral forces in play, the evolution of the lateral force and the position of the finger. Around time $t = 1.5$ s, the finger is above the actuated area and 300, 600 and 900 Hz frequency components appear in the lateral force spectrogram. Friction being modulated by the absolute amplitude of the displacement, the actual friction frequency is twice the signal modulation frequency ($f = 300$ Hz) which also explains the presence of an harmonic frequency at 900 Hz in the spectrogram. At the same time-stamp, we should be able to see a reduction of lateral forces but Figure 5.15 (middle) do not show a noticeable change. This observation is surprising as notable frequency component are appearing in the spectogram and haptic feedbacks were felt during the experiment while sliding above the actuated zone. A first thought would explain this fact to be linked with the carrier frequency. Most studies implying active lubrication seem to work above 25 kHz. Taking Biet et al. [10] research, it seems, in our current configuration, that frequency and vibration amplitude are not sufficient enough to strongly lower the friction coefficient. Yet, this first assumption do not explain why a haptic feedback while sliding a finger over the localized area was felt and further investigation is still required.

5.5. Discussion

Localized ultrasonic lubrication through the use of non-radiating frequencies born from an interference phenomena implied by the actuation nature of a bonded piezoelectric actuator is feasible. We found that implementation of such phenomena is not reduced to circular piezoelectric actuator alone but can also happen with hexagonal shaped actuator with a triangular meshing. Thus, providing feedback continuity regarding a moving finger becomes possible. Trough careful powering of each piezoelectric area we can produce multiple friction reduction areas. By powering areas of interest in counter-phase, overlapping configurations do not need to be activated which could reduce the power used to provide a continuous feedback throughout the plate. The different mappings of the out-of-plane displacement showed an important amount of leaks which could hinder the user interaction. We believe that those leaks can be reduced to a minimum if proper integration is assured i.e. thin film deposition of actuators, proper stacking (for added damping)...

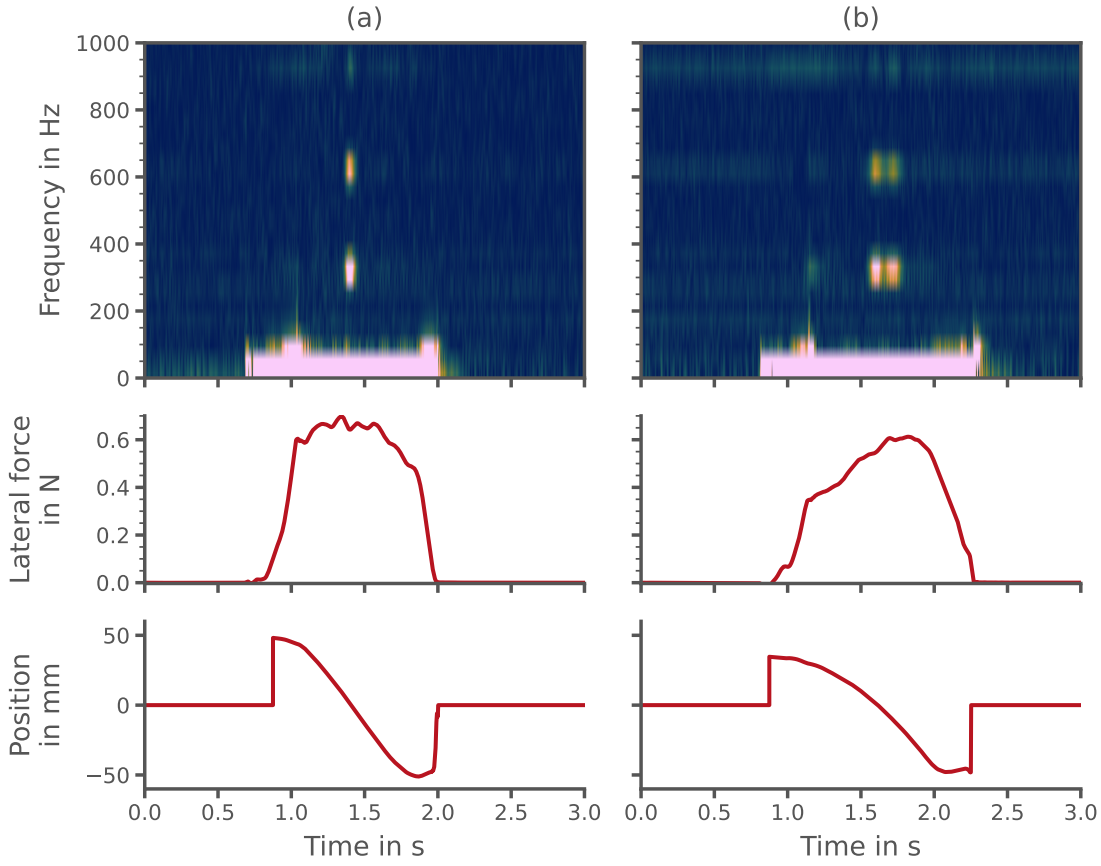

Figure 5.15: Friction analysis for one activated area (a) and two activated areas (b) with non-radiating carrier frequencies modulated at 300 Hz. (bottom) Position of the finger and actuator position and corresponding time. (middle) Corresponding friction force implied by the finger. (top) Spectrogram of the friction force. Even though $n \times 300$ frequency components are present in the spectrogram, friction reduction when the finger passes over an actuated area is not noticeable.

It is also important to keep in mind that this localized friction modulation is not meant for static or passive interaction as the change in tangential force only happens for a moving finger. New approaches have been considered by researchers to provide feedback for static interaction (like indentation). Monnoyer et al. [11] showed that by using rapid changes in friction to store elastic energy in the finger-pulp, it is possible to create a stimulus when the energy is released. One of the important point here resides in the detection threshold which is higher than the one produced by lateral motion [12]. To bypass this limitation and lower the detection threshold, traveling ultrasonic waves were used by Gueorguiev et al. [13] which increased the tangential force through an elliptical motion of particles. Following this idea of elliptical motion, Garcia et al. [14] implemented a button click by superposition of two ultrasonic waves creating a pseudo-travelling wave on a plate. The application of those solutions to our case do not seem possible for the moment, but a way to allow static feedback would be to use non-radiating frequencies with geometries allowing low-frequency band-gaps (chapter 3 and chapter 4) thus allowing the use of low-frequency feedback for static interactions and high-frequency for dynamic interactions. An other way would be to implement the inverse-filtering technique for static interactions in parallel with non-radiating frequencies. Those solutions would lead us to interfaces providing a full range of interaction (key-clicks, texture, compliance...).

Two important interrogations regarding the finger effect on frequency location of non-radiating frequencies and power consumption remain to be investigated. However, we would like to provide some guidance in this regard.

On a vibrating plate, finger interaction brings an added mechanical loading which can be viewed as an added rigidity and mass. The evolution of there impact is yet to be perfectly documented as the mechanical finger behavior is highly non-linear and difficult to simulate. On a side note, given the anatomy of the finger, the finger pulp is a three-dimensional fibro-fat composite tissue (numerous adipocyte cells held together by fibers) capable of withstanding composite stresses (torsion, compression, traction and torsion) [15]. This also explains that getting definitive values (regarding mass, rigidity, attenuation..) is a tedious work with strict experimental conditions and obtained values cannot be generalized. But even-though we cannot precisely predict the effect of finger interaction, we can still be confident on how it will impact our technique. In our case we can see with the non-radiating frequency expression $f_n = \frac{1}{2\pi}\sqrt{\frac{D}{m}}\left(\frac{\alpha_n}{R}\right)^2$ that rigidity and mass do have an influence on the non-radiating frequency. It is of interest to notice that, compared to techniques involving resonant frequencies whose amplitudes can get strongly reduced by the finger, in our case, it is the localization ratio that is concerned. Again, we cannot extrapolate by how

much the non-radiating frequency can be shifted and further experimental studies with controlled conditions are necessary.

Concerning power consumption, the use of piezoelectric actuator outside mode frequencies implies that more voltage have to be used. As we can notice on previous measurements, we needed 200 V peak-to-peak (V_{RMS} = 70.7 Vrms) in order to obtain 1 μm amplitude. If we take a simple model (capacitor equivalent) for our actuator with the measured capacitance C = 14 nF and the frequency f = 20 kHz, we have I_{peak} = 0.176 A (I_{RMS} = 0.124 A). Thus the power supplied to load is equal to P = 8.8 VA. This first approximation shows that piezoelectric actuators draw little power but this estimation needs to be considered with precaution as the use of piezoelectricity imply a two way exchange and the estimation of the actual energy would hold more meaning here. Providing a good amplification circuit, energy recovery can be implemented to reduce power-consumption to a minimum (CapDriveTM is an example of haptic driver applying this concept). We could also recover this energy with a passive inductor circuit, this though would need fine tuning and an important number of big inductors.

5.6. CONCLUSION

A piezoelectric actuator bonded to a plate can display at certain discrete frequencies a non-radiating behavior. At those frequencies, waves, that propagates throughout the plate in normal circumstances, are confined to the actuated areas. This allows for the creation of local tactile friction reduction by driving actuators with a harmonic signal at a non-radiating frequency. Modulating this harmonic signal thus leads to local friction modulation. This effect can be implemented with hexagonal piezoelectric actuators formed by a set of triangular electrodes. This triangular meshing allows to multiply the number of interaction areas while preserving the vibration amplitudes. Thanks to the thinness of OLED screens, having transparent actuators becomes unnecessary as they can be directly applied at the back cover-glass of the screen. In case of normal screens, where actuators should be directly applied between glass and screen, recent advances showed that transparent ferroelectric cristals with ultrahigh piezoelectricity are achievable [16].

NOMENCLATURE

ABBREVIATIONS

Abbreviation	Definition
FRF	Frequency Response Function
OLED	Organic Light-Emitting Diode
rms	Root-Mean-Square (power measurement)

SYMBOLS

Symbol	Definition	Unit
A_1, A_2, A_3, A_4	Amplitudes	~
d_{31}	Piezoelectric actuator coefficient	m/V
D	Bending stiffness	N.m
D_a	Actuator bending stiffness	N.m
D_i	Bending stiffness inside the actuator zone	N.m
E	Young's modulus	GPa
E_a	Actuator Young's modulus	GPa
E_p	Plate Young's modulus	GPa
f_n	Non-radiating frequency	Hz
H	Average transfer function	m/V m/s/V
H_{ref}	Reference H transfer function value	m/V m/s/V
H_{dB}	Average transfer function	dB
h	Thickness	m
h_a	Actuator thickness	m
h_p	Plate thickness	m
k	Wave number	m^{-1}
k_i	Interior wave number	m^{-1}
k_e	Exterior wave number	m^{-1}
M	Bending moments	N.m
M_r	Bending moments	N.m
M_p	Bending moments exerted on the plate	N.m
m	Mass	kg
m_e	Exterior mass	kg
m_i	Interior mass	kg
n	Mode index	~
r	Radius	m
R	Radius	m
u	Transverse motion	m
V	Voltage	V
V_r	Shear stress	N/m

Symbol	Definition	Unit
α_n	Solutions of $J_1(\alpha_n) = 0$	~
∇^4	Biharmonic operator	m^{-4}
ν	Poisson's ratio	~
ν_a	Poisson's ratio of the actuator	~
ν_p	Poisson's ratio of the plate	~
ω	Circular frequency	rad/s
J_0	Bessel function of the 1^{st} kind of order 0	
J_1	Bessel function of the 1^{st} kind of order 1	
Y_0	Bessel function of the 2^{nd} kind of order 0	
I_0	Modified Bessel of the 1^{st} kind of order 0	
I_1	Modified Bessel of the 1^{st} kind of order 1	
K_0	Modified Bessel of the 2^{nd} kind of order 0	
$H_0^{(1)}$	Hankel function of the 1^{st} kind of order 0	
$H_1^{(1)}$	Hankel function of the 1^{st} kind of order 1	
$\mathbb{G}\downarrow_{3,3}$	sub-matrix of $\mathbb{G}$ without 3rd line and column	

REFERENCES

[1] Ronald T. Verrillo. Psychophysics of vibrotactile stimulation. *The Journal of the Acoustical Society of America*, 77(1):225–232, January 1985. ISSN 0001-4966. doi: 10.1121/1.392263. URL https://asa.scitation.org/doi/abs/10.1121/1.392263.

[2] Cagatay Basdogan, Frederic Giraud, Vincent Levesque, and Seungmoon Choi. A Review of Surface Haptics: Enabling Tactile Effects on Touch Surfaces. *IEEE Transactions on Haptics*, pages 1–1, 2020. ISSN 2329-4051. doi: 10.1109/TOH.2020.2990712.

[3] Michaël Wiertlewski, Rebecca Fenton Friesen, and J. Edward Colgate. Partial squeeze film levitation modulates fingertip friction. *Proceedings of the National Academy of Sciences*, 113(33):9210–9215, August 2016. ISSN 0027-8424, 1091-6490. doi: 10.1073/pnas.1603908113. URL https://www.pnas.org/content/113/33/9210. Publisher: National Academy of Sciences Section: Physical Sciences.

[4] T. Watanabe and S. Fukui. A method for controlling tactile sensation of surface roughness using ultrasonic vibration. In *Proceedings of 1995 IEEE International Conference on Robotics and Automation*, volume 1, pages 1134–1139 vol.1, May 1995. doi: 10.1109/ROBOT.1995.525433. ISSN: 1050-4729.

[5] Roberta L. Klatzky and Susan J. Lederman. Touch. In *Handbook of psychology: Experimental psychology, Vol. 4, 2nd ed*, pages 152–178. John Wiley & Sons, Inc., Hoboken, NJ, US, 2013. ISBN 978-0-470-64993-0 978-1-118-28515-2 978-1-118-28194-9 978-1-118-28377-6.

[6] C. Hudin. Local friction modulation using non-radiating ultrasonic vibrations. In *2017 IEEE World Haptics Conference (WHC)*, pages 19–24, June 2017. doi: 10.1109/WHC.2017.7989850.

[7] Victor Giurgiutiu. Chapter 10 - High-Frequency Vibration SHM with PWAS Modal Sensors –the Electromechanical Impedance Method. In Victor Giurgiutiu, editor, *Structural Health Monitoring with Piezoelectric Wafer Active Sensors (Second Edition)*, pages 509–572. Academic Press, Oxford, January 2014. ISBN 978-0-12-418691-0. doi: 10.1016/B978-0-12-418691-0.00011-3. URL https://www.sciencedirect.com/science/article/pii/B9780124186910000113.

[8] Karl F Graff. *Wave motion in elastic solids*. Dover Publications, New York, 1991. ISBN 978-0-486-13957-9 978-1-62198-646-1. URL http://www.freading.com/ebooks/details/r:download/ZnJlYWQ6OTc4MDQ4NjEzOTU3OTpl. OCLC: 829198880.

[9] Victor Giurgiutiu. Chapter 8 - Coupling of PWAS Transducers to the Monitored Structure. In Victor Giurgiutiu, editor, *Structural Health Monitoring with Piezoelectric Wafer Active Sensors (Second Edition)*, pages 395–443. Academic Press, Oxford, January 2014. ISBN 978-0-12-418691-0. doi: 10.

1016/B978-0-12-418691-0.00008-3. URL https://www.sciencedirect.com/science/article/pii/B9780124186910000083.

[10] Mélisande Biet, Frédéric Giraud, and Betty Lemaire-Semail. Squeeze film effect for the design of an ultrasonic tactile plate. *IEEE Transactions on Ultrasonics, Ferroelectrics, and Frequency Control*, 54(12):2678–2688, December 2007. ISSN 1525-8955. doi: 10.1109/TUFFC.2007.596. Conference Name: IEEE Transactions on Ultrasonics, Ferroelectrics, and Frequency Control.

[11] Jocelyn Monnoyer, Emmanuelle Diaz, Christophe Bourdin, and Michaël Wiertlewski. Ultrasonic Friction Modulation While Pressing Induces a Tactile Feedback. In Fernando Bello, Hiroyuki Kajimoto, and Yon Visell, editors, *Haptics: Perception, Devices, Control, and Applications*, Lecture Notes in Computer Science, pages 171–179, Cham, 2016. Springer International Publishing. ISBN 978-3-319-42321-0. doi: 10.1007/978-3-319-42321-0_16.

[12] Muhammad Khurram Saleem, Cetin Yilmaz, and Cagatay Basdogan. Psychophysical Evaluation of Change in Friction on an Ultrasonically-Actuated Touchscreen. *IEEE Transactions on Haptics*, 11(4):599–610, October 2018. ISSN 1939-1412. doi: 10.1109/TOH.2018.2830790. URL https://doi.org/10.1109/TOH.2018.2830790.

[13] David Gueorguiev, Anis Kaci, Michel Amberg, Frédéric Giraud, and Betty Lemaire-Semail. Travelling Ultrasonic Wave Enhances Keyclick Sensation. In Domenico Prattichizzo, Hiroyuki Shinoda, Hong Z. Tan, Emanuele Ruffaldi, and Antonio Frisoli, editors, *Haptics: Science, Technology, and Applications*, Lecture Notes in Computer Science, pages 302–312, Cham, 2018. Springer International Publishing. ISBN 978-3-319-93399-3. doi: 10.1007/978-3-319-93399-3_27.

[14] Pierre Garcia, Frédéric Giraud, Betty Lemaire-Semail, Matthieu Rupin, and Michel Amberg. 2MoTac: Simulation of Button Click by Superposition of Two Ultrasonic Plate Waves. In Ilana Nisky, Jess Hartcher-O'Brien, Michaël Wiertlewski, and Jeroen Smeets, editors, *Haptics: Science, Technology, Applications*, Lecture Notes in Computer Science, pages 343–352, Cham, 2020. Springer International Publishing. ISBN 978-3-030-58147-3. doi: 10.1007/978-3-030-58147-3_38.

[15] Marvin M. Shrewsbury and Richard K. Johnson. Form, function, and evolution of the distal phalanx. *The Journal of Hand Surgery*, 8(4):475–479, July 1983. ISSN 0363-5023. doi: 10.1016/S0363-5023(83)80211-1. URL https://www.sciencedirect.com/science/article/pii/S0363502383802111.

[16] Chaorui Qiu, Bo Wang, Nan Zhang, Shujun Zhang, Jinfeng Liu, David Walker, Yu Wang, Hao Tian, Thomas R. Shrout, Zhuo Xu, Long-Qing Chen, and Fei Li. Transparent ferroelectric crystals with ultrahigh piezoelectricity. *Nature*, 577(7790):350–354, January 2020. ISSN 1476-4687. doi: 10.1038/s41586-019-1891-y. URL https://doi.org/10.1038/s41586-019-1891-y.

6

General Conclusion

The present work sought technical solution to spatially localize vibration stimuli on a flat continuous medium with the intention to enrich tactile interactions and allow for a more natural exploration of everyday tactile surfaces. This thesis introduced three methods to localize haptic stimuli. Taking a very different path from control-based approaches, these techniques propose a matrix-based solution where each actuator provides a stimulus in its actuation area. By tweaking the geometry of the propagation medium and the boundary conditions, we found that waveguides could provide a low frequency band gap allowing us to localize vibrotactile stimuli on narrow thin plates. Associated theory as well as practical measurements showed that applications for haptics were possible and the resulting prototype received good reviews in the haptic community. Its extension to wider surfaces was possible thanks to the use of periodic supports which also provided a low frequency band-gap. A 2D prototype was implemented and allowed the user, through different exploratory procedures, to find a vibrating target area and experience phantom sensations such as apparent movement and saltation. It was shown that the effect of the finger on those geometry was close to null for light and heavy force by the finger. Seeking a full haptic experience, we also wanted to provide, in addition to normal force modulation, lateral force modulation through friction modulation. This was achieved thanks to an interference phenomena appearing in ultrasonic frequencies implied by the bounding nature of a piezoelectric actuator to a plate. Application to an OLED screen was also proven possible through a matrix of triangular electrodes powered in sets to form hexagonal piezoelectric actuators.

Now, taking a product approach, several aspects for further development of the present work can be identified: *hardware*, *interaction design* and *software*.

Regarding *hardware*, the developed techniques are based on matrices of actuators. We preferred the use of piezoelectric actuators as they have a high level of integrability in tactile devices and allow high displacement accuracy and fast response speed. In our case, their use outside surface resonance frequencies imply the need of high-voltage for each actuator to get sufficient amplitudes for haptics. As we imagine the development of a full haptic experience, the powering electronic would have to be able to amplify, up to a 100 V amplitude, low-frequency (< 1 kHz) as well as high-frequency (> 25 kHz) signals for a matrix of actuator. Powering an effector matrix is not a new problem and is already implemented in many systems i.e. screens. The difficulty here lies in the way we use it and especially in its application to piezoelectric actuators. Indeed, a piezoelectric actuator is equivalent to a capacitor. Driving a capacitive load has a strong chance to destabilize the upstream amplification system, leading to overshoot and electrical oscillation accompanied by important current calls due to the voltage inertia inherent to capacitors. Furthermore, charging and discharging of the capacitor leads to high energy loss. To a avoid the latter, recycling the energy used to charge the actuator is possible but would need an added control electronic. Also, if we wish to control each $N\times$actuator individually we would need $N\times$amplification electronic. A better trade-off would be to limit the number of simultaneously activated actuators and develop an electronic with commutation to reduce the number of component used. Moreover, if we imagine a two way exchange and use this matrix as sensor, we would have yet again to adapt the electronic or add a parallel one to each channels with a charge amplifier which would have to be protected in both ways to ensure proper sensing and isolation when actuators are powered. As we can see, the powering and signal generation/acquisition through a dense matrix of piezoelectric actuator is rather tricky and constitute one of the future challenges linked to our approach.

Regarding *interaction design*, a full device based on the state of the art methods and on our approaches, for instance the use of the inverse filtering technique in harmony with non-radiating frequencies, would open the way to new kind of interactions. Such device, merging vibrotactile feedback and friction modulation in a localized fashion, would allow us to manage both static and dynamic multi-touch/multi-user interactions in an HMI setting. Applications in design, online shopping (i.e. feeling the fabric of clothes as you purchase them online), gaming and entertainment, education, health and rehabilitation, accessibility (i.e. visually impaired person navigation), arts, automotive (i.e. feeling the detents of a digital knob or identifying an option through touch alone on a tactile dashboard) and more can be imagined. The implementation of new interactions needs to be accompanied with user and psy-

chophysical studies to carefully design haptic signal which will affect the hardware specifications.

Regarding *software*, with new interactions comes the need of an adapted API. Present haptic APIs (i.e. Google and Apple) only allow for temporal modulated stimuli thus it is necessary to build a "multi-haptic API" which takes into account the spatial dimension allowed by our technologies in addition to the temporal modulation. As the nature of piezoelectric materials allow for a two way operation, in the same way we provide localized haptic feedback we can also use the actuators as localized sensors. We could therefore imagine a two way haptic communication between users. This raise questions about haptic data stream encoding or decoding for digital transmission and storage. Like video and sound codecs, the construction of a haptic codec will soon become essential.

Taking some distance from surface haptics, there are numerous fields that could be inspired by the ideas developed in this thesis. As waveguides allow for the localization of low-frequencies, if used as sensor, they could constitute spatial filters for robotic applications (i.e. in grasping task or affective touch). We can also think of applications in positioning and vibration isolation in micro-systems for instance (i.e. micro-organism manipulation and micro-particle arrangement).

To conclude, I would like to put the work presented in this thesis into a larger perspective. All things considered, the usefulness of extending haptic feedback to multi-touch on tactile surfaces is still an open question. We touched on the topic slightly in chapter 2 and pointed that certain exploratory tasks are best performed by augmenting tactile vision through the use of multiple fingers. The usefulness of multi-touch is therefore task-specific. Tasks that are thus essential to characterize if we want to judge the usefulness of the developed technologies. Considering the increasing number of worldwide shortages of electronic components and the deterioration of earth resources, if technologies based on actuator matrix approaches for haptic feedback become preponderant in consumer products, they can in no way be used solely for haptic feedback but should ensure a plurality of functions to justify the energy and materials used for its design. Future developments of the presented methods should therefore be subject to user-centered scenarios and ethically justifiable.

Appendices

A

Laser Vibrometers

A

A.1. OFV-505 SENSOR HEAD

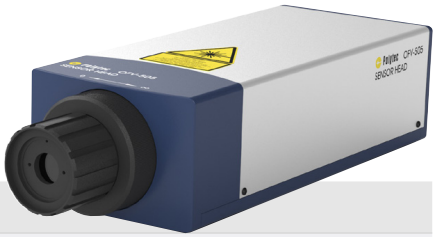

Polytec

Optical Specifications	
Laser type	Helium Neon (HeNe)
Laser class	Class 2, < 1 mW, eye-safe
Laser wavelength	633 nm, visible red laser beam
Focus	Auto focus, remote focus, manual focus [1]
Maximum stand-off distance	Up to 300 m (with OFV-SLR, surface dependent)
Visibility maxima	234 mm + n · 204 mm; n = 0, 1, 2, 3, ... measured from the focusing ring

General Specifications	
Operating temperature	+5 °C ... +40 °C (41 °F ... 104 °F)
Relative humidity	Max. 80%, non-condensing
Weight	3.4 kg
Dimensions [W x H x L]	120 x 80 x 345 mm (4.7 x 3.2 x 13.6 in)
Controller compatibility	OFV-5000, OFV-2520, OFV-2570 Vibrometer Controller, VDD-E-600 Digital Front-End

Compliance with Standards	
Laser safety	IEC/EN 60825-1; CFR 1040.10 and 1040.11
Electrical safety	IEC/EN 61010-1
EMC	IEC/EN 61326-1

Options and Accessories

Front lens	OFV-SR short range	OFV-MR mid range	OFV-LR² long range	OFV-SLR super long range
Focal length [mm]	30	60	100	200
Min. stand-off distance [mm]	100	200	530	1,800
Aperture diameter (1/e²) [mm]	3.4	6.8	11.3	22.6
Typical spot size in µm at				
100 mm	25	-	-	-
200 mm	49	25	-	-
500 mm	121	54	18	-
1,000 mm	245	112	62	-
2,000 mm	500	235	135	60
3,000 mm	750	356	210	96
5,000 mm distance	1,260	604	356	168
Each additional meter add [µm]	240	126	74	36

A.2. OFV-534 Sensor Head

Optical Specifications	
Laser type	Helium Neon (HeNe)
Laser class	Class 2, < 1 mW
Laser wavelength	633 nm, visible red laser beam
Focus	Manual focus
Minimum stand-off distance	Up to 200 mm
Visibility maxima	295 mm + n · 204 mm; n = 0, 1, 2, 3, ... measured from the focusing ring
General Specifications	
Operating temperature	+5 °C ... +40 °C (41 °F ... 104 °F)
Relative humidity	Max. 80%, non-condensing
Weight	1 kg
Dimensions [W x H x L]	201 x 39 x 71 mm
Controller compatibility	OFV-5000, OFV-2500, OFV-2570 Vibrometer Controller, VDD-E-600 Digital Front-End
Compliance with Standards	
Laser safety	IEC/EN 60825-1; CFR 1040.10 and 1040.11
Electrical safety	IEC/EN 61010-1
EMC	IEC/EN 61326-1

Characteristics		[2]	[3]			[4]				
Stand-off distance [1]	mm	21.7	37.3	200	300	320	500	1,000	2,000	each m
Laser depth of field	mm	0.012	0.048	±1	±3	±0.08	±10	±40	±170	–
Spot diameter ($1/e^2$)	µm	1.5	3.0	25	40	15	70	148	302	add 150
Camera field of view	mm x mm	0.68 x 0.52	1.36 x 1.04	10 x 8	17 x 13	3.8 x 2.9	31 x 24	64 x 49	130 x 100	–

[1] Measured from the front edge of the sensor head housing; as for the 10X-, 20X-microscope lens and the telephoto lens measured from the front edge of the lens
[2] With VIB-A-20xLENS 20X Microscope Lens
[3] With VIB-A-10xLENS 10X Microscope Lens
[4] With VIB-A-520 Telephoto Lens

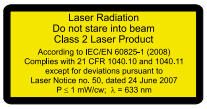

B

Actuators

B.1. PIEZOELECTRIC ACTUATORS

PI / *STEMiNC*

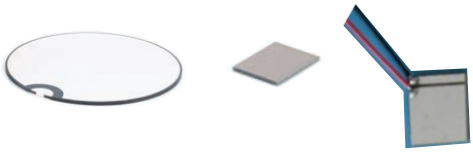

Material type			PIC 151	PIC 255	SM412
Parameter					
Physical and dielectric properties					
Density	ρ (g/cm^3)		7.80	7.80	7.80
Curie temperature	Tc (°C)		250	350	320
Permittivity in the polarization direction perpendiculaer to the polarity	$\varepsilon_{33}^T/\varepsilon_0$ $\varepsilon_{31}^T/\varepsilon_0$		2400 1980	1750 1650	1850
Dielectric loss factor	tan δ (10^{-3})		20	20	12
Electromechanical properties					
Coupling factors	k_p k_t k_{31} k_{33} k_{15}		0.62 0.53 0.38 0.69	0.62 0.47 0.35 0.69 0.66	0.63 0.42 0.35
Piezoelectric charge constants	d_{31} d_{33} d_{15}	(10^{-12} C/N)	-210 500	-180 400 550	-190 450
Piezoelectric charge voltage constants	g_{31} g_{33}	(10^{-3} Vm/N)	-11.5 22	-11.3 25	25.6 -12.6
Acousto-mechanical properties					
Frequency constants	N_p N_1 N_3 N_t	(Hz.m)	1950 1500 1750 1950	2000 1420 2000	2080 1560 2080
Elastic constants (compliance)	S^E_{11} S^E_{33}	(10^{-12}m^2/N)	15.0 19.0	16.1 20.7	
Elastic constants (stiffness)	C^D_{33}	(10^{10}N/m^2)		10.0	5.6
Mechanical quality factor	Qm		100	80	100
Temperature stability					
Temperature coefficient of ε_{33} [-20, +125]°C	TK ε_{33}	(x10^{-3}/K)	6	4	
Aging stability (relative change of the parameter per decade in %)					
Relative dielectric constant	C	(%)		-1.0	
Coupling factor	C_k			-1.0	

muRata
INNOVATOR IN ELECTRONICS

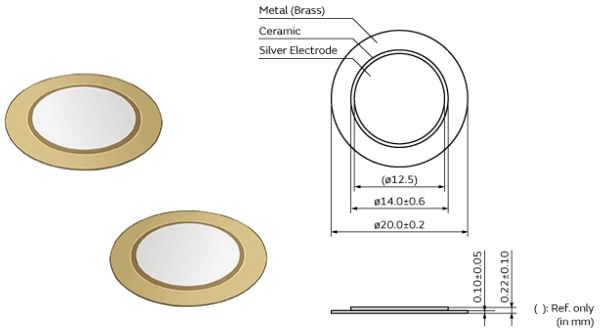

7BB-20-3

Features	1. Clear sound 2. Ultrathin and lightweight No contacts: therefore, no noise and highly reliable 4. Low power consumption for voltage type

Specifications	
Resonant frequency	3.6 kHz
Resonant frequency tolerance	±0.6 kHz
Resonant impedance (R1)	500 Ω
Capacitance	20 nF
Capacitance Tolerance	±30%
Measurement condition of capacitance	[1 kHz]
Operating temperature range	-20°C to 70°C
Storage temperature range	-30°C to 80°C
Shape	No lead wire
Plate size	20 mm
Element size	14 mm
Plate material	Brass
Drive type	External drive
EIAJ Part number	PD-SU2-C20-36
Mass	360 mg

Applications	
Other usage	Consumer/Idustrial

Packaging information	
Packaging	-
Specifications	Bulk
Standard packing quantity	3000

B

B.2. INERTIAL ACTUATORS

PRECISION MICRODRIVES™
www.precisionmicrodrives.com

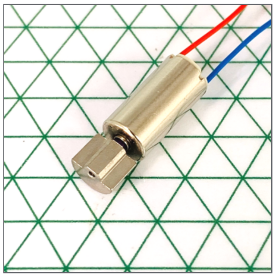

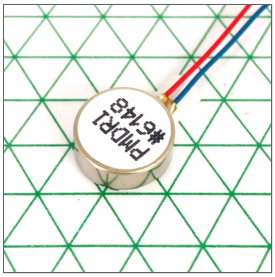

Material type	306-109	C10-100
Key features		
Body diameter	6 mm [±0.1]	10 mm [±0.1]
Body length	12.2 mm [±0.2]	3.7 mm [±0.15]
Ecc. weight radius	2.9 mm [±0.1]	-
Acc weight length	14.5 mm [±0.2]	-
Rated voltage	3 V	2 V
Rated vibration	14,300 rpm[±3,500]	175 Hz
Typical rated operating current	66 mA	69 mA
Typical norm. amplitude	4.51 G	1.5 G

Typical DC Motor Performance Characteristics

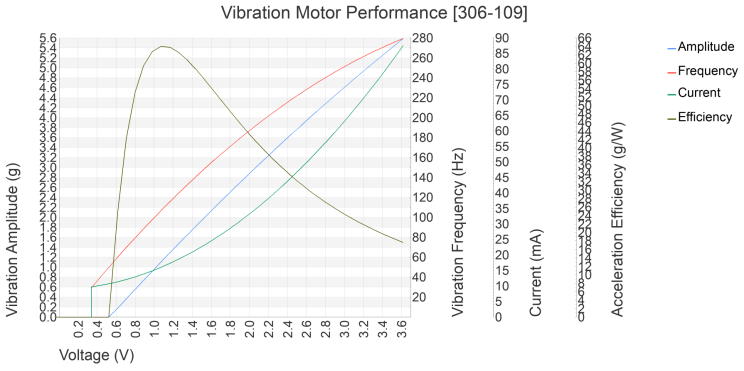

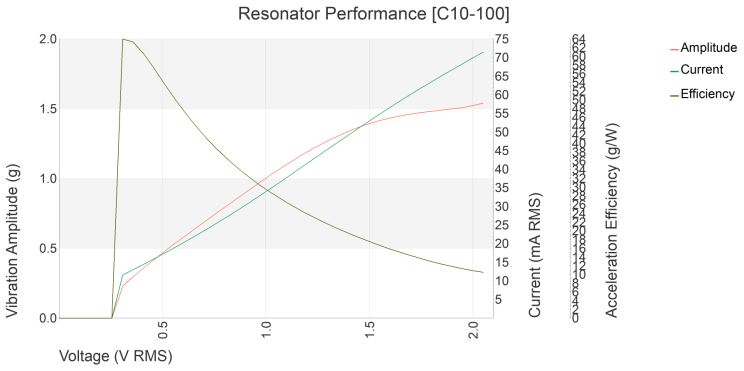

C

Electronics

C.1. AMPLIFICATION

C.1.1. TI DRV8662

TEXAS INSTRUMENTS

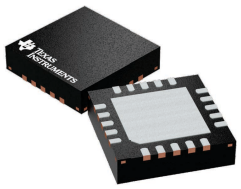

Specifications		MIN	TYP	MAX	UNIT
Absolute maximum ratings					
Supply voltage		-0.3		6.0	V
Input voltage		-0.3		6.3	V
Boost/output voltage				120	V
Operating free-air temperature range		-40		70	°C
Operating junction temperature range		-40		150	°C
Storage temperature		-65		85	°C
Recommended operating conditions					
Supply voltage		3.0		5.5	V
Boost voltage		15		105	V
Differentail input voltage			1.8		V
Load capacitance	Boost 105 V / 500 Hz / OUT 200 V			50	nF
	Boost 105 V / 300 Hz / OUT 200 V			100	
	Boost 80 V / 300 Hz / OUT 150 V			150	
	Boost 55 V / 300 Hz / OUT 100 V			330	
	Boost 30 V / 300 Hz / OUT 50 V			680	
	Boost 25 V / 300 Hz / OUT 40 V			1000	
	Boost 15 V / 300 Hz / OUT 20 V			3000	
Electrical characteristics					
Quiescent current	IN 3.6 V / boost 105 V / no signal			24	mA
	IN 3.6 V / boost 80 V / no signal			13	
	IN 3.6 V / boost 55 V / no signal			9	
	IN 3.6 V / boost 30 V / no signal			5	
Amplifier bandwidth	28.8 dB / OUT 50 V / No Load			20	kHz
	34.8 dB / OUT 100 V / No Load			10	
	38.4 dB / OUT 150 V / No Load			7.5	
	40.7 dB / OUT 200 V / No Load			5	
Average battery current during operation	IN 3.6 V / 10 nF / 150 Hz / OUT 200 V			75	mA
	IN 3.6 V / 10 nF / 300 Hz / OUT 200 V			115	
	IN 3.6 V / 47 nF / 150 Hz / OUT 200 V			210	
	IN 3.6 V / 47 nF / 300 Hz / OUT 200 V			400	
Total harmonic distortion + noise	300 Hz @ 200 V		1%		

C.1.2. ELBATECH T-500

ElbaTech srl
Soluzioni elettroniche e Innovazione

Specifications	
Multiple gain selector	x ± 2 V or x ± 20 V
Max input voltage	± 10 V
Max output voltage	± 200 V
Bandwidth (-N, without load)	DC to 100 kHz
Bandwidth (-F, without load)	DC to 500 kHz
Channels	up to 6
Power supply	230 Vac 50-60 Hz
Load	capacitive, resistive, inductive
Output current	400 mA peak-to-peak max
Ripple voltage	2 mV max full bandwidth
RMS noise absolute	RMS noise absolute 1.2 mV (typical)

Physical dimensions	
Width	84 TE
Heigth	3 U
Deoth	480 mm
Weight	10 kg
Operating temperature	-10°C to 50°C
Humidity	0 to 95%

T-500 Output voltage vs. load capacitance

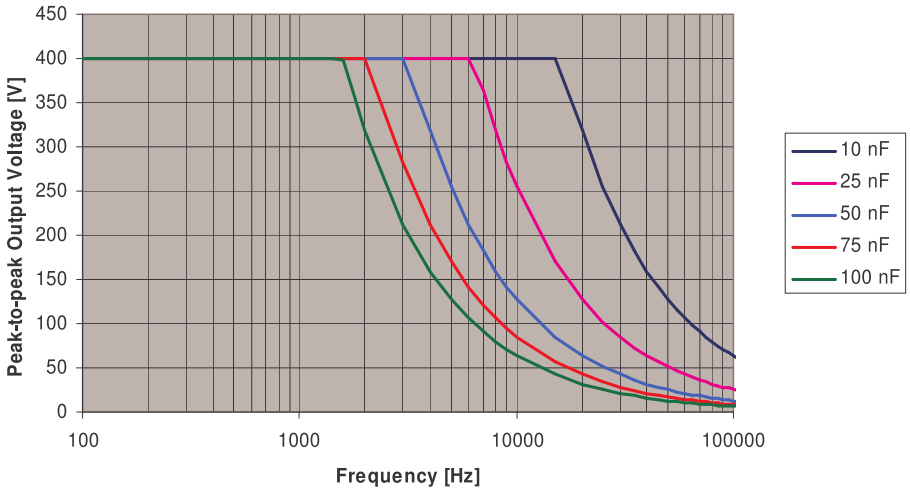

C.2. ACQUISITION

C.2.1. NI-USB-6363

NI - USB - 6363	
Analog input	
Number of channels	32 single-ended or 16 differential
ADC resolution	16 bits
DNL	No missing codes guaranteed
INL	Refer to *AI Absolute Accuracy*
Sample rate single channel max	2.00 MSample/s
Sample rate multi channel max	1.00 MSample/s
Timing resolution	10 ns
Timing accuracy	50 ppm of sample rate
Input coupling	DC
Input range	± 0.1/0.2/0.5/1/2/5/10 V
Maximum working voltage for analog inputs	± 11 V of AI GND
CMRR (DC to 60 Hz)	100 dB
Analog output	
Number of channels	4
DAC resolution	16 bits
DNL	± 1 LSB
Monotonicty	16 bit guaranteed
Maximum update rate 1/2/3/4 channels	2.86/2.00/1.54/1.25 MSample/s
Timing accuracy	50 ppm of sample rate
Timing resolution	10 ns
Output range	± 10 V, ± 5 V ± external reference on APFI <0.1>
Output coupling	DC
Output impedance	0.2
Output current drive	± 5 mA
Overdrive protection	± 25 V
Overdrive current	26 mA
Power-on state	± 5 mV

C.2.2. NI-9264 (AO output)

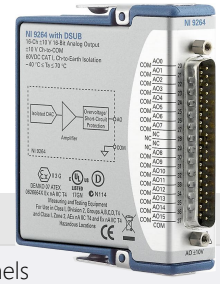

NI 9264		
Number of channels		16 analog output channels
DAC resolution		16 bits
Type of DAC		String
Power-on output state		Channels off
Startup voltage		0 V
Power-down voltage		0 V
Output range	Nominal	± 10 V
	Minimum	± 10.35 V
	Typical	± 10.5 V
	Maximum	± 16.65 V
Current drive		± 16 mA all channels maximum ± 4 mA per channel typical
Output impedance		2.0 Ω

C.2.3. NI-9205 (AI input)

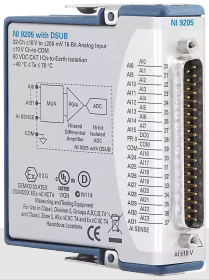

NI 9205		
Number of channels		16 differential / 32 single-ended channels
ADC resolution		16 bits
Input coupling		DC
Nominal input ranges		± 10 / ± 5 / ± 1 / ± 0.2 V
Maximum sampling rate		250 kSamples/s
Minimum overrange		4%
Input impedance ON/OFF		> 10 GΩ in parallel with 100 pF / 4.7 kΩ minimum
Analog bandwidth		370 kHz
Scaling coefficient	± 10 V	328 µV / LSB
	± 5 V	164.2 µV / LSB
	± 1 V	32.8 µV / LSB
	± 0.2 V	6.57 µV / LSB

D

Sensors

D.1. ATI MINI-40

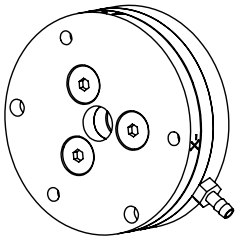

Six-axis Force/Torque sensor system

Physical properties	
Single-axis overload	
Fxy	±810 N
Fz	±2400 N
Txy	±19 N.m
Tz	±20 N.m
Stiffness (calculated)	
X-axis & Y-axis forces (Kx, Ky)	$\pm 1.1 \times 10^7$ N/m
Z-axis force (Kz)	$\pm 2.0 \times 10^7$ N/m
X-axis & Y-axis torque (Ktx, Kty)	$\pm 2.8 \times 10^3$ N.m/rad
Z-axis torque (Ktz)	$\pm 4.0 \times 10^3$ N.m/rad
Resonant frequency	
Fx, Fy, Tz	3200 Hz
Fz, Tx, Ty	4900 Hz
Physical specifications	
Weight	0.0499 kg
Diameter	40 mm
Height	12.2 mm

Calibration specifications		SI-20-1	SI-40-2	SI-80-4
Fx, Fy	(N)	20	60	80
Fz	(N)	60	120	240
Tx, Ty	(N.m)	1	2	4
Tz	(N.m)	1	2	4
Fx, Fy	(N)	1/200	1/100	1/50
Fz	(N)	1/100	1/50	1/25
Tx, Ty	(N.m)	1/8000	1/4000	1/2000
Tz	(N.m)	1/8000	1/4000	1/2000

D.2. S2M

Force Transducer
Special features
- Tensile/compressive force transducer
- Nominal (rated) forces : 10 ... 1000 N
- High protection class (IP67)
- High lateral force stability
- Six-wire circuit

Specifications							
Nominal (rated) force	10	20	50	100	200	500	1000
Accuracy class	0.02						
Electrical characteristic values							
Nominal (rated) sensitivity	2 mV/V						
Relative zero signal error	5%						
Relative sensitivity error	0.25%						
Rel. tensile/compression sensitivity variation	0.1%						
Input resistance	> 345 Ω						
Output resistance	350 ± 50 Ω						
Insulation resistance	> 2 GΩ						
Operating range of the excitation voltage	0.5 ... 12 V						
Reference excitation voltage	5 V						
Connection	Six-wires circuit						
Mechanical characteristic quantities							
Max. operating force	150%						
Limit force	1000%						
Breaking force	1000%						
Limit torque (N.m)	4	8	25	28			
Limit bending moment (N.m)	6	25	34	50	71	95	125
Static lateral limit force (% of F_{nom})	100						
Nominal (rated) displacement (mm)	0.27	0.21	0.18	0.15	0.13	0.12	0.13
Fundamental resonance frequency (Hz)	94.4	146	243	358	475	582	618
Relative permissible oscillatory stress (% of F_{nom})	140						

E

Adhesive

E.1. 3M DP490

3M Scotch-Weld EPX Adhesive DP490	Base	Accelerator
Specific gravity	1.00	1.00
Consistency	Non-sag paste	Non-sag paste
Mix ratio	100	50
Colour	Black	Off-white
Work life	1.5 hours minimum at 23°C	
Time to handling strength	4 to 6 hours at 23°	
Time to full strength	7 days (test to full performance at one week)	
Shelf life	15 months at 21°C & 50% relative humidity	

E.2. LOCTITE 401

LOCTITE 401	
Chemical type	Ethyl cyanoacrylate
Appearance	Transparent
Components	One part - requires no mixing
Viscosity	Low
Cure	Humidity
Application	Bonding
Key substrates	Metals, plastics & elastomers
Specific gravity	1.10
Cure speed	5 seconds

List of Figures

List of Tables

Curriculum Vitæ

Ayoub Ben Dhiab

08-08-1994	Born in Sousse, Tunisia.

Education

2009–2012	High-School Diploma Scientific Curriculum with focus on Engineering Sciences Jean Perrin, Lambersart, France. (2009–2010) Jean Prouvé, Lomme, France. (2010–2012)
2012–2014	Associate's Degree Speciality in Physics Measurements University Institute of Technology Lille 1, France.
2014-2015	Undergraduate courses to prepare nationwide competitive exams in sciences. Prépa ATS, Lycée Baggio, Lille, France. Year obtained with ECTS A Mention.
2015-2018	Engineering Diploma & Research Master Degree. Speciality in Advanced Systems and Robotics, with focus on Haptics and Medical Robotics. Arts et Métiers, Lille, France. (2015–2017) Arts et Métiers & Sorbonne Université, Paris, France. (2017–2018)
2018–2021	PhD on "Confinement of Vibration for Localized Surface Haptics". Doctoral School of Mechanical Sciences, Acoustics, Electronics and Robotics. ED SMAER, Sorbonne Université, Paris, France. CEA-List, Palaisseau, France.
2021-Current	Permanent Position as a Research Engineer. CEA-List, Palaisseau, France.

Awards

2019	Best Student Paper at IEEE World Haptics Conference 2019 Tokyo
2020	Best Short Presentation at CEA PhD Day

List of Publications

5. M. Jeannin, **A. Ben Dhiab**, L. Pantera, C. Hudin, et S. Panëels, *The Funneling Illusion Using the Confinement of Vibrotactile Stimuli in Narrow Plates*, in 2021 IEEE World Haptics Conference (WHC), juill. 2021, p. 1147-1147. DOI.

4. **A. Ben Dhiab** et C. Hudin, *Confinement of Vibrotactile Stimuli in Periodically Supported Plates*, in Haptics: Science, Technology, Applications, Cham, 2020, p. 334-342. DOI.

3. **A. Ben Dhiab** et C. Hudin, *Confinement of Vibrotactile Stimuli in Narrow Plates: Principle and Effect of Finger Loading*, IEEE Transactions on Haptics, vol. 13, n°3, p. 471-482, juill. 2020, DOI.

2. **A. Ben Dhiab** et C. Hudin, *Touch interface offering improved localised vibrotactile feedback*, European Patent EP3942392 A1, 2022 Jan 26, French, ONLINE.

1. **A. Ben Dhiab** et C. Hudin, *Confinement of Vibrotactile Stimuli in Narrow Plates*, in 2019 IEEE World Haptics Conference (WHC), juill. 2019, p. 431-436. DOI.

The French Atomic Energy and Alternative Energies Commission (CEA) is a public research organization of a scientific, technical and industrial nature (EPIC). Key player in research, development and innovation, the CEA is active in six major sectors: defense and national security, nuclear and renewable energies, biotechnology and medical research, technological research for industry, fundamental research (material and life sciences) and the cleanup and dismantling of nuclear facilities. For 75 years, thanks to the excellence of its research and its partnerships, the CEA has been at the origin of many applications that influence our daily lives

The CEA-List is one of CEA Tech's three technological research institutes. Dedicated to intelligent digital systems, its mission is to carry out excellent technological developments on behalf of industrial partners, and to create value. The activities of the List's research engineers are the subject of publications in leading international conferences and journals. The List is also involved in more than 200 European collaborative projects, collaborates with leading foreign academic laboratories, and conducts research activities at the international level.

Short abstract. On a tactile surface, providing vibrotactile feedback improves interaction. Doing so in a localized manner allows for a more natural multi-finger exploration of these surfaces. While the propagation of vibrations generally prevents this localization, in this thesis we present technical solutions to spatially localize vibratory stimuli on continuous surfaces. Taking a route opposite to control-based approaches, we propose three methods where each actuator provides a stimulus confined to its actuation area. By adjusting the geometry of the propagation medium and the boundary conditions, we show that waveguides constitute high-pass filters allowing localized vibrotactile stimulation on thin and narrow plates. The extension of the method to larger surfaces was made possible by the use of periodic supports that also provide frequency band gaps. Seeking a complete haptic experience, in addition to normal force modulation, lateral force modulation was provided by friction modulation. This was achieved through an interference phenomenon occurring in so-called non-radiating ultrasonic frequencies involved by the mechanical bonding of a piezoelectric actuator to a plate. The extension to an actuator array was then achieved by creating a triangular electrode array. By feeding sets of triangles to form hexagonal piezoelectric actuators, localized friction modulation was found to be possible on an OLED display.

Biography

Hi ! My name is Ayoub Ben Dhiab and I received in 2018 a Master of Engineering (MEng) in General Engineering from Arts et Métiers and a Master of Research (MRes) in Advanced Systems and Robotics from Sorbonne University, Paris, France. I defended my thesis and received my PhD degree in 2022 from Sorbonne University which was completed at the CEA within the Laboratory of Sensory and Ambient Interfaces (LISA). This manuscript reports 3 years of work on localized surface haptics through confinement of vibrations and present novel ways to provide enhanced interactions on future smart surfaces. I am now working as a permanent researcher at the CEA-List institute working on various topics including acoustics, signal processing, multi-touch and multi-user surface haptics.